Poly(ethylene glycol)-Based Hydrogels to Support Vascularization and Reendothelialization by Endothelial Colony Forming Cells

by

Yuan Tian

A dissertation submitted to the Graduate Faculty of
Auburn University
in partial fulfillment of the
requirements for the Degree of
Doctor of Philosophy

Auburn, Alabama
May 2, 2020

Keywords: Hydrogels, Endothelial Colony Forming Cells, Microfluidics

Approved by

Elizabeth A. Lipke, Chair, Mary and John H. Sanders Endowed Associate Professor of Chemical Engineering
Rajesh Amin, Associate Professor of Drug Discovery and Development
Bryan S. Beckingham, Assistant Professor of Chemical Engineering
Allan E. David, John W. Brown Associate Professor of Chemical Engineering
Anne A. Wooldridge, Professor of Clinical Sciences

Abstract

Endothelial colony forming cells (ECFCs) have a high proliferative capability and can differentiate into endothelial cells, making them a promising cell source for vascularization of ischemic tissues and reendothelialization of injured vasculature. However, it is challenging to deliver the ECFCs to a target site and ensure that their therapeutic functionality is preserved. This research focuses on the development of approaches for subcutaneous and intravascular ECFC delivery with the aid of biomimetic poly(ethylene glycol) (PEG)-based hydrogels.

Chapter 1 introduces current treatment for cardiovascular disease (CVD), endothelial cell (EC) sources for treating CVD, and the use of biomaterials to support the functionality of ECs. Chapter 2 describes the development of a microfluidic encapsulation platform that enables rapid production of highly uniform cell-laden hydrogel microspheres, which can be used for numerous applications including supporting injectable cell delivery. Chapter 3 presents the further exploration of the microfluidic platform for production of microspheroids with different geometric shapes, including axial ratio and diameter, and understanding of the underlying mechanism controlling microspheroidal geometry. In chapter 4, autologous equine ECFCs were encapsulated in PEG-fibrinogen hydrogel microspheres using the microfluidic platform and subcutaneously injected into distal limb wounds of horses, demonstrating the feasibility of scalable production of cell-laden microspheres for large animal cell therapy and realization of cell retention and survival after local injection. Results from this study can provide insight on ECFC delivery for vascularization of ischemic tissues for enhancing the wound healing process. In chapter 5, a study investigating the dynamic adhesion of ECFCs on peptide-grafted hydrogels under shear condition is reported. Novel peptide combinations were designed and evaluated for their ability to support

ECFC tethering and adhesion. These results can be applied for modification of vascular graft and stent surface for preventing restenosis, which is one of the main long-term causes of failed heart surgery. Overall, new approaches were developed for more efficient delivery of ECFCs subcutaneously and intravascularly to restore blood flow to ischemic tissues.

Acknowledgments

Graduate studies at Auburn University have been a great part of my life, and I cannot get this far without the help of many individuals. I am grateful to my advisor, Dr. Elizabeth Lipke, for her continued dedication and guidance throughout my Ph.D. project. I would also like to thank members of Lipke Lab, specifically, Aaron Seeto, Benjamin Anbiah, Ferdous Finklea, Morgan Ellis, and Iman Hassani for their assistance and friendship. I would like to thank my committee members, Dr. Anne Wooldridge, Dr. Allan David, Dr. Bryan Beckingham, and university reader, Dr. Rajesh Amin for their time and knowledge in the preparation and critical review of this manuscript.

Furthermore, I would like to thank my parents, Hong Wei and Jinzhong Tian, for all the support they have given me during this process. Lastly, I would like to acknowledge and thank my wife, Wen Shi, for her support and love.

Table of Contents

List of Tables

List of Illustrations

List of Abbreviations

ABS	Acrylonitrile butadiene styrene
ANOVA	Analysis of variance
AR	Axial ratio
BAEC	Bovine aortic endothelial cell
BMP	Bone morphogenetic protein
BMS	Bare-metal stent
Ca	Capillary number
CABG	Coronary artery bypass graft
CAD	Coronary artery disease
CFU	Colony forming unit
CVD	Cardiovascular disease
DAPI	4',6-diamidino-2-phenylindole
Dil-Ac-LDL	Dil-conjugated acetylated low-density lipoproteins
DES	Drug-eluting stent
DMEM	Dulbecco's Modified Eagle's Medium
DMSO	Dimethyl sulfoxide
EC	Endothelial cell
ECFC	Endothelial colony forming cell
ECM	Extracellular matrix
EG	Ethylene glycol
EPC	Endothelial progenitor cell

Fb	Fibrinogen
FBS	Fetal bovine serum
GelMA	Gelatin methacryloyl
hESC	Human embryonic stem cell
hiPSC	Human induced pluripotent stem cell
HSD	Honestly significant difference
HUVEC	Human umbilical vein endothelial cell
IFA	Immunofluorescence assay
ISR	In-stent restenosis
MCF7	Michigan cancer foundation 7
MNC	Mononuclear cell
MS	Microspheres
NMR	Nuclear magnetic resonance
NO	Nitric oxide
NR	Narrowing ratio
OCT	Optimal cutting temperature
PAD	Peripheral artery disease
PBS	Phosphate-buffered saline
PCI	Percutaneous coronary intervention
PDMS	Polydimethylsiloxane
PEG	Poly(ethylene glycol)
PEGDA	Poly(ethylene glycol) diacrylate
PF	Poly(ethylene glycol) diacrylate-fibrinogen

PFA	Paraformaldehyde
SD	Standard deviation
SEM	Scanning electron microscope
SMC	Smooth muscle cell
TCPS	Tissue culture polystyrene
VEGF	Vascular endothelial growth factor
vWF	von Willebrand factor

1. CHAPTER 1: Introduction

1.1 Motivation for treating cardiovascular disease

Cardiovascular disease (CVD) includes a variety of diseases that can affect the heart and the blood vessels, such as angina, myocardial infarction, stroke, hypertensive heart disease, and peripheral artery disease. CVD is a major cause of death worldwide. More than 17 million people died from CVD in 2008 (Mendis et al. 2011). Based on a report from American Heart Association, 800,937 deaths were caused by CVD in the year of 2013 in the United States, which was 37 % more than cancer-related deaths (Mozaffarian et al. 2016). Though CVD can be caused by different factors, a major cause of CVD is atherosclerosis, where a plaque is formed within the artery wall. The plaque comes from the accumulation of leukocytes, cholesterol, triglycerides, and the proliferation of smooth muscle cells (SMCs), leading to the narrowing of the artery. As a result, blood flow through the artery is limited, causing regional ischemia. For years, numerous studies have explored the methods for treating CVD, and many effective medications as well as surgical therapies have emerged. However, many current treatments only have a limited therapeutic effect on CVD. Therefore, more work is still needed to identify better ways of treating CVD.

1.1.1 Peripheral artery disease and injectable cell therapy

Peripheral artery disease (PAD) is a common circulatory problem in which narrowed arteries cannot provide enough blood flow to the limbs. One of the major reasons for PAD is atherosclerosis in the arteries of the legs. PAD can lead to pain, numbness, and weakness in the limbs and diabetic foot ulceration for diabetic patients. Angiogenesis is the growth of blood vessels from pre-existing vasculature and has been studied extensively as a therapeutic approach to treat patients with PAD. Major strategies focus on intra-arterial and intramuscular injection of growth factors, such as vascular endothelial growth factor (VEGF), and therapeutic cells, such as bone

marrow mononuclear cells (Iyer and Annex 2017). For cell-based therapies, despite the promising results of many preclinical studies, the outcome from human clinical studies thus far have been disappointing. This is largely due to the use of a direct cell injection method, which may cause low cell viability and retention rates caused by the high shear forces in the needle and mechanical washout. Encapsulation of therapeutic cells in hydrogels has been shown to support cell proliferation and long-term survival (Nicodemus and Bryant 2008). Hydrogels can protect the cells from shear stress and significantly improve cell retention (Bidarra, Barrias, and Granja 2014). Therefore, cell encapsulation in hydrogel scaffolds could advance the potential of cell-based therapies.

1.1.2 Coronary artery disease and restenosis

When atherosclerosis develops within the coronary arteries, the blockage causes coronary artery disease (CAD). The shortage of blood supply to cardiomyocyte can lead to angina and even cardiac ischemia. For patients with mild CAD, medication is normally used to alleviate the symptoms. However, when severe atherosclerosis has developed, meaning more than 70 % occlusion has been detected in the coronary artery, surgical treatments will be necessary to restore enough blood flow to the affected region of the heart. The two most common surgical treatments for CAD are coronary artery bypass graft (CABG) and percutaneous coronary intervention (PCI), commonly known as angioplasty.

CABG treatment bypasses the partially blocked portion of the coronary artery using a healthy vessel from other parts of the body, such as the great saphenous vein of the leg. However, in many patients, it is difficult to obtain vessels that are healthy and long enough for effective bypass. In these cases, synthetic vascular grafts are used as substitutes. Most of the artificial vascular grafts are made of polymer plastics such as expanded polytetrafluoroethylene, polyethylene terephthalate,

or polyurethane (Avci-Adali, Ziemer, and Wendel 2010). These materials have relatively poor biocompatibility compared to native vessels and can have stenosis, as well as thrombosis. Every 10 years, the artificial vascular graft needs to be replaced due to occlusion. Although studies have shown that CABG is effective in lowering death and myocardial infarction rates (Hawkes et al. 2006), it is a more invasive surgery with higher risk and cost when compared to angioplasty.

As an alternative to replacing the narrowed portion of the coronary artery, the goal of angioplasty treatment is to widen the blocked portion by inflating a balloon guided with a catheter and place a stent to keep the portion open. Various types of stents have been developed for angioplasty; the two most commonly used are bare-metal stents (BMS) and drug-eluting stents (DES). BMS are small metal wire mesh tubes without coating, which expand after inflation of the balloon catheter and open the artery. Compared to balloon angioplasty alone, patients with BMS implantation had a significantly lower rate of restenosis at seven months (Serruys et al. 1994) and a reduced requirement for repeat intervention at one year (Macaya et al. 1996). However, in 15 % to 60 % of cases, bare-metal in-stent restenosis (ISR) still occurs with more challenging syndromes compared with conventional balloon angioplasty (Greenberg, Bakhai, and Cohen 2004). The ISR is believed to be the result of a vascular injury caused by angioplasty and stenting. The insertion of a stent will lead to endothelial denudation, followed by platelet adhesion and thrombus formation (Faxon, Sanborn, and Haudenschild 1987). Then a series of inflammatory responses cause endothelial proliferation and smooth muscle migration, resulting in neointimal hyperplasia (Mitra and Agrawal 2006).

To prevent restenosis, DES were introduced to inhibit biological processes that lead to neointimal hyperplasia, as well as to deliver higher concentration of drugs directly to the site of the target lesion without systemic effects (Sousa, Serruys, and Costa 2003). The drugs, such as

Sirolimus and Zotarolimus, work as immunosuppressants with anti-proliferative effects on vascular SMCs (Puranik, Dawson, and Peppas 2013). Despite the significant advances of DES to reduce ISR, the incidence of ISR requiring target vessel revascularization and DES failure are still 5 % to 10 %, which translates to 200,000 cases annually in the United States alone (Farooq, Gogas, and Serruys 2011, Lloyd-Jones et al. 2009). One of the reasons for DES failure is that the delivered drug not only inhibits the proliferation of SMCs but also impairs the recovery of the endothelium, causing late restenosis.

Besides DES with anti-restenotic drugs, numerous studies have been conducted to prevent thrombosis and neointimal proliferation, such as utilizing nitric oxide (NO)-generating polymeric hydrogels to inhibit neointima formation (Lipke and West 2005) or employing endothelial progenitor cells (EPCs)-capturing stents to promote reendothelialization (Aoki et al. 2005). The captured EPCs can differentiate into endothelial cells (ECs) which form the endothelial lining on the interior surface of the blood vessels. Despite the enormous progress in artificial biocompatible surface technologies, the endothelium remains to be the ideal surface for preventing thrombogenesis and restenosis. Healthy ECs express antiplatelet and anticoagulant agents that prevent platelet aggregation and fibrin formation (Yau, Teoh, and Verma 2015). Studies have shown that facilitated reendothelialization attenuates intimal hyperplasia (Asahara et al. 1995, Wang, Cherng, et al. 2008). This may be achieved through the generation of nitric oxide by ECs to inhibit the mitogenesis and proliferation of SMCs (Garg and Hassid 1989).

Intensive research has been conducted to promote reendothelialization by capturing circulating EPCs and various strategies for EPC capture have been developed, including capturing with antibodies (Aoki et al. 2005), peptides (Jun and West 2004, Seeto, Tian, and Lipke 2013), magnetic molecules, oligosaccharides, and aptamers (Avci-Adali, Ziemer, and Wendel 2010). All the

techniques mentioned above may also be applied to artificial vascular graft to capture EPCs. A confluent endothelial layer on the inner surface of grafts can improve the biocompatibility and thus reduce the frequency of invasive surgery to replace vascular grafts.

1.2 Cell sources for treating vascular disease

The endothelium, which is the lining of the blood vessel, consists of a monolayer of ECs. ECs have many physiological properties to ensure the normal function of blood vessels, including providing a non-thrombogenic surface, controlling the blood pressure through vasoconstriction and vasodilation (Furchgott and Vanhoutte 1989), and regulating gene expression and cell behavior by sensing the fluid shear stress from blood flow (Baeyens et al. 2016). Multiple sources of ECs have been used for investigation over the years including isolated mature ECs, such as human umbilical vein endothelial cells (HUVECs) and bovine aortic endothelial cells (BAECs), EPCs, and ECs derived from human induced pluripotent stem cells (hiPSCs), for which differentiation protocols were recently developed.

1.2.1 Isolated endothelial cells

Mature ECs can be isolated directly from human or animals. HUVECs are isolated from the luminal surface of human umbilical veins (Davis, Crampton, and Hughes 2007, Baudin et al. 2007) and are widely used in research as models providing general properties of human ECs due to their easy accessibility. Also, HUVECs are a good cell source that can provide a large number of cells. Even though HUVECs are normally considered differentiated, mature ECs, they still carry high proliferative potential, and at least 22 population doublings can be achieved through subculture (Bompais et al. 2004, Ingram et al. 2005).

Besides HUVECs, BAECs are also widely used in EC research because of their well-established isolation method and high proliferative potential (Voyta et al. 1984, Schwartz 1978).

Moreover, many other EC sources isolated from the human body are also available such as human coronary artery endothelial cells, human iliac artery endothelial cells, and human pulmonary artery endothelial cells. While there are multiple sources to obtain primary ECs for research, for disease treatment, an autologous source of ECs is highly preferable to avoid rejection by the immune system. However, due to low proliferative capacity or difficulty in maintaining phenotype in culture, autologous mature ECs are not the best sources for therapeutic purposes.

1.2.2 Endothelial progenitor cells and endothelial colony forming cells

EPCs are an important autologous EC source for many tissue engineering applications. They are unipotent stem cells that are capable of differentiating into ECs. Unlike ECs, EPCs have a high proliferative capability making them an ideal cell type for tissue repair, which requires a large number of cells. Many clinical research studies have been conducted using EPCs for reendothelialization such as vessel repair (Kong et al. 2004), coating of vascular grafts (Avci-Adali, Ziemer, and Wendel 2010), and for neovascularization of ischemic tissues (Gaffey et al. 2015). EPCs originate from bone marrow or the vessel wall and circulate in peripheral blood. A specific marker for EPCs has yet to be identified; instead, they are generally defined by possessing a variety of cell surface markers including CD34, CD133, and VEGFR2, similar to those expressed by vascular endothelial cells (Yoder 2012).

EPCs can be separated into two types: early and late outgrowth EPCs, which can be isolated using different methods. The early outgrowth EPCs (Hur et al. 2004), also called colony forming units (CFUs), are isolated by plating peripheral blood mononuclear cells (MNCs) on fibronectin-coated dishes, removing non-adherent cells, and are recognized at day 5 to 7 as elongated sprouting cells within discrete colonies. The late outgrowth EPCs (Ingram et al. 2004), also known as endothelial colony forming cells (ECFCs), are isolated by seeding peripheral blood mononuclear

cells on collagen-coated plates, removing non-adherent cells, and culturing for a much longer time than CFU cells. ECFCs carry a cobblestone morphology, are highly proliferative compared to CFUs, and actively participate in neovascularization.

1.2.3 Induced pluripotent stem cell-derived endothelial cells

HiPSCs are a promising cell source for creating ECs owing to their capability of unlimited proliferation. HiPSCs technology, which reprograms adult cells into pluripotent stem cells, was first introduced in 2006 (Takahashi and Yamanaka 2006). Unlike human embryonic stem cells (hESCs), hiPSCs can be used for deriving large quantities of autologous ECs, making them a good choice for regenerative medicine (Choi et al. 2009). Many studies have explored the therapeutic potential of human induced pluripotent stem cell-derived endothelial cells (hiPSC-ECs) in ischemic disease. Induced by bone morphogenetic protein-4 (BMP-4) and vascular endothelial growth factor-A (VEGF-A), hiPSCs can be differentiated into ECs. By following slightly different protocols, ECs subtypes such as arterial hiPSC-ECs, venous hiPSC-ECs, and lymphatic hiPSC-ECs can be obtained (Rufaihah et al. 2013). Carrying endothelial phenotypes, the hiPSC-ECs are able to form a capillary-like network in 3D tissue-engineered constructs *in vitro* and increase capillary density and improve perfusion on *in vivo* animal models with a peripheral arterial disease (Rufaihah et al. 2011, Belair et al. 2015).

1.3 The need for microengineered tissues

Traditionally, researchers culture cells on a two-dimensional (2D) plastic or glass surfaces such as tissue culture flasks or well plates. However, in a real-world situation, cells inhabit an environment surrounded by other cells and extracellular matrix in three-dimensional (3D) space. Researchers realized that the gap between *in vivo* and *in vitro* condition may result in highly divergent cell function. Thus, many studies have been done in creating scaffolds that can support

3D cell culture and simultaneously mimic mechanical, structural, and compositional properties of native tissue.

1.3.1 Biomaterials supporting endothelial cells

A biomaterial is a substance that is engineered to interact with biological systems for directing therapeutic or diagnostic procedures. Many studies have been done in developing biomaterials that facilitate viability, attachment, and phenotypic maintenance of ECs. Among all the biomaterials, polymers have the mechanical, structural, and compositional properties that can be easily customized, making them a good option for tissue engineering (Chen, Liang, and Thouas 2013).

Nanofiber mesh consisting of different copolymers modified with ECM proteins are explored as potential materials for tissue engineered vascular graft (He et al. 2005, Ma et al. 2005). The presence of ECM proteins can enhance the attachment and spreading of ECs. Besides nanofiber mesh, polymers can also be fabricated into thin films as coating for vascular grafts. Polyelectrolyte multilayered thin films with customized surface properties are suitable for attachment and proliferation of ECs (Boura et al. 2003).

The research work mentioned above is mainly focused on developing biomaterials supporting ECs in 2D. However, the cellular environment is not a flat plastic or glass surface *in vivo*. Cell-cell and cell-extracellular matrix (ECM) interaction are not limited in a 2D plane. Instead, cells are surrounded by abundant ECM which provides structural and biochemical support in a 3D environment. To better understand the interaction between biomaterials and ECs for therapeutic and diagnostic purposes, it is important to assess cell behavior in a 3D environment.

Various types of biomaterials have been introduced for cell culture, aiming for the control of mechanical, structural, and compositional properties that can accurately represent features of native tissues, such as patterned glass substrates, elastomeric films, hydroxyapatite ceramics, and

fibrillary foams (Caliari and Burdick 2016). Among all the biomaterial systems, hydrogels are considered the most promising. Hydrogels are polymeric materials with a hydrophilic structure that can hold a large amount of water in the network. Compared to other biomaterials, hydrogels are capable of mimicking the mechanical properties of those soft native tissues and providing constructs for 3D cell culture. Their porous structure facilitates diffusion of oxygen and nutrients, which are essential for cell metabolism. Generally, hydrogels can be classified into two groups based on their natural or synthetic origins. Hydrogels with natural origins include proteins such as collagen and gelatin and polysaccharides such as alginate and hyaluronic acid. Synthetic hydrogels are formed through a chemical crosslinking reaction between polymer chains initiated with different mechanisms such as photo-initiation or thermal-initiation. Compared to natural hydrogels, synthetic hydrogels have the advantage of high reproducibility with limited batch to batch variation. Synthetic hydrogels can also be modified with natural components such as protein or peptides, extending their applications greatly. With the modification from natural components, hydrogels can provide the cells with binding sites and can be biodegraded later. They are able to protect the embedded cells and will not block the transportation of the nutrients because of the porous structure.

Poly(ethylene glycol) (PEG) is a synthetic polymer that has attracted a lot of research interest in tissue engineering due to its biocompatibility. PEG has very minimal protein adsorption due to its steric hindrance of negative charges (Lasic et al. 1991); thus, it can minimize thrombogenic or inflammatory responses. To form a hydrogel with crosslinked polymeric network, PEG is first acrylated into poly(ethylene glycol) diacrylate (PEGDA) with a carbon-carbon double bond on each side. The chemical structure of PEGDA is shown in Figure 1.1. By exposing the photo-initiator to light with a specific wavelength, the PEGDA hydrogel is formed after a rapid free

radical chain reaction. The light sources for activating the photo-initiator can be visible or ultraviolet light, and they are able to photocrosslink the hydrogel *in vitro* or *in vivo.* Compared to other approaches for crosslinking hydrogels, photocrosslinking is a relatively gentle procedure for the cells. The reaction happens in aqueous conditions without changing the temperature or pH. Therefore, the encapsulation of cells can be conducted simultaneously during the photocrosslinking process. Based on the advantages discussed above, PEGDA-based hydrogel was chosen as the biomaterial for the project.

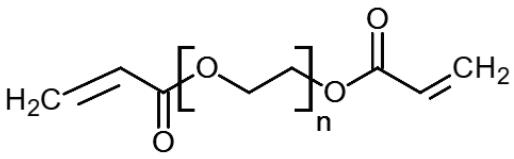

Figure 1.1 The chemical structure of PEGDA.

1.3.2 Fabrication techniques for forming 3D hydrogel scaffolds

Encapsulation of cells into 3D hydrogel scaffolds can provide the 3D environment for the cells. A number of techniques have been developed to fabricate hydrogel scaffolds with different geometric shapes. These techniques can be categorized into the following categories: molding, emulsification, microfluidics, and 3D printing.

Molding

Polydimethylsiloxane (PDMS) is a kind of polymeric organosilicon and is optically transparent, inert, non-toxic, and non-flammable. It is a viscous liquid that can be processed into any shape or size at the beginning and then crosslinked into a solid elastic state. Therefore, PDMS is an ideal choice as a mold for creating 3D cell culture scaffolds. For example, PDMS molds can work as reservoirs holding the hydrogel precursor solution with cells before conducting photo-

crosslinking on the hydrogel. 3D hydrogel scaffolds containing cancer cell lines can be used as cancer models for investigations of cancer biology or pre-clinical testing of anti-cancer drugs (Roudsari et al. 2016, Pradhan, Clary, et al. 2017). Also, encapsulation of human pluripotent stem cells can be used for differentiation and growth of engineered human heart tissues (Kerscher et al. 2016). Encapsulation of cells within PDMS molds is a straightforward method for preparing 3D cell culture scaffolds.

Emulsification

Though encapsulation of cells within PDMS mold is straight-forward, it has limited applications in creating spherical tissue constructs on a millimeter or micron scale. Thus, researchers developed a technique based on surface tension in a liquid-liquid dual-phase system. By adding a specific small amount of hydrogel precursor solution, which is the aqueous phase, into the oil phase, which is another immiscible phase, spherical hydrogel precursor droplet with a certain size can be formed within the oil. Exposed to light, the hydrogel can then be formed through a photo-crosslinking reaction. Millimeter-scale hydrogel beads containing cancer cells can be prepared as a 3D cell culture model, which closely mimics the native tumor microenvironment, and can be used as models for anti-cancer drug testing (Pradhan, Chaudhury, and Lipke 2014).

Microfluidics

Microfluidic systems are system processes with low volumes of fluids to achieve automated, high-throughput production. Compared to the two methods described above, microfluidic systems are capable of making highly uniform, micron-scale, spherical cell culturing scaffolds with high efficiency. The most common approach to preparing microfluidic systems is photolithography. A precleaned wafer is spin-coated with a thin layer of photoresist and then covered with an optical mask with a printed design of microfluidic channels. After exposure to ultra-violet (UV) light, the

photoresist will have a change in solubility, and thus can be rinsed away. Without the protection of photoresist, the oxide layer on the wafer can be etched with chemicals. After removal of leftover photoresist, the etched wafer can be used as a mold for preparing PDMS microfluidic devices. The development of microfluidic techniques significantly promotes the progress in tissue engineering. For example, Yu et al. used a droplet-based microfluidic system to encapsulate cancer cells within alginate microbeads and then trapped the cell-laden alginate beads in microsieve structure with continuous perfusion to investigate the response of the tumor spheroids to an anticancer drug (Yu, Chen, and Cheung 2010). Efforts are also made in optimizing the microfluidic system aiming for producing large quantities of highly uniform microgels with high post-encapsulation viability (Choi et al. 2016).

3D printing

As described above, most of the microfluidic systems are built with PDMS using soft photolithography, and numerous research fields have been benefited from the sophisticated-designed PDMS devices. However, the fabrication process is typically labor-intensive, and the 3D complexity of the devices is limited due to the layered design on the wafer. 3D printing, as a rapidly developing technique, has been used to make complex microfluidic systems due to its 3D spatial fabrication ability as well as increasing resolution (Lee et al. 2010, Kolesky et al. 2014). Besides printing the microfluidic system used for making 3D cell culture scaffolds, 3D printing is also capable of printing the scaffold directly. Compared to other approaches, a 3D printer is able to manipulate multiple materials simultaneously and build heterogeneous structures with encapsulated cells and micro-channels for better nutrient diffusion (Hong et al. 2015). In this way, the engineered in vitro tissue model can best mimic the real physiological environment, making

these molds promising choices for drug screening and other fundamental studies such as wound healing and angiogenesis.

By using the fabrication techniques mentioned above, hydrogels can be engineered into different geometric shapes, which are critical for their applications such as cell delivery, bioreactor-based cell production, high throughput screening, and 3D bioprinting (Seeto et al. 2017, Highley et al. 2019, Kropp, Massai, and Zweigerdt 2017, Brouzes et al. 2009). Different purpose can require a different geometric shape. For example, microspherical hydrogels are widely used for injectable cell delivery(Seeto et al. 2017, Zhao et al. 2016, Oliveira et al. 2015, Yao et al. 2013), and properly controlled sizes can improve cell retention while allowing for a smooth injection process. In a stirred tank or fluidized bed bioreactor system, hydrogels with different ARs will lead to different flow properties, which can be used to control the mixing and sedimentation process. Encapsulation of islets in fiber-shaped hydrogels were reported by An et al. to make delivered cells conveniently retrievable. Rapid production of hydrogels with a wide range of geometric shapes and physiologically relevant dimensions (10^{-1}-10^{3} μm) is important to meet the various needs for differing biomedical uses.

2. CHAPTER 2: Rapid Production of Cell-laden Microspheres Using a Flexible Microfluidic Encapsulation Platform

2.1 Introduction

Hydrogel microspheres are advantageous for use in a wide range of regenerative medicine applications (Lutolf and Hubbell 2005), including 3D cell culture (Workman et al. 2014), injectable cell delivery (Yao et al. 2012), disease modeling (Horning et al. 2008), cell differentiation (Shofuda et al. 2013), drug delivery (Dini, Alexandridou, and Kiparissides 2003), vaccine production (Tree et al. 2001), and cell production (Tashiro, Tsumoto, and Sano 2012). Depending on the application, cells can be either encapsulated within or seeded on the surface of the microspheres, in which case they are referred to as microcarriers.

Microspheres can be fabricated using extrusion, atomization, emulsion, and microfluidics. Among these methods, emulsion and microfluidics are used more widely because they do not require the specialized equipment necessary for the other methods (Leong and Wang 2015). Although emulsion allows for scalable production and has been used successfully for mammalian cell encapsulation (Franco, Price, and West 2011, Pradhan, Clary, et al. 2017), this method of microsphere production has some inherent challenges. The emulsion process can require the use of harsh chemical solvents, necessitating further processing steps to minimize the negative impact on downstream cell viability, and can be time-consuming depending on the crosslinking method (Yang, Chung, and Ng 2001, King and Patrick 2000). Incorporating cells directly is also challenging; the high levels of shear stress make consistent maintenance of high cell viability during the emulsion process difficult. In addition, microspheres produced from emulsion usually have a broad size distribution which can be problematic for downstream applications where tight size distribution is critical (Khademhosseini and Langer 2007). In contrast, microfluidic

approaches can precisely produce uniform microspheres with a very narrow size distribution (coefficient of variance, CV < 5 %) (Headen et al. 2014). However, due to constraints in channel dimensions imposed by the use of photolithography for microfluidic chip fabrication, resulting microspheres typically have a maximum diameter of around 200 μm (Velasco, Tumarkin, and Kumacheva 2012). Furthermore, pressure differences and changes in flow stability within these smaller channels make it more challenging to encapsulate cells at high densities or in cell clusters, which tend to clog the microfluidic channels and junctions (Headen et al. 2014). High cell density is critical for therapeutic cell delivery as we have shown in previous work, where millions of cells were used for large animal cell therapy (Seeto et al. 2017). To minimize the delivered volume and fabrication time while achieving the desired therapeutic dose, high cell densities are required. However, the small dimensions of microfluidic chips limit the total number of cells that can be encapsulated per time, failing to meet the needs for therapeutic cell delivery. Additionally, there are other restrictions on the applications of microspheres where larger size microspheres are desired, for example, modeling large tumors for induction of hypoxia and necrosis, providing shear-protection for bioreactor-based cell production, and improving retention of injected therapeutic cells. In addition to the limitation on channel size, the complex process of photolithography makes adjustment of the channel dimensions of microfluidic chip difficult. It requires a substantial investment of time and resources to produce a microfluidic chip with a different design during process optimization.

Having reported the use of hydrogel microspheres for large animal cell therapy (Seeto et al. 2017), here we present for the first time the design of the custom-built microfluidic platform that overcomes some of the challenges inherent to microfluidic cell encapsulation using standard microfluidic chips. The microfluidic device, which is the major component of the platform,

leverages the use of 3D printing for scalable mold production and a custom-developed molding technique that does not require expensive reagents and facilities for photolithography. With a custom-designed T-junction and readily adjustable assembling components, the platform enables rapid production of microspheres with a wide range of diameters from 300 μm to 1100 μm. This robust platform also has the potential to be used with a variety of natural and synthetic polymers; here we have demonstrated microspheres produced with PEGDA, poly(ethylene glycol)-fibrinogen (PF), and gelatin methacryloyl (GelMA) through rapid photocrosslinking. With the use of Eosin Y as the photoinitiator and a full spectrum light source, cells at high density (10-60 million cells mL^{-1} of hydrogel precursor solution, depending on application) were encapsulated including horse ECFCs, breast cancer cells, or human induced pluripotent stem cells (hiPSCs). The encapsulated cells were evenly distributed through the microspheres and maintained high viability and functional cellular activities. These results demonstrate the capabilities of this microfluidic encapsulation platform and show its potential for various regenerative medicine applications.

2.2 Experimental Section

2.2.1 Cell culture

Isolation and culture of horse ECFCs from horse peripheral blood were performed based on a method that was previously published (Salter et al. 2015). All procedures involving animals were approved by the Auburn University Animal Care and Use Committee. ECFCs were cultured in Endothelial Cell Basal Medium-2 (Lonza) containing 5 % horse serum (HyClone) and SingleQuots Kit (Lonza) at 37 °C and 5 % CO_2. The ECFCs were seeded and expanded on collagen-coated tissue culture polystyrene flask. When ECFCs reached 90 % confluency, trypsin/EDTA (Lonza) was added to detach the cells at 37 °C for 50 s and was neutralized by ECFCs medium followed by centrifugation at 200 g for 5 minutes. ECFCs were resuspended in medium and then

subcultured at a ratio of 1:6 or immediately used for experiment. Cells between passage 2-7 were used for all experiments.

MCF7 (ATCC®HTB-22™) and MDA-MB-231 (ATCC®HTB-26™) human breast cancer cells were maintained in Dulbecco's Modified Eagle's Medium (DMEM, Gibco) supplemented with 10 % fetal bovine serum (FBS, Atlanta Biologicals), 1 % (v/v) non-essential amino acids (Lonza), 1 % (v/v) penicillin/streptomycin, 1 % (v/v) Glutamax (Gibco), and 1 % (v/v) sodium pyruvate. Cells were expanded and dissociated with trypsin/EDTA when reaching 90 % confluency.

IMR-90 Clone 1 and 19-9-11 (WiCell) human induced pluripotent stem cells (hiPSCs) were cultured on human embryonic stem cell (hESC) qualified Matrigel (Corning) using mTeSR-1 medium (Stem Cell Technologies) and passaged using Versene (Invitrogen).

2.2.2 PEGDA synthesis

PEG (10 kDa; Sigma) was acrylated to form PEGDA following a method from a previously published literature (DeLong, Moon, and West 2005). Briefly, PEG was first lyophilized, and then reacted with 0.4 M acryloyl chloride (Alfa Aesar) and 0.2 M triethyl amine (TEA, Sigma) in anhydrous dichloromethane (Acros) under argon overnight. 1.5 M K_2CO_3 (Fisher) was then added, and the solution was separated into aqueous and organic phase. The organic phase was collected and dried with anhydrous $MgSO_4$ (Fisher). The PEGDA was then precipitated by cold ethyl ether, filtered, dried, and stored under argon at -20 °C. The degree of acrylation was estimated to be 96 % by nuclear magnetic resonance (NMR). PEGDA was dissolved in phosphate-buffered saline (PBS, Lonza) to 10 % (w/v) prior to use.

2.2.3 PEG-fibrinogen synthesis

PEG-fibrinogen (PF) was synthesized by following a previously published method (Almany and Seliktar 2005). In brief, fibrinogen (Type I-S; Sigma) was dissolved in 8 M urea (Sigma) in

PBS (Lonza) solution to a final concentration of 7 mg mL^{-1} with pH of 7.4. Then tris(2-carboxyethyl) phosphine (Acros Organics) was added to the solution and reacted at pH of 8. PEGDA was dissolved in urea-PBS to a final concentration of 280 mg mL^{-1} and then slowly added to fibrinogen solution to react for 3 hours in dark at room temperature. After reaction, PEGylated fibrinogen was precipitated with acetone, followed by centrifugation to remove acetone, and then dissolved in urea-PBS again for dialysis. The product was dialyzed in sterile PBS over 24 hours in dark at 4 °C, and then stored at -80 °C. Protein content was calculated to be 12.5 mg mL^{-1} using a Pierce BCA protein assay kit (Thermo Fisher). PEGylation efficiency ($\varepsilon_{PEGylation}$) was calculated to be 98 % using Equation 1 (Dikovsky, Bianco-Peled, and Seliktar 2006).

$$\varepsilon_{PEGylation} = \frac{[PEG]}{[Fibrinogen]} \times theoretical\{\frac{MW_{fibrinogen}}{29 \times MW_{PEG}}\}$$

$$= \frac{[PEG]}{[Fibrinogen]} \times \frac{166000}{29 \times 10000} \qquad (1)$$

2.2.4 GelMA synthesis

GelMA was synthesized following previous protocols (Nichol et al. 2010, Van Den Bulcke et al. 2000) with modifications. Briefly, gelatin (Type B, bovine) was mixed at 5 % (w/v) into phosphate buffered solution (PBS, Gibco) at 60 °C with constant stirring until fully dissolved. Methacrylic anhydride (MA) was slowly added until the target concentration was reached (15 % w/v) and reacted at 60 °C for 2 hours. The reaction was stopped with PBS; methacrylated gelatin was dialyzed for seven days and lyophilized for five days. Lyophilized GelMA was dissolved in deuterium oxide (Fisher Scientific) for NMR analysis. ^{1}H NMR spectra were collected using a Bruker 600 MHz NMR spectrometer. Before integration, phase and baseline corrections were applied to ensure accurate methacrylation calculations. GelMA was dissolved in PBS to 1.5 % (w/v) and kept at 37 °C prior to use.

2.2.5 3D printed bracket for scale up production of microfluidic device

A bracket was 3D printed to hold the mold for creating the junction and the channels for the microfluidic device. The bracket was designed in Blender 2.77 and printed using the LulzBot TAZ 5 with an acrylonitrile butadiene styrene (ABS) filament. The T-junction and the channels were molded with Teflon tubes and metal wires. To assemble the mold, two hollow Teflon tubes were inserted into the holes on the jig as shown in Figure 2.1 and Figure 2.2D. The top Teflon tube had a cylindrical end and the bottom one had a conical end for making the conical region at the junction. A metal wire was inserted into the hollow center of both Teflon tubes, and the uncovered part of the wire in between tubes could form a restriction segment. Another metal wire with tapered end was introduced through the third hole on the jig and inserted right below the conical end of the Teflon tube to make the outlet channel. The metal wires have different sizes and can be easily machined to obtain desired tapered end, providing flexibility in adjusting channel size and junction geometry. Multiple design parameters of assembled junction, including junction size, tapered end length, and outlet channel size were then checked under microscope to ensure consistency in device fabrication.

After the channels were assembled to achieve the desired junction design, the bracket was fixed on a glass using binder clips. Polydimethylsiloxane (PDMS) microfluidic device was created with Sylgard 184 silicone elastomer kit (Dow Corning) by pouring the mixture of base and cure component into the bracket, and air bubbles were removed by vacuum. Then the PDMS was cured at 70 °C for 2 hours. Once the PDMS was cured, the channel molds were removed and the PDMS was extracted from the bracket. The PDMS was cleaned by sonicating in 70 % ethanol before and after each use. The total cost of each microfluidic device was estimated to be $2.90, which included

the cost of all components of the channels ($0.80 per device), the jig ($0.16 per device), and PDMS (14 g, $1.94 per device).

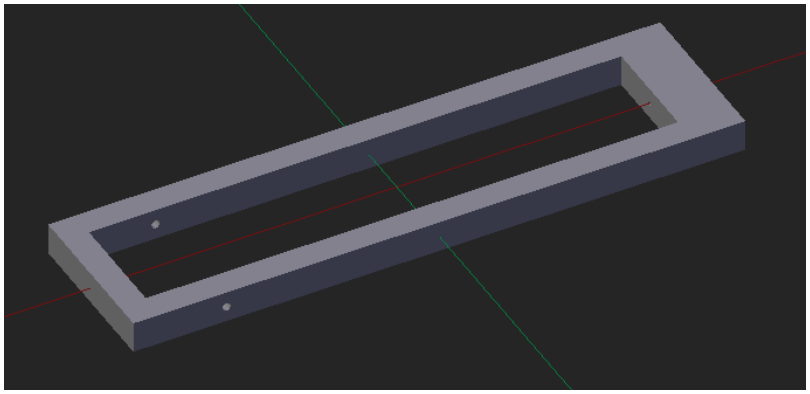

Figure 2.1 Design of a reusable channel mold-holding jig for 3D printing, which is essential for consistent and scalable production of microfluidic devices.

2.2.6 Cell encapsulation in hydrogel microspheres

Cell encapsulation in hydrogel microspheres was achieved through the novel microfluidic encapsulation platform. Before cell encapsulation, hydrogel precursor solution was prepared by mixing the polymer solution (PEGDA, PF, or GelMA) with 0.1 % (w/v) of Pluronic F68 (Sigma), 0.1 mM of Eosin Y photoinitiator (Fisher Scientific), 1.5 % (v/v) triethanolamine (Acros Organics), and 0.39 % (v/v) of N-vinylpyrrolidone (Sigma). Cells including equine ECFCs, MCF7 cells, MDA-MB-231 cells, IMR90 hiPSCs, and 19-9-11 hiPSCs were detached from tissue culture flask, centrifuged, and resuspended in crosslinking precursor solution to the desired, application-specific cell density of 10-60 million cells mL^{-1}.

Cells encapsulation and hydrogel photocrosslinking were conducted in a biosafety cabinet to keep the process sterile. The device had two inlets and one outlet where cells and hydrogel precursor mixtures were flowed from the top inlet, and mineral oil was flowed from the bottom inlet by using syringe pumps. When the two streams meet at the junction, microspheres were

formed due to emulsification and the cell-encapsulated microspheres were crosslinked by a 2.8 W cm^{-2} full spectrum visible light (Prior Lumen 200). A mirror was placed behind the microfluidic device near the outlet to aid the crosslinking by reflecting the light that passed through the device. The microspheres were washed down from the outlet with cell media by using a third syringe pump. The microspheres were then washed twice with media by centrifugation at 200 g for 3 minutes to remove the residual mineral oil and cultured in well plates at 37 °C and 5 % CO_2.

To prepare the microspheres shown in Figure 2.2G-J, the following experimental parameters were employed. The flow rates for mineral oil were 4, 10, 10, and 9 mL h^{-1}, respectively from G to J. The flow rates for hydrogel precursor solution were 0.8, 1, 0.5, and 1 mL h^{-1}, respectively. The flow rates for washing were 10 mL h^{-1} for all conditions. The junction diameters of microfluidic device were 240, 460, 520, and 460 μm, respectively. The outlet channel diameters of microfluidic device were 380, 960, 770, and 960 μm, respectively.

2.2.7 Microsphere geometry characterization:

The uniformity of the microspheres was evaluated by measuring their maximum diameter and roundness on one and three days after cell encapsulation. Three batches of microspheres with at least 30 microspheres per batch were measured and the measurements were performed using ImageJ. Roundness measured in ImageJ is defined by Equation 2.

$$Roundness = \frac{Area}{\pi \times Major\ axis^2} \qquad (2)$$

Uniformity was also analyzed by coefficient of variance (CV) which is defined by Equation 3.

$$Coefficient\ of\ variance = \frac{Standard\ deviation}{Mean} \quad (3)$$

2.2.8 Post-cell encapsulation cell viability assay

Cell viability after encapsulation was assessed by Live/Dead viability/cytotoxicity kit (Invitrogen). Cell-laden microspheres were incubated for 30 minutes with Calcein AM and

Ethidium homodimer-1, and then Z-stack-images were obtained with fluorescence microscopy (Nikon Eclipse Ti). Three regions with same size (250 × 250 μm) were randomly selected from each microsphere using ImageJ, and both live and dead cells were counted through the optical slices along the z-axis for approximately 550 μm.

2.2.9 Scanning electron microscopy

The ultrastructural features of the microspheres and the cell-laden microspheres were visualized through scanning electron microscopy (SEM). Microspheres were washed with PBS, fixed with 4 % glutaraldehyde (Electron Microscopy Sciences) for 1 hour and then fixed with 2 % osmium tetroxide (Electron Microscopy Sciences) for 1 hour, all at room temperature. The fixed microspheres were frozen in liquid nitrogen for 2 minutes and then dried in a freeze dryer (Labconco). Dried samples were mounted on carbon taped-aluminum stubs, sputter-coated with gold (Pelco SC-6 sputter coater) and imaged using scanning electron microscope (JEOL JSM-7000F).

2.2.10 Microsphere stiffness

In order to measure the Young's modulus of the hydrogel microspheres, they were subjected to compression testing under physiological conditions using MicroSquisher (CellScale). Briefly, cell-laden hydrogel microspheres were loaded onto the MicroSquisher platform maintained at 37 °C in PBS, preconditioned for compression testing and made to undergo cycles of compression and relaxation at a rate of 2.5 μm s^{-1} for a minimum of 15 % strain. The force-displacement data obtained from the stress were converted to stress-strain curves and the lower portion of the curve (5-15 % strain) was used to estimate the Young's moduli of microspheres.

2.2.11 Immunocytochemistry

Encapsulated horse ECFCs were evaluated for the expression of cell proliferation maker Ki67 with indirect immunofluorescence assay (IFA). Microspheres cryosection containing ECFCs were fixed with 4 % paraformaldehyde (PFA) solution and rinsed with PBS solution. ECFCs were then permeabilized with PBS-T containing 0.2 % Triton X 100 (Sigma) in PBS for 30 minutes and blocked with 3 % FBS at 4 °C overnight. The encapsulated cells were then incubated at room temperature for 2 hours with primary antibody solution which was rabbit anti-Ki67 (Abcam) at 1:100 dilution in 3 % FBS solution. After incubation, cells were washed with PBS-T before applying secondary antibody. Alexa Fluor 680-conjugated goat anti-rabbit IgG diluted at 1:200 in 3 % FBS solution was used as secondary antibody and incubated with cells at room temperature in dark for 2 hours. Cells were counterstained with DAPI, washed with PBS, mounted with ProLong Gold antifade reagent (Life technologies), and imaged with fluorescent microscopy.

2.2.12 Statistical analysis

All data were presented as mean ± standard deviation (SD). All statistical analysis was performed using Minitab 17 Statistical Software (Minitab Inc.). After verifying equal variances using F-test, Student's t-test was performed to evaluate statistical significance between two groups. After checking for normality of distribution, one-way analysis of variance (ANOVA) followed by the Tukey-Kramer honest significant difference (HSD) test was performed to evaluate statistical significance between multiple groups. Statistical significance was declared if $p<0.05$.

2.3 Results and Discussion

This study established a novel microfluidic encapsulation platform and developed a new method for microfluidic device fabrication to overcome the limitations imposed by photolithography. Deviating from traditional microfluidic chip fabrication, this study established

a novel molding technique for fabricating microfluidic devices. The resulting devices employ a custom-designed T-junction and continue to provide the important advantages of using microfluidic systems for production of hydrogel microspheres. This new molding technique supports designing microfluidic devices with a wider range of dimensions for various components, including junction geometry, channel width, and device length. The ease and flexibility provided by this technique enables quick fabrication of prototypes for ready testing and design iteration, which is beneficial for understanding the fluid dynamics of microsphere production. The established microfluidic encapsulation platform was shown to be compatible with multiple polymers and cell types, and was able to produce highly uniform microspheres with high cell densities and a wide range of diameters through rapid photocrosslinking. The encapsulated cells were evenly distributed through the microspheres and could maintain high viability and cellular activities in long-term culture post-encapsulation.

2.3.1 Microfluidic encapsulation platform using a novel custom design and device molding technique

A novel microfluidic encapsulation platform was developed in this study. As shown in Figure 2.2A-B, the microfluidic encapsulation platform is composed of three syringe pumps, a collection vessel, and the novel custom-designed polydimethylsiloxane (PDMS) microfluidic device. Aqueous polymer precursor solution, the discrete phase, flows into the device through the top inlet channel and the oil, the continuous phase, flows in through the bottom channel. The flow rate of the polymer precursor and oil can be independently adjusted using two syringe pumps, providing control over the polymer precursor/oil flow rate ratio. Microspheres are formed at the T-junction due to emulsification and then photocrosslinked in the outlet channel of the microfluidic device,

using a wide spectrum visible light source with a liquid light guide. At the end of the outlet, the microsphere hydrogels are washed down with and collected in media, controlled by a syringe pump.

This encapsulation platform uses a high power visible light source to perform rapid photocrosslinking, which leads to a much higher production rate. Compared to other microfluidic platforms, microspheres here have a much shorter residence time passing through the light beam. It takes approximately 1 s for photocrosslinking, whereas other platforms take up to 20 s or longer per microsphere (Jiang et al. 2017, Zhao et al. 2016). As previously reported, using this platform 4 million cells were encapsulated in 400 μL of PF precursor solution in 24 minutes, resulting in approximately 1500 cell-laden microspheres with diameters of 800 μm (Seeto et al. 2017). A range of power output (0.5 W- >3 W, 10 %-100 %) of the light source has been tested. In order to achieve rapid photocrosslinking, a minimum of 2.8 W cm^{-2} light was necessary to form microspheres with stable boundaries and structural integrity, and a mirror was placed behind the device to reflect the light for higher crosslinking efficiency. Power output can be increased for photocrosslinking without affecting the microsphere size and geometry. In addition to the light source power output, many other platform parameters were established through extensive iterative testing. For example, the distance of the light source from the outlet channel was optimized to support rapid photocrosslinking while keeping heat generation low enough to maintain high cell viability. Further improvements could be achieved by the use of an LED light source.

As the major component of the platform, the microfluidic devices are fabricated using a new molding technique that is more flexible than the standard microfabrication techniques. When using standard photolithography microfabrication techniques, the maximum diameter of fabricated microspheres is generally determined by the height of microfluidic channels, which is usually around 200 μm (Velasco, Tumarkin, and Kumacheva 2012). This limitation is a result of the

channel height being dictated by the maximum thickness of photoresist that can be cast onto a wafer and depends on the series and choice of the photoresist. As a result, traditional microfluidic device fabrication is not suitable when microspheres with larger diameters are desired. This study overcomes the size limitation by employing a molding technique and designing a suitable T-junction in the fabrication of the microfluidic device.

The design of the microfluidic device channels is assembled with easily acquired components as shown in Figure 2.2D. Numerous iterations were able to be performed in the design of the reported device due to the ease of fabrication using the molding technique. In order to hold the assembly of the channels together and control the dimension of the microfluidic device, a reusable channel mold-holding jig was designed (Figure 2.1) and 3D printed (Figure 2.2C) with acrylonitrile butadiene styrene (ABS) filament (The 3D printable file of the jig is available upon request). The 3D printed jig is essential for consistent and scalable production of microfluidic devices. In addition, the cost of all components is relatively low (Figure 2.2D, detailed cost listed in Experimental Section). After the PDMS is cured, the molds of the channels can be easily removed (Figure 2.2E). Producing a microfluidic device with new channel dimensions takes approximately 1 hour, which allows for quick testing during prototype development. Although this molding fabrication approach may not provide the high level of consistency needed to commercially manufacture numerous identical microfluidic devices, it eliminates the need to use photolithography, making it advantageous for research groups wanting to do rapid, iterative design testing or for those who do not have ready access to expensive microfabrication facilities.

Based on iterative testing, the final design of the microfluidic device is shown in Figure 2.2F. The T-junction and the channels are molded with Teflon tubes and metal wires, providing channels with a circular cross-sectional area instead of the rectangular cross-sectional area produced using

photolithography. In typical T-junction designs, the two inlet channels are perpendicular to each other, with the discrete phase entering the continuous phase channel at an angle and then progressing linearly to the outlet (Baah and Floyd-Smith 2014, Xu et al. 2008). Here, however, the discrete and continuous phase inlet channels are collinear with each other and the joint outlet channel is perpendicular to both inlets. When the microfluidic device is placed vertically, the collinear inlet channels can maximally exploit the density difference between two fluids to assist droplet formation, which will be discussed in the following paragraph. This unique design leverages the simplicity of the T-junction design while providing additional control over microsphere size and operational stability, typically only achieved using much more complex flow focusing microfluidic designs. In particular, manipulation of the inlet flow ratio enables control over microsphere size. This T-junction design has not to our knowledge been used before for microsphere fabrication. The top inlet channel was designed to contain a restriction segment as indicated by an asterisk. This was implemented to stabilize the precursor/oil interface prior to entering the outlet channel; without this restriction segment some of the denser precursor tends to escape from the aqueous flow into the oil phase and form unwanted droplets that sink to the bottom inlet in the vertically oriented device. Beneath the restriction segment is a conical region instead of a cylindrical region, which was introduced to eliminate the dead volume of hydrogel precursor solution. The metal wire has a tapered end that can be inserted into the Teflon tube forming the T-junction. The tapered end slightly increases the flow speed at the T-junction to aid in microsphere formation. This approach is commonly used in microfluidic flow focusing techniques (Kim et al. 2007, Anna, Bontoux, and Stone 2003) but not in standard T-junctions, where only the discrete stream (aqueous/polymer precursor) is entering the continuous stream at an angle, versus our modified T-junction design where both the continuous and discrete streams are perpendicular to

the outlet channel. The metal wires have different sizes and can be easily machined to obtain desired tapered end, providing flexibility in adjusting channel size and junction geometry. Since rapid photocrosslinking requires a high-power light source, the outlet channel length in this design was increased to achieve an optimal distance between the T-junction and the light source to minimize the influence of light back scattering. Previously, multiple methods were reported to prevent scattered light from reaching the junction, including embedding opaque materials in the device and reducing light power which resulted in extended crosslinking time (Wang et al. 2018). External shielding methods combined with opaque material embedding were tested in earlier iterations of the reported platform. However, it was determined that light was traveling down the interior of the outlet channel itself. As readily facilitated by the employed molding technique, the device length was extended to 10 cm, which provided the distance between the light source and the T-junction needed to eliminate this issue.

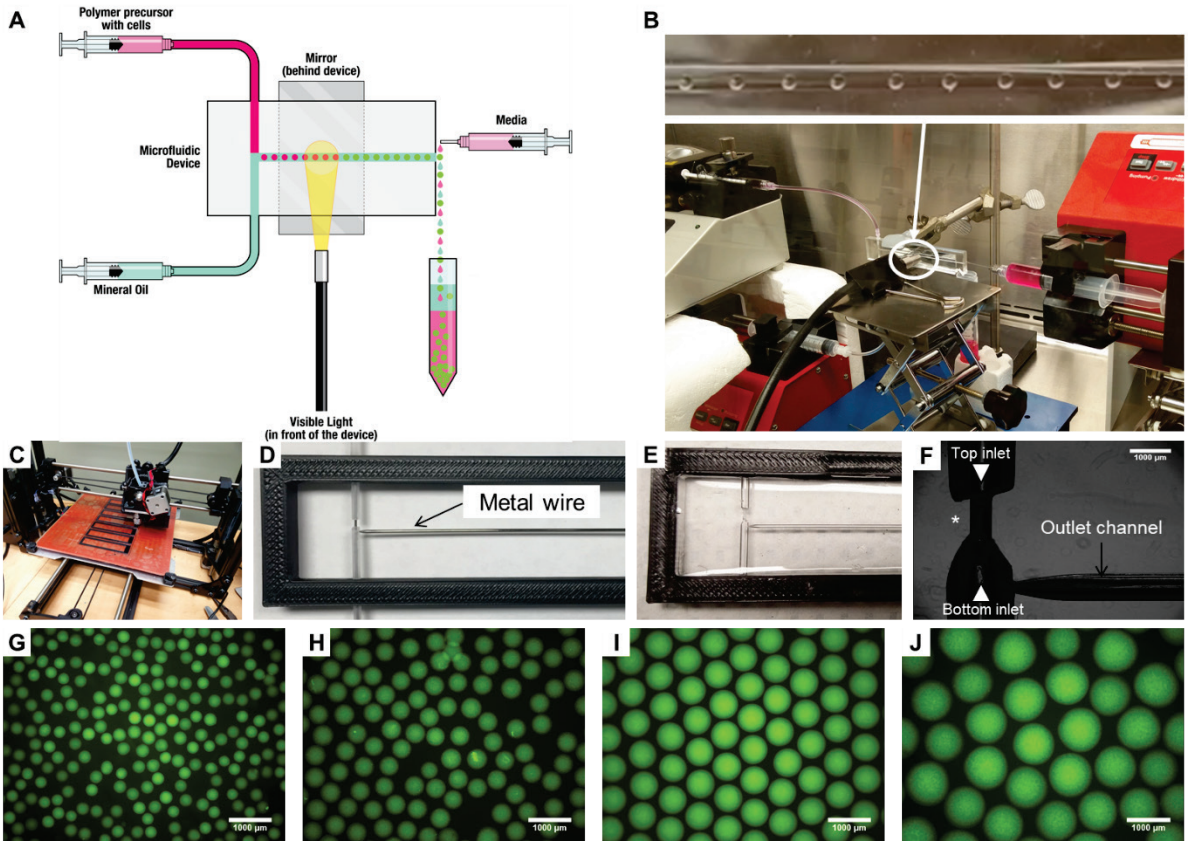

Figure 2.2 Microfluidic encapsulation platform using a novel custom design and device molding technique enables production of uniform hydrogel microspheres with a wide range of diameters. A) Schematic of the microfluidic encapsulation platform. B) Setup of the microfluidic encapsulation platform in a biosafety cabinet. C) 3D printing of the jig. The jig helps with consistent, low-cost, and scalable production of microfluidic devices. Design of the jig is shown in Figure 2.1. D) The printed reusable jig holds the assembly of the channels together. The T-junction and the channels are molded with Teflon tubes and metal wires, enabling quick fabrication of prototypes for ready testing and design iteration, which is beneficial for understanding the fluid dynamics during microsphere production. E) PDMS microfluidic device after curing and channel mold removal. F) T-junction of the microfluidic device with precursor inlet on top and mineral oil inlet from bottom. The restriction segment for stabilization of the precursor/oil interface is indicated by an asterisk. (G-J) Hydrogel microspheres with a wide range of diameters (from 300

μm to 1100 μm) can be produced using the microfluidic encapsulation platform. The diameters of microspheres shown in the figures are 312 ± 13, 473 ± 15, 723 ± 7, and 1008 ± 47 μm respectively (n>20 microspheres per condition, experimental parameters are included in the Experimental Section). The hydrogel microspheres are shown in fluorescent green due to the Eosin Y used during photocrosslinking.

The microfluidic device orientation within this platform is also a critical design parameter. In contrast to typical microfluidic device operation, the one in this study is orientated vertically instead of lying flat horizontally (Clausell-Tormos et al. 2008). Since the channel sizes are much larger than in traditional microfluidic chips, gravity is an important factor in successful device operation and needs to be considered. According to our preliminary studies during platform development, the vertical orientation allows the less dense oil, which is flowing in from the bottom inlet, to separate the denser hydrogel precursor/cell-precursor suspension, which is flowing in from the top inlet, in a more stable manner. Combining all the new design features mentioned above, the resulting microfluidic encapsulation system is able to rapidly produce uniform microspheres with a wide range of diameters from 300 μm to 1100 μm (Figure 2.2G-J) that can be used for numerous applications, including injectable cell delivery, bioreactor-based cell expansion and differentiation, and tissue sphere-based drug testing assays.

In addition to the design of the microfluidic device itself, the collection wash fluid that flows over the outlet port at the end of the device is also critical to flow stabilization. Exiting microspheres are washed down from the end of the outlet channel into the collection tube resulting in them being immediately immersed in cell culture media. Without this wash stream, accumulation of microspheres at the outlet introduces unstable flow within the upstream channels which results in wide distribution of microsphere diameter and geometry. This is a novel approach

that to our knowledge has not been employed in other systems. Furthermore, such stable system flow enables the formation of a range of microsphere diameters within a range of flow rates by using a single microfluidic device design. More details will be discussed in a later section. Taken together with the novel custom-designed microfluidic device made by molding, this encapsulation platform can overcome the limitations of traditional microfluidic chip-based production and produce uniform microspheres with a wide range of diameters.

2.3.2 Established microfluidic encapsulation platform is compatible with multiple photocrosslinkable polymers

Using the established microfluidic encapsulation platform, microspheres have been produced using multiple photocrosslinkable polymers that have been widely employed for various tissue engineering applications (Nguyen and West 2002, Seliktar 2012). Here, we examined the photocrosslinkable hydrogel materials PF, GelMA, and PEGDA; these materials have been used for cancer tissue engineering (Pradhan, Hassani, et al. 2017), cardiac tissue engineering (Kerscher et al. 2017, Shin et al. 2016), and bone regeneration (Sonnet et al. 2013). These polymers were selected to demonstrate the compatibility of this setup with various polymers. The presence of the acrylate groups allows crosslinking and formation of hydrogels through free-radical chemistry (Odian 2004). The photoinitiator in polymer precursor solution triggers the photocrosslinking reaction once exposed to light. Acellular microspheres were fabricated with each of these polymers; scanning electron microscopy (SEM) images of the microspheres showed the typical porous structure present in these hydrogel scaffolds (Figure 2.3A-D) (Annabi et al. 2010). Using the same parameters for microsphere production, elastic moduli of microspheres formed using the three different polymers were evaluated by a compression testing (Figure 2.3E and F). All microspheres were observed to regain their initial geometries following compression. Elastic

moduli of PF, GelMA, and PEGDA were found to be 127.3 ± 24.4 Pa, 1894 ± 257 Pa, and 31,800 ± 5,280 Pa respectively (Figure 2.3G). Collectively, these results demonstrate that this microfluidic encapsulation platform has the capability to be used for producing microspheres with various polymer systems.

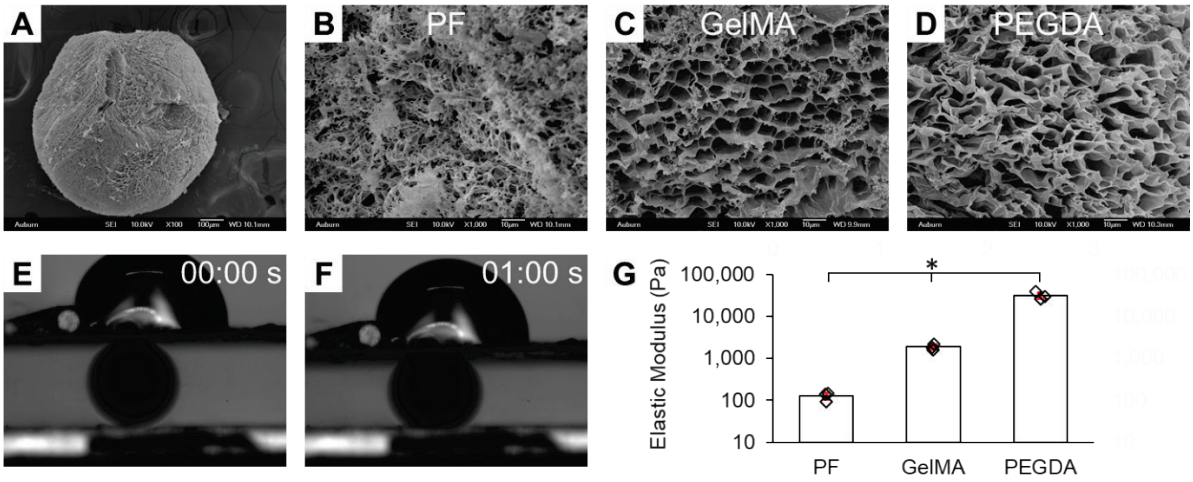

Figure 2.3 Microspheres were able to be formed using a range of photocrosslinkable hydrogel materials. Porous structure of the hydrogel scaffolds shown by SEM of (A) GelMA microspheres (100x), (B) PF microspheres (1000x), (C) GelMA microspheres (1000x), and (D) PEGDA microspheres (1000x). (E-F) Compression testing was used to assess elastic moduli of the microspheres. G) Elastic moduli of PF, GelMA, and PEGDA were found to be 127.3 ± 24.4 Pa, 1894 ± 257 Pa, and 31,800 ± 5,280 Pa respectively (n=3 separate measurements for each material). Elastic moduli were found to be significantly different between different materials (*$p<0.05$).

2.3.3 Straightforward control of microsphere diameters by varying inlet flowrates and outlet channel diameter.

In addition to fabricating microspheres with various materials, this microfluidic device also provides tight control over microsphere diameter. Based on extensive testing during platform development using multiple microfluidic device designs, the ratio of precursor to oil flow rate and

outlet channel diameter were found to be the critical parameters in controlling microsphere diameter. For example, by changing the precursor: oil flow rate ratio from 1:10 to 2:9 in a microfluidic device with 750 μm outlet channel diameter, the microsphere diameter increased from 746 ± 46 μm to 788 ± 40 μm (Figure 2.4A). Similarly, microspheres increased in diameter from 811 ± 22 μm to 951 ± 25 μm when changing the precursor: oil flow rate ratio from 1:10 to 2:9 in the microfluidic device with 920 μm outlet channel diameter (Figure 2.4A). These results demonstrate the diameters of microspheres can be changed by varying just the precursor: oil flow rate ratio without changing the outlet channel diameter. Conversely, when holding the flow rate ratio constant, the resulting microspheres were bigger in size as the outlet channel diameter was increased (Figure 2.4A). Roundness was found to be above 0.95 for all microspheres (Figure 2.4B). Representative images are shown in Figure 2.4C-F.

In flow focusing and co-flow microfluidic chips, varying the inlet flow rate ratio is a common approach to adjust the size of the microspheres, and both experimental (Xu et al. 2006) and computational (Dupin, Halliday, and Care 2006) studies have been done. Channel diameter is the limiting factor in determining the maximum size of produced microspheres. Because of the constraints imposed by photolithography, traditional microfluidic chip fabrication is time-consuming and has an upper limit of 200 μm for channel diameter (McDonald et al. 2000). By employing the molding technique used here in microfluidic device fabrication, the outlet channel diameter can be altered simply by selecting a different wire size for molding. The metal wire used in molding the outlet channel is commercially available in a wide range of diameters (250 μm – 25 mm). This is highly advantageous for maximizing the microsphere diameter options available for specific applications, providing much greater flexibility than microfabrication. Together these

results show that microsphere diameter can be readily controlled by adjusting inlet flowrates and altering outlet channel diameter.

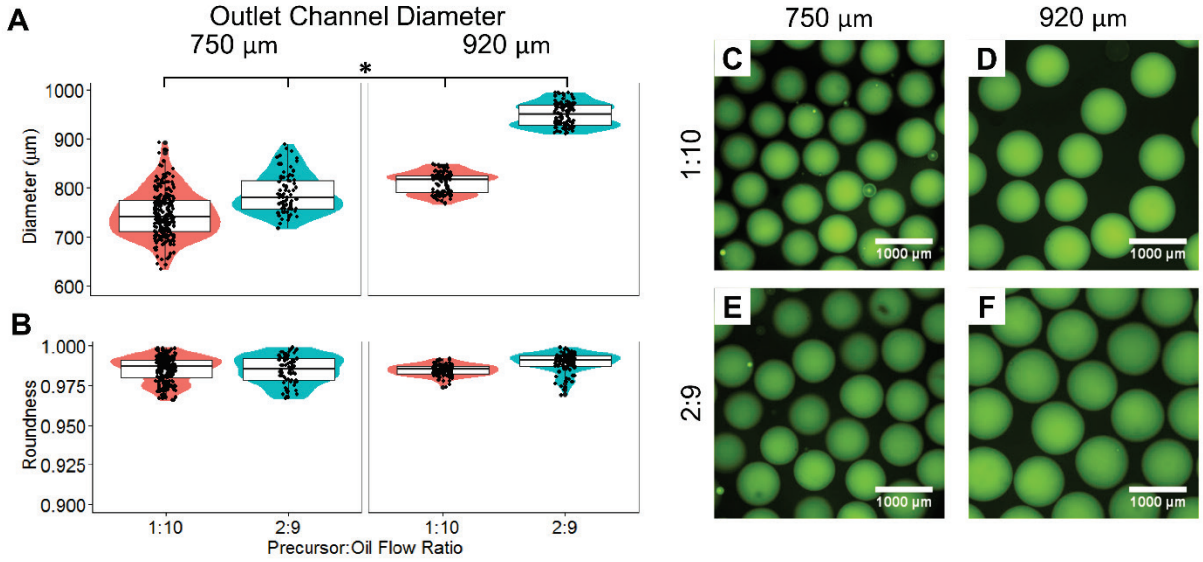

Figure 2.4 Microfluidic device provides tight control over microsphere diameter. A) Hydrogel precursor to oil flow rate ratio and outlet channel diameter are critical in determining microsphere diameter. By changing the flow ratio or the outlet channel diameter, the size of microspheres can be adjusted. Diameters were found to be significantly different between all pairs (*$p<0.05$, $n>78$ microspheres per condition). B) Roundness (above 0.95) was maintained under all conditions. (C-F) The change of microspheres in size under different experimental conditions shown by fluorescent images.

2.3.4 Highly uniform microspheres produced within and between batches

Tight control over the size and shape of microspheres is critical for various applications, such as high-throughput drug screening (Brouzes et al. 2009), cell production (Kropp, Massai, and Zweigerdt 2017), bioprinting using microspheres as building blocks (Mironov et al. 2009), and cell delivery (Seeto et al. 2017). For regenerative medicine, high uniformity of microspheres prepared from multiple batches is needed to ensure smooth and consistent cell delivery by injection.

For high-throughput drug screening, tight control over size and shape of microspheres enables a better comparison of drug effects and reduces the number of required replicates. The microfluidic encapsulation platform presented in this study provides high uniformity of produced microspheres both between and within batches. As shown in Figure 2.5A-C, horse ECFCs were encapsulated within PF hydrogel microspheres at the high cell densities required for therapeutic cell delivery; these ECFC-laden microspheres, which are shown in fluorescent green, were highly consistent. Five separately prepared batches of ECFCs-laden microspheres were analyzed quantitatively for intra- and inter-batch comparison (Figure 2.5D); average microsphere diameter ranged from 740 μm to 793 μm between batches with low variance (CV < 2 %) within each batch. For each of the five batches, average roundness was above 0.980 with a standard deviation of 0.01 between microspheres.

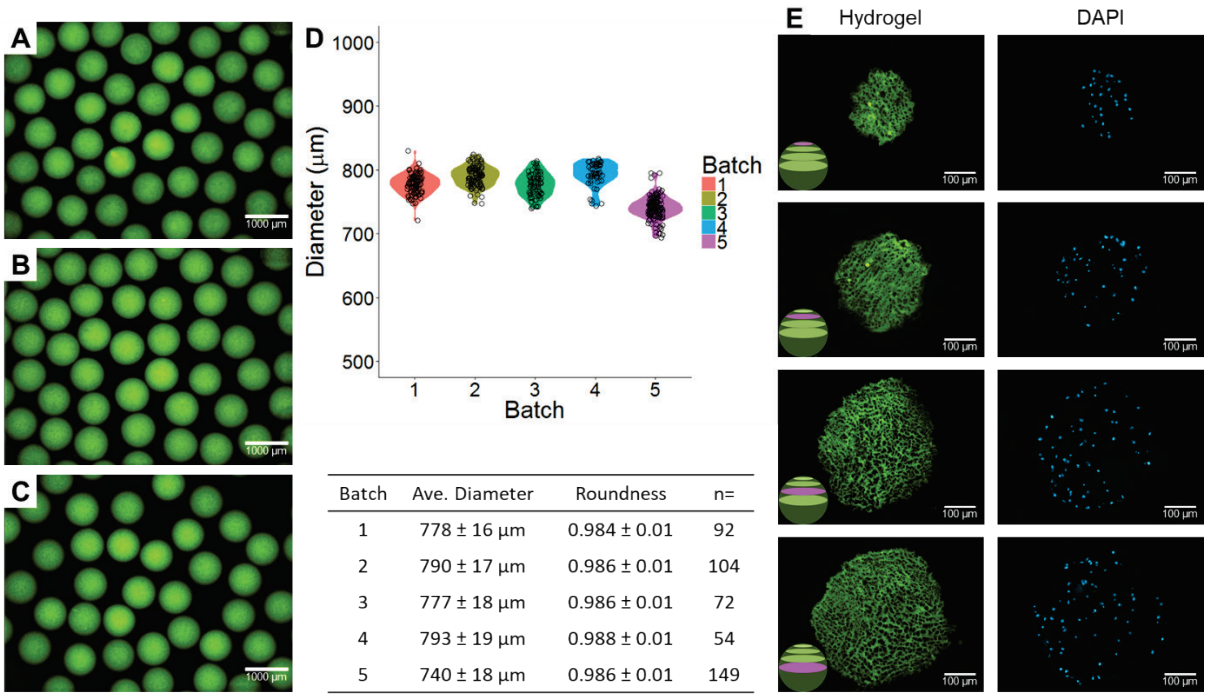

Batch	Ave. Diameter	Roundness	n=
1	778 ± 16 µm	0.984 ± 0.01	92
2	790 ± 17 µm	0.986 ± 0.01	104
3	777 ± 18 µm	0.986 ± 0.01	72
4	793 ± 19 µm	0.988 ± 0.01	54
5	740 ± 18 µm	0.986 ± 0.01	149

Figure 2.5 Microfluidic encapsulation platform enables high uniformity of microspheres both between and within batches. (A-C) PF microspheres with encapsulated horse ECFCs from 3 separate batches. D) Tight control of microsphere size and shape was achieved by the microfluidic encapsulation platform within and between batches (n>54 microspheres per batch). Microsphere average diameter ranged from 740 µm to 793 µm between batches with low variance within each batch. The roundness was above 0.980 with the standard deviation of 0.01 for all batches. E) Cell distribution throughout the microsphere post-encapsulation shown by cryosections of ECFC microspheres. Hydrogel structure visualized in green (Eosin Y), nuclei in blue (DAPI). Inset schematic shows slice location based on measured diameter (Pink).

Moreover, cell distribution within the microspheres was also assessed. Horse ECFC microspheres were cryosectioned after encapsulation. Cells were found to be distributed evenly throughout the microsphere volume as shown in Figure 2.5E. Collectively, these results show that

the microspheres produced by this microfluidic encapsulation platform have highly uniform size, shape, and inner cell distribution.

2.3.5 Established microfluidic platform enables encapsulation with high cell density

Encapsulation of cells at high densities and/or in clusters, rather than as single cells, creates substantial additional technical challenges, particularly in maintaining microsphere uniformity. Most studies on microfluidic encapsulation have reported producing microspheres with low cell densities (Choi et al. 2007, Koster et al. 2008), and very few studies have been conducted using higher cell densities (1-10 million cells mL^{-1}) (Kumachev et al. 2011). This limitation is due to the junction becoming clogged and/or changes in the precursor viscosity. However, producing microspheres with a high cell density is critical for many downstream applications, including delivery of sufficient numbers of cells to achieve therapeutic benefit without exceeding limitations on injection volume.

Encapsulation at high cell density for both single cells and cell clusters was tested. Following the design modifications described above for enhanced operational stability, the microfluidic device operated robustly under these challenging conditions. Single cells including horse ECFCs and MCF7 cells, and clusters of hiPSC were encapsulated at 10 million cells mL^{-1}, 20 million cells mL^{-1}, and 25 million cells mL^{-1}, respectively (Table 2.1). The hiPSC clusters did not clog the junction. Resulting microspheres were uniform in size and shape for all encapsulation densities and had similar diameters post-encapsulation as shown in Figure 2.6A-C. Diameters of hiPSC, horse ECFC, and MCF7 microspheres were 878 ± 29 μm, 957 ± 31 μm, and 939 ± 26 μm (n>20 microspheres for each cell type), which all show low standard deviation. High degree of roundness (above 0.95) was maintained for all cell types (Figure 2.6D). Furthermore, MCF7 cells at 60 million cells mL^{-1} could be encapsulated without clogging the microfluidic device and the resulting

microspheres were highly uniform with diameters of 979 ± 13 μm and roundness of 0.98 ± 0.01 (Table 2.1).

Table 2.1 Cells encapsulated with high densities.

Cell Type	Initial Cell Concentration Used [x 10^6 cells mL^{-1}]	Diameter (μm) (CV)	Roundness (CV)	Potential Applications
ECFC	10	957 ± 31 (0.03)	0.98 ± 0.01 (0.01)	Cell delivery
hiPSC	25	878 ± 29 (0.03)	0.98 ± 0.01 (0.01)	Stem cell differentiation
Breast cancer (MCF7)	20	939 ± 26 (0.03)	0.98 ± 0.01 (0.01)	Cancer tissue model
Breast cancer (MCF7)	60	979 ± 13 (0.01)	0.98 ± 0.01 (0.01)	Cancer tissue model

Cell viability was evaluated post-encapsulation in all design iterations to assess the effect of device-associated shear stress and light exposure on the cells during encapsulation with this platform. Horse ECFCs, MCF7 cells, and MDA-MB-231 cells were found to have a high post-encapsulation viability of 97 ± 1 %, 98 ± 1 %, and 97 ± 1 %, respectively. Microsphere encapsulated hiPSC clusters were also found to have high viability (Figure 2.6E). Accurate quantification without further processing to dissociate the cell clusters, which inherently reduces viability, was not possible. Results indicate that the microfluidic platform enables encapsulation at high cell densities while maintaining high cell viability. These results advance the ability to achieve commercial applications of cell-laden microspheres, such as therapeutic cell delivery, stem cell differentiation, and cancer tissue modeling.

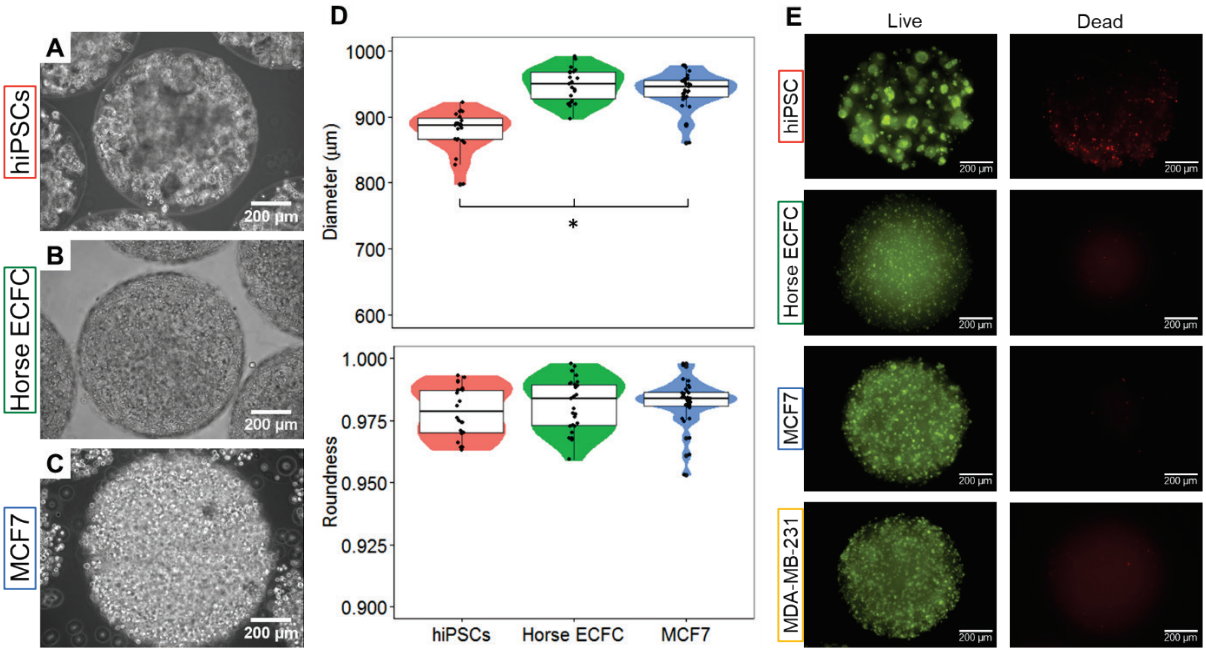

Figure 2.6 Uniform microspheres with high cell densities can be fabricated for a range of cell types using the microfluidic encapsulation platform. Phase contrast images of (A) hiPSCs (25 million cells mL^{-1}) (B) horse ECFCs (10 million cells mL^{-1}), and (C) MCF7 breast cancer cells (20 million cells mL^{-1}) encapsulated in PF microspheres. Encapsulation of single cells (ECFCs, MCF7 cells) and cell clusters (hiPSCs) was readily achievable; Figure 2.7A-B shows batch-to-batch comparisons for each cell type. D) Diameters of hiPSCs, horse ECFC, and MCF7 microspheres are 878 ± 29 µm, 957 ± 31 µm, and 939 ± 26 µm (n>20 microspheres for each cell type). Microsphere diameter was found to differ significantly between cell types (*$p<0.05$), possibly as a result of differences in cell size, cell encapsulation density, and pre-encapsulation cell dissociation method (clusters versus single cells). High degree of roundness (above 0.95) was maintained for all cell types. E) All tested cell types maintained high viability post encapsulation within PF microspheres (Live Green: Calcein AM, Dead Red: Ethidium homodimer).

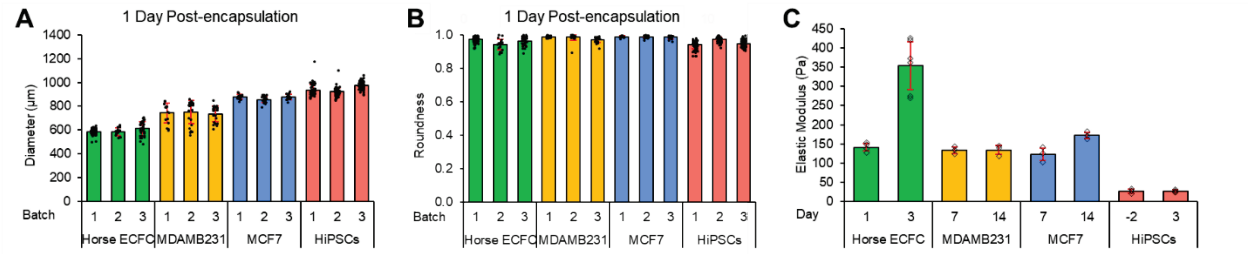

Figure 2.7 Characterization of cell-laden PF hydrogel microspheres. (A-B) Cell-laden PF hydrogel microspheres with different cell types are uniform in size and shape within and between batches. C) Evaluation of elastic modulus of different cell-laden PF hydrogel microspheres at different time points.

2.3.6 Cells maintain normal cellular activities post encapsulation

Following encapsulation in the microfluidic platform, understanding the potential impact of this process on subsequent cellular function is important for downstream applications. Cells were found to maintain normal cellular activities after being encapsulated, including the ability to proliferate within the microspheres and to remodel the microsphere structure. As a proof-of-concept, horse ECFCs were encapsulated in PF hydrogel microspheres and their cellular activities were assessed, including cell outgrowth, alteration of microsphere stiffness and morphology, and cell proliferation marker expression. When culturing the ECFC-laden microspheres in collagen-coated well plates, ECFCs had round morphology upon encapsulation. Then the cells were seen to elongate and align along the edges of the hydrogel microspheres one day after encapsulation (Figure 2.8A). Generally, changes in cell morphology can be caused by external force exerted on cells from different sources, such as magnetic forces (Zhang, Le, et al. 2019), shear stress (Jadhav, Eggleton, and Konstantopoulos 2005), or interaction between cell adhesion molecules and their ligands (Zhang, Rejeeth, et al. 2019). Here, ECFC morphology changed through cellular binding to cell-adhesion sites provided by the fibrinogen in the PF hydrogel as shown in Figure 2.9A.

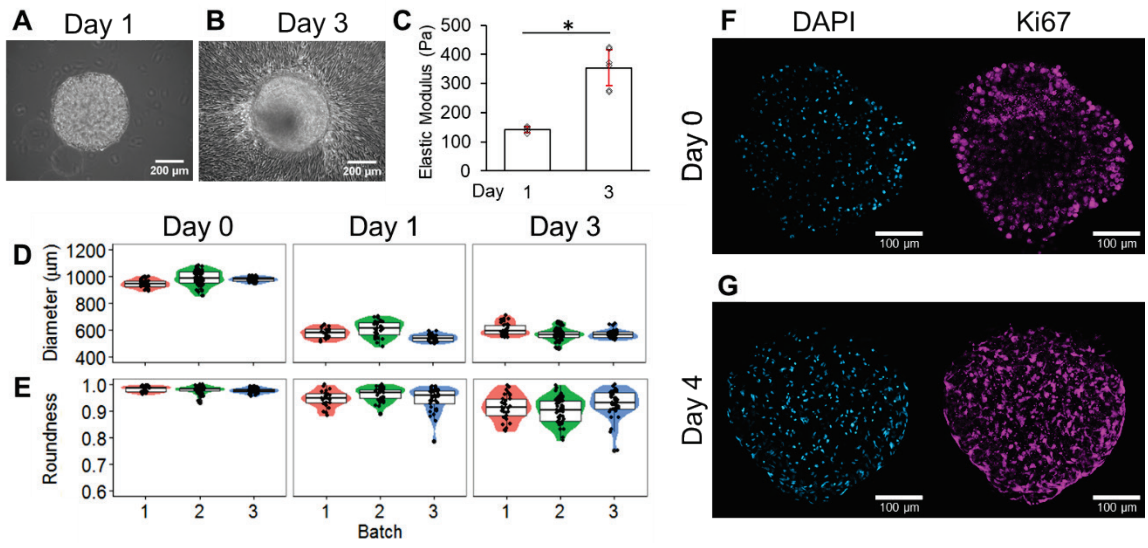

Figure 2.8 ECFCs maintained their highly proliferative phenotype post-encapsulation in PF microspheres. (A-B) Outgrowth of ECFCs from microspheres indicating high proliferative capability was maintained post encapsulation. C) The elastic modulus of microspheres with horse ECFCs have significantly increased from 142 ± 10 Pa on day 1 to 354 ± 62 Pa on day 3 (*$p<0.05$, $n>4$ microspheres per condition). Changes in elastic modulus were also measured for microspheres with cancer cells and hiPSCs (results shown in Figure 2.7C). (D-E) ECFCs remodeled the microsphere size and shape during culture. Similar cellular activities were observed over time on multiple batches of ECFC-laden microspheres cultured over a month (shown in Figure 2.9B). (F-G) Encapsulated ECFCs remained proliferative within the microspheres as shown by the expression of cell proliferation marker Ki67 (Blue: DAPI, Magenta: Ki67).

On day 3, cell outgrowth from the microsphere was observed, and these cells formed a confluent layer (Figure 2.8B). The elastic modulus of the ECFC-laden microspheres was measured and found to increase significantly from day 1 to day 3 (Figure 2.8C), indicating the encapsulated cells were actively remodeling the microspheres. In-depth analysis for all cell types, although beyond the scope of this study, is ongoing for horse ECFCs (Seeto et al. 2017), breast cancer cells,

and hiPSCs. Cellular activity of encapsulated cells was found to differ between cell types, as expected based on the phenotypic differences. For example, rate of remodeling and changes in elastic modulus have been observed to be cell type dependent (results shown in Figure 2.7C). Additionally, size and shape of the ECFC-laden microspheres from 3 batches were quantified on day 0, 1, and 3 (Figure 2.8D-E). Both the diameter and roundness of the microspheres decreased along with time as a result of cellular activities of the encapsulated cells. Encapsulation did not substantially impact cell proliferation; the vast majority of ECFCs continued to show positive Ki67 expression on both day 0 and day 4 post-encapsulation as shown in Figure 2.8F-G. Multiple batches of ECFC microspheres were maintained in culture for over one month; similar cellular growth and PF microsphere remodeling was observed over time as shown in Figure 2.9B. Taken together, these results provide initial evidence that the cells maintain viability and basic cellular activities following encapsulation using the microfluidic platform and justify further in-depth application-specific studies.

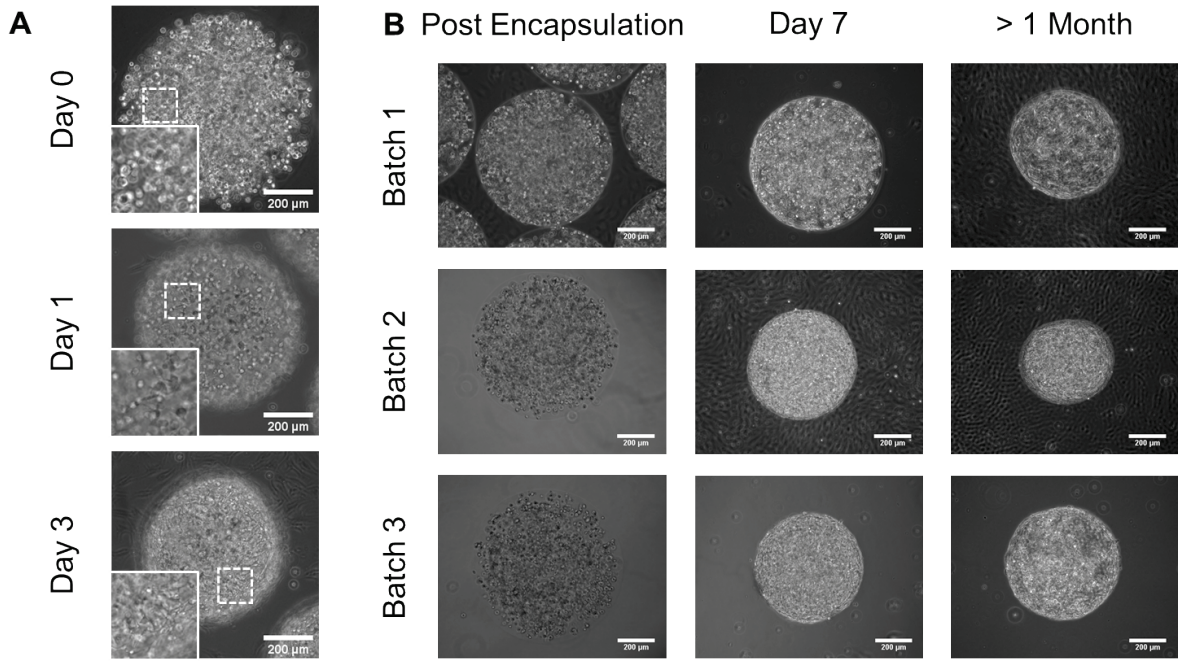

Figure 2.9 A) Morphology of encapsulated ECFCs changed along with time. B) Horse ECFC microspheres from 3 batches over time frame.

2.3.7 Resulting microspheres enable long term cell culture

Encapsulated cells can be cultured long-term within the microspheres. To demonstrate this, MCF7 breast cancer cells and MDA-MB-231 breast cancer cells were separately encapsulated in PF hydrogel microspheres (20 million cells mL^{-1}) and cultured for at least one month. MCF7 cells grew as distinct local colonies with tight cell packing, as is characteristic of this cell type in 3D culture, and colonies were distributed uniformly throughout the microsphere. Colony outgrowth of MCF7 cells was observed under phase contrast microscope from day 14 to day 28 after encapsulation as shown in Figure 2.10A-C. In SEM images of the microspheres, increasing outgrowth of MCF7 cell colonies from the hydrogel material was seen over time (Figure 2.10E-H). Encapsulated MDA-MB-231 cells were cultured for over 38 days, with continued maintenance of cell viability (Figure 2.10D). Multiple cell types have been tested and were able to maintain

viable for an extended period of time. Comprehensive studies of long-term culture are in progress for breast cancer cells, horse ECFCs (Seeto et al. 2017), and hiPSCs. Together, these results suggest that microspheres produced using the microfluidic encapsulation platform can be used for long term cell culture.

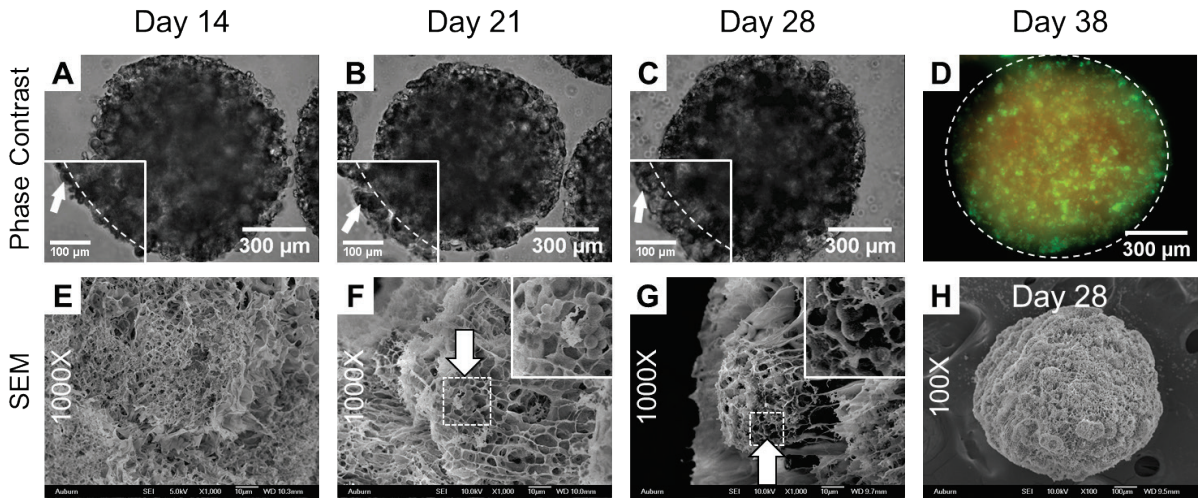

Figure 2.10 Encapsulated cells were able to be cultured for an extended time post-encapsulation. (A-C) Increasing colony outgrowth of cancer cells from MCF7 microspheres, indicating proliferation of cells during long-term culture. Initial microsphere boundaries are indicated by a dashed line. D) Encapsulated MDA-MB-231 cells maintained high viability for a long-term. Viability assay was conducted on day 38 post-encapsulation (Live Green: Calcein AM, Dead Red: Ethidium homodimer). Separate live, dead, and nuclei images are shown in Figure 2.11. (E-H) SEM images of MCF7 microspheres with magnification of 1000x and 100x. Cancer cell colonies are indicated by arrows.

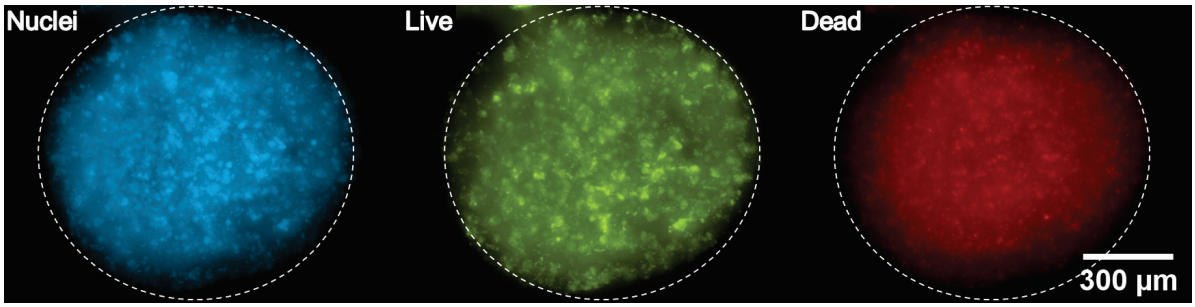

Figure 2.11 Viability of encapsulated MDA-MB-231 on day 38.

To meet the need for a wide range of downstream applications, the field of tissue engineering needs to be able to rapidly encapsulate mammalian cells at high cell density in uniform microspheres using clinically applicable materials with tight control over microsphere shape and size, while maintaining high cell viability and cellular phenotype. However, the commercially available systems for cell-laden hydrogel microspheres production are mainly based on electrostatically assisted spraying (or electrospray) technology. Produced cell-laden droplets are polymerized through exposure to ions in the collection solution. Limited by this polymerization approach, encapsulation systems using electrospray are limited to use with only a few types of materials, such as alginate and agarose-based materials, and polymerization time can be up to 5-10 minutes. Given the tighter control over microsphere size and more flexibility in terms of crosslinking approach and material selection, microfluidic systems have the potential to bridge the technological gap for realizing downstream commercial applications and have a competitive advantage in the marketplace. However, most microfluidic systems on the market and reported previously in the scientific literature only work with acellular materials or very low cell densities, and the resulting microspheres are small in size, which is limited by microfabrication technique used during microfluidic device production. Here we have described multiple advantageous features that can be employed to advance microfluidic platforms towards commercially applicable

production, including rapid production rate, wide range of sizes, materials selections, cell densities, and cell types, and easy device fabrication method, making the platform to be adopted by others easily. A table comparing current encapsulation systems and the novel microfluidic platform we developed is shown in Table 2.2, and more detailed information is shown in Table 2.3 and Table 2.4.

Table 2.2 Comparison of established microfluidic platform attributes to existing cell-laden microsphere production systems.

Production method (References)	Microfluidic (This dissertation)	Microfluidic (Headen et al. 2014, Hidalgo San Jose et al. 2018, Tan and Takeuchi 2007, Capretto et al. 2010)	Nozzle-based droplet generator (Orive et al. 2005, Bidarra et al. 2010)	Microfluidic (Kumachev et al. 2011, Sakai et al. 2011)	Microfluidic (Jiang et al. 2017, Zhao et al. 2016)
Crosslinking method	Photo	Chemical	Chemical	Thermal	Photo
Rapid crosslinking	++	-	-	-	+
Junction design	Modified T-junction with vertical orientation	T-junction/ Flow focusing	n/a	T-junction/ Flow focusing	T-junction/ Flow focusing
Rapid/simple device fabrication with low cost	+ (Molding)	- (Photolithography)	-	- (Photolithography)	- (Photolithography)
Wide range of sizes	++	-	+	-	-
Support multiple materials	+	-	-	-	+
High cell density ($>10^6$ mL^{-1})	++	-	+	+	-
High production rate (>1 mL h^{-1})	+	+	++	+	-
High uniformity	+	+	+	+	+

Table 2.3 Microfluidic encapsulation platform support rapid production.

Diameter (μm)*	Volume per microsphere (mL)#	Preparation time per microsphere (s)#	Flow rate of discrete phase (mL h^{-1})*	Microspheres prepared per hour#
300	$1.4x10^{-5}$	0.1	0.5	36000
800	$2.7x10^{-4}$	1.0	1	3600
1000	$5.2x10^{-4}$	1.9	1	1900

* indicates data collected from direct measurement.

# indicates calculated result based on directly measured data.

Table 2.4 Examples of rapid production when producing microspheres with 800 μm diameter.

Cell density (million mL^{-1})*	Cells per microsphere#	Encapsulation time per million cells (min)*
10	2700	6
20	5400	3
60	16000	1

* indicates data collected from direct measurement.

# indicates calculated result based on directly measured data.

2.4 Conclusion

This study established a robust microfluidic cell encapsulation platform, including developing a new molding technique for microfluidic device fabrication (Figure 2.12). This new method overcomes the limitations imposed by traditional microfluidic chip fabrication using photolithography and provides great flexibility for altering the design of the microfluidic device. With a custom-designed T-junction and readily adjustable channel sizes, the established microfluidic encapsulation platform is compatible with multiple polymers and cell types; furthermore it can be used to produce highly uniform microspheres with high cell densities and a wide range of diameters through rapid photocrosslinking. The encapsulated cells are evenly distributed through the microspheres and can maintain high viability and appropriate cellular

activities in long-term culture. This microfluidic encapsulation platform can be a valuable tool for tissue engineered microsphere production for use in regenerative medicine applications. More studies for a thorough understanding of the fluid dynamics during microsphere production will be carried out in the future.

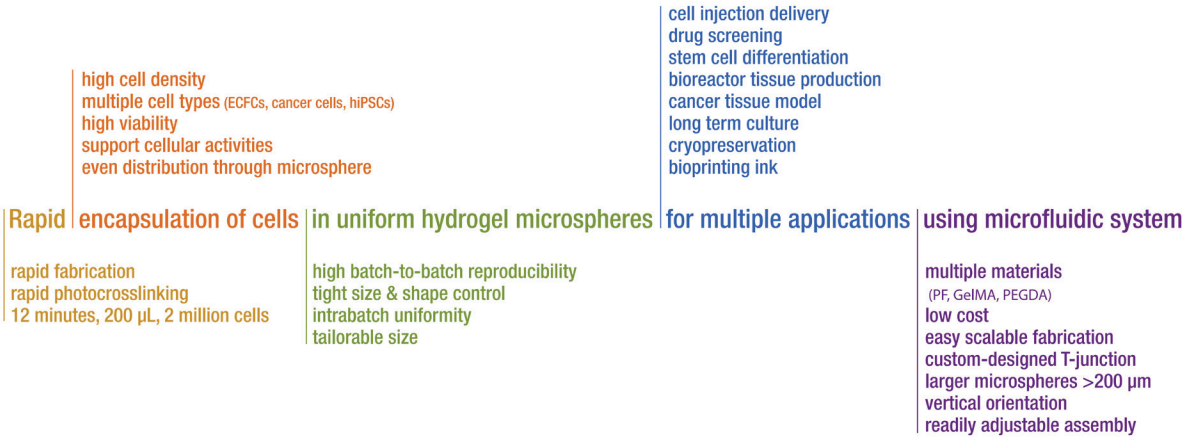

Figure 2.12 Summary of the advantages of the established microfluidic encapsulation platform.

3. CHAPTER 3: Microfluidic Production of Microspheroidal Hydrogels with Different Geometric Shapes

3.1 Introduction

Microfluidics has become one of the most commonly used platform technologies for production of microspheroidal droplets, including microspheres and microrods, which can be used for encapsulation of cells, functional macro- or super- molecules, and drugs (Seeto et al. 2017, Hindson et al. 2011, Xu et al. 2009). Compared to other production approaches, such as electrospray and non-microfluidic emulsion techniques, microfluidics can produce microspheroids with higher uniformity and production throughput, and importantly, with different geometries, which influence many aspects of microspheroid function (Headen et al. 2014, Khademhosseini and Langer 2007, Baah and Floyd-Smith 2014). Towards that end, significant attention has been paid to geometry control in microfluidic production, such as control over microspheroid size and axial ratio (AR), the ratio of axial diameter to radial diameter (Garstecki et al. 2006, Kim et al. 2007).

The geometric shape plays an important role in microspheroid function. Champion et al. reported that particle shape played a dominant role in the process of particle uptake by macrophages; thus leveraging control over shape expands possibilities in engineering drug delivery carriers (Champion and Mitragotri 2006). Von Maltzahn et al. showed the gold nanorods exhibited superior intrinsic absorption and photothermal efficacy as well as much longer circulation times *in vivo* compared with gold nanospheres, thereby working as more effective reagents for photothermal tumor therapy (von Maltzahn et al. 2009). De Vicente et al. demonstrated the importance of shape for sphere- and rod- based magnetorheological fluids, including differences in rheological properties (de Vicente et al. 2009).

Particularly in the tissue engineering field where hydrogels are commonly used for cell encapsulation, providing control over hydrogel geometry can be beneficial for various applications such as cell delivery, bioreactor-based cell production, high throughput screening, and 3D bioprinting (Seeto et al. 2017, Highley et al. 2019, Kropp, Massai, and Zweigerdt 2017, Brouzes et al. 2009). Each purpose requires a certain geometric shape for the hydrogels. For example, microspherical hydrogels are widely used for injectable cell delivery (Seeto et al. 2017, Zhao et al. 2016, Oliveira et al. 2015, Yao et al. 2013), and properly controlled sizes can improve cell retention while allowing for a smooth injection process. In a stirred tank or fluidized bed bioreactor system, hydrogels with different ARs will lead to different flow properties, which can be used to control the mixing and sedimentation process (Xia et al. 2009). Encapsulation of islets in fiber-shaped hydrogels were reported by An et al. to make delivered cells conveniently retrievable (An et al. 2018). Rapid production of hydrogels with a wide range of geometric shapes and physiologically relevant dimensions (10^{-1}-10^{3} μm) is important to meet the various needs for differing biomedical uses.

Geometric shape has been varied in microspheroids with dimensions ranging from the microscale down to the nanoscale using various techniques. Rolland et al. utilized non-wetting molding techniques to produce a number of shapes as small as 200 nm (Rolland et al. 2005). Champion et al. reported a film-stretching method that can generate microspheroids with various axial diameter ranging from 200 nm to 10 μm (Champion and Mitragotri 2006). Karp et al. use template-assisted self-assembly to form cell aggregates with defined shape and size from 40 to 150 μm (Karp et al. 2007). Compared to these techniques, microfluidic technology is advantageous when higher throughput production is needed. However, despite the advancements achieved by current microfluidic devices, most of the resulting microspheroids have relatively small sizes. This

limitation is due to the utilization of photolithography for microfluidic device fabrication. During fabrication of devices, the thickness of the spin-coated photoresist constrains the size of microfluidic channels, which thereby restricts resulting microspheroid size. Previously, we reported a custom-developed molding technique for fabrication of our microfluidic device (Seeto et al. 2019). With this technique, the diameter of the cylindrical microfluidic channels can be increased to 300-1100 μm compared to the typical photolithography upper limit of 200 μm (Velasco, Tumarkin, and Kumacheva 2012).

Using our previously established microfluidic encapsulation platform, we have shown the capability to rapidly produce highly uniform, cell-laden hydrogel microspheres on a large-scale (Seeto et al. 2019, Seeto et al. 2017). Our microfluidic device uses a modified T-junction design, which combines the features from two commonly used microfluidic junction designs, the T-junction and flow focusing designs. In this study, we explore for the first time the ability to produce microspheroids with different geometric shapes and focus on understanding the governing fundamental physical principles of this platform. In particular we leverage this junction design's control over capillary number, enabling production of microspheroids with varying ARs and diameters. These principles provide a better understanding of how to adjust the geometric shape of microspheroids by changing device design and experimental parameters including junction/outlet diameter ratio and continuous/discrete phase flow rate ratio.

3.2 Experimental Section

3.2.1 Microspheroid Production Using Microfluidic Platform.

For microfluidic device fabrication, molding technique was employed where a 3D printed jig was used to hold the molds. The jig with molds was then fixed on a glass surface using binder clips. Polydimethylsiloxane (PDMS; Sylgard 184 silicone elastomer kit, Dow Corning) was

poured into the jig, degassed by vacuum, and cured at 70 °C for 2 hours. The molds were then removed. The PDMS microfluidic device was sterilized by sonicating in 70 % ethanol before and after each use.

To produce hydrogel microspheroids using the microfluidic platform, hydrogel precursor solution was first prepared by mixing PEG-fibrinogen solution with 0.1 % (w/v) of Pluronic F68 (Sigma-Aldrich), 0.1 mM of Eosin Y photoinitiator (Fisher Scientific), 1.5 % (v/v) triethanolamine (Acros Organics), and 0.39 % (v/v) of N-vinylpyrrolidone (Sigma-Aldrich). For cell-laden microspheroids production, cells were detached from tissue culture flask, centrifuged, and resuspended in hydrogel precursor solution to desired cell density.

Microspheroid production was conducted in a biosafety cabinet to keep the process clean. The microfluidic device had two inlets and one outlet where the hydrogel precursor solution was pumped in from the top inlet, and the mineral oil was pumped in from the bottom inlet. Both flow rates were controlled by syringe pumps separately. Microspheroids were formed at the junction of the microfluidic device due to emulsification and then photocrosslinked by a high intensity visible light source (2.8 W/cm^2; Prior Lumen 200). The microspheroids were washed down at the end of the outlet channel by using a third syringe pump and collected in a centrifuge tube. The residual mineral oil was removed through centrifugation.

3.2.2 Microspheroid Geometry Characterization.

The resulting hydrogel microspheroids, including microspheres and microrods, were imaged using an inverted Nikon Eclipse Ti microscope. Using ImageJ software (NIH), axial diameter and radial diameter of the microspheroids were determined. The Axial Ratio (AR) was calculated using the formula:

$$Axial\ Ratio = \frac{Axial\ diameter}{Radial\ diameter}$$

A higher AR value means a longer microrod, and a perfect microsphere has an AR value of 1. For clarification purposes, a microspheroid is named as microsphere when its AR is smaller than 1.05, and axial diameter is reported as diameter in the text when the difference between axial and radial diameter is small (<5 %).

Uniformity was analyzed by coefficient of variance (CV) which is defined as:

$$Coefficient\ of\ variance = \frac{Standard\ deviation}{Mean}$$

3.2.3 Cell Culture and Maintenance.

BJ-5ta (ATCC® CRL4001™) normal human foreskin immortalized fibroblasts were obtained from ATCC (Manassas, VA). The cells were cultured in media containing 70.6 % (v/v) Dulbecco's Modified Eagle's Medium (DMEM; Gibco), 18 % (v/v) Medium 199 (Gibco), 10 % (v/v) fetal bovine serum (FBS; Atlanta Biologicals), 1.4 % (v/v) glutaGRO (Corning), and 0.02 % (v/v) hygromycin B (Millipore). The cells were maintained at 37 °C with 5 % CO_2. Cells cultured in tissue-culture flask were detached with TypLE™ Express Enzyme (Gibco) and used for 3D encapsulation.

3.2.4 Cell Viability Assay.

Cell viability after encapsulation was assessed using Live/Dead™ Viability/Cytotoxicity Kit (Invitrogen). Cell-laden microspheroids were incubated with Calcein-AM and Ethidium Homodimer-1 for 30 minutes. Z-stack images were then taken with fluorescence microscope (Nikon Eclipse Ti). Three regions with same size (192×192 μm) were randomly selected on each microspheroids using ImageJ, and live/dead cells were counted through the optical slices along the z-axis for approximately 350 μm.

3.2.5 Phalloidin Staining.

Fibroblast-laden microspheroids were rinsed with PBS to remove media and fixed with 4 % paraformaldehyde for 30 minutes at room temperature. They were subsequently rinsed with PBS and stained with Alexa Fluor 568 Phalloidin and Hoechst 33342 for 1 hour. After washing with PBS, fluorescence images were obtained using confocal microscopy (Nikon AI Confocal Scanning Laser Microscope).

3.2.6 Statistical Analysis.

All data are presented as mean ± standard deviation. All statistical analysis was performed using Minitab 18 Statistical Software (Minitab Inc.). After checking for normality of distribution, one-way analysis of variance (ANOVA) followed by Tukey-Kramer honest significant difference (HSD) test was performed to evaluate statistical significance between multiple groups. Statistical significance was declared if $p<0.05$.

3.3 Results and Discussion

3.3.1 Modified T-Junction Design for Geometry Control.

The control over microspheroid geometry, including AR and diameter, comes from the precise liquid manipulation provided by design of the microfluidic devices, especially the junction design. There are three commonly used junction designs for microfluidic devices: T-junction, flow focusing, and co-flow (Christopher and Anna 2007). Each design individually provides different advantages for controlling microspheroid size and AR during the production process. For T-junctions, varying the flow ratio, the ratio of discrete phase to continuous phase, enables the resulting microspheroids to have various ARs (Tice et al. 2003). For flow focusing and co-flow junction design, changing the flow ratio influences the final microspheroid diameter, whereas it is challenging to control AR through changes in flow ratio. Due to the complex and resource-

intensive nature of traditional microfluidic device fabrication, computational simulation has previously been done for a range of junction designs to provide researchers with a better understanding of the mechanisms controlling microspheroid geometries (Dupin, Halliday, and Care 2006, Liu and Zhang 2009, Hong and Wang 2007).

As the central component of the microfluidic platform employed in this study (Figure 3.1A), the microfluidic device uses a modified T-junction design, which combines the features from both T-junction and flow focusing designs. Here we examine the ability to use this design to control both diameters and ARs of resulting microspheroids by changing experimental conditions such as the flow fraction. In our modified T-junction design, the discrete phase is aqueous hydrogel precursor solution which flows into the microfluidic device from the top inlet. Mineral oil, the continuous phase, flows in from the bottom inlet. Microspheroidal droplets are formed at the junction and are photocrosslinked in the outlet channel. As shown in Figure 3.1B, after entering from the top inlet, the precursor solution flows into a restriction segment functioning as a flow stabilizer. Under the stabilizer is a conical region, which serves to eliminate dead volume of precursor solution. The outlet channel starts with a relatively small diameter at the junction and gradually increases to a constant size. Adjusting the size of this tapered end of outlet channel enables differing flow speed at the junction, providing control over the viscous force in microspheroid formation. Compared to traditional microfluidics, the modified T-junction design has larger channels with circular cross-sectional area which is achieved by the previously reported molding technique (Seeto et al. 2019). Unlike traditional microfluidics, this device is operated vertically instead of horizontally. The buoyant force caused by the difference in inlet fluid densities is more substantial with larger channel sizes. The vertical orientation exploits this density difference to assist microspheroid formation. Together, with all the design parameters mentioned

above, the modified T-junction design makes it possible to produce larger microspheroids with different ARs and sizes.

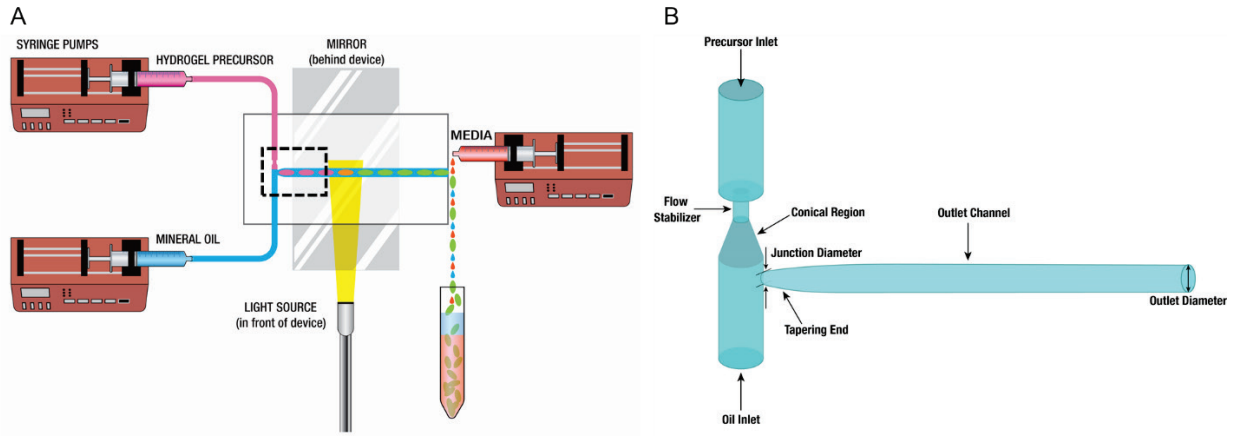

Figure 3.1 Microfluidic platform with modified T-junction design. Schematic of the (A) microfluidic platform and (B) modified T-junction design.

3.3.2 Uniform Microspheroids with a Wide Range of Geometric Shapes.

In initial testing, this platform using the microfluidic device with modified T-junction design was able to produce uniform hydrogel microspheroids, including microspheres and microrods, with a wide range of geometric shapes. As shown in Figure 3.2(A-D), the resulting microspheres had diameters of 320 ± 13 μm, 585 ± 19 μm, and 1002 ± 56 μm (CV = 0.04, 0.03, and 0.06), respectively. This is a much wider range of diameters compared to the ones achieved by microfluidic devices fabricated through photolithography (Seeto et al. 2019). Even at the largest end of the diameter range, production of spherical hydrogels is possible with AR of 1.03 ± 0.02, 1.02 ± 0.02, and 1.02 ± 0.02 that are close to 1, indicating high roundness.

Leveraging the ability to readily fabricate microfluidic devices with varying design parameters, we probed the ability of this microfluidic platform to produce microspheroids with higher AR, or microrods. Changing inlet flow rates and design parameters, including junction diameter and outlet

diameter, enabled modulation of the resulting microrods AR; example microrods are shown in (Figure 3.2 E-H) with AR of 1.37 ± 0.04, 1.98 ± 0.10, and 3.54 ± 0.37 (CV = 0.03, 0.05, 0.10), respectively.

Previously, microfluidic platforms with flow focusing and T-junction design were often used to produce microspheres and microrods (Wan et al. 2012, Seemann et al. 2012). However, they were small in size, restricting their use in downstream applications. The microfluidic platform used in this study was able to achieve similar goals, which is to produce highly uniform microspheroids while varying diameters and ARs in a much wider size ranges, greatly broadening the scope of their functions.

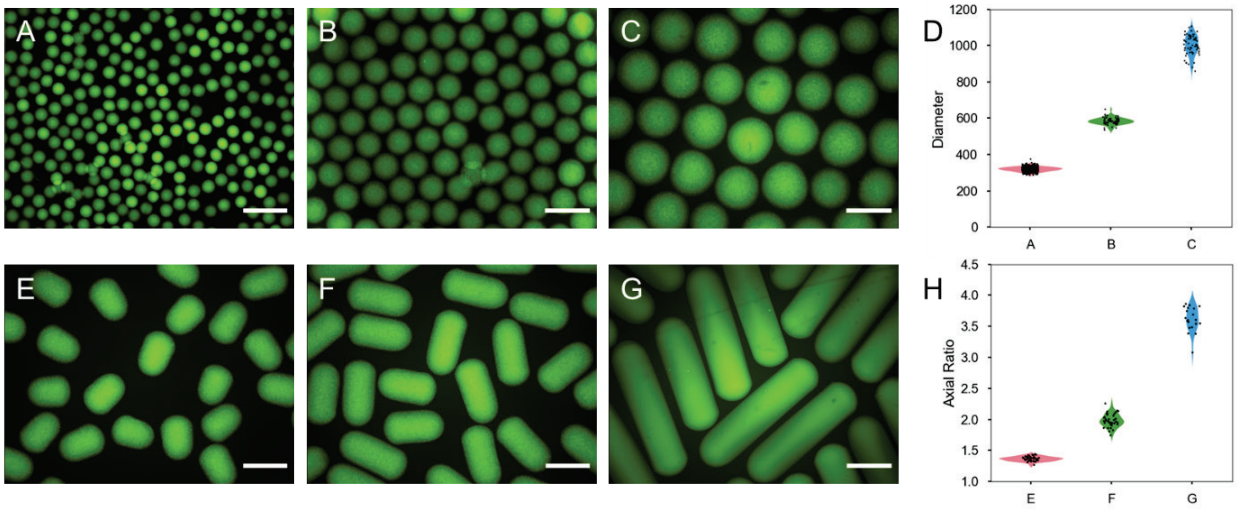

Figure 3.2 Hydrogel microspheroids with different geometric shapes. (A-C) Imaged by a fluorescence microscope, hydrogel microspheres were shown to have high uniformity, high roundness, and a wide range of diameters. The green color came from the auto-fluorescence of the photoinitiator Eosin Y used in hydrogel photocrosslinking. (D) The hydrogel microspheres had diameters of 320 ± 13 µm (CV = 0.04), 585 ± 19 µm (CV = 0.03), and 1002 ± 56 µm (CV = 0.06), respectively (n>59 microspheres per condition). (E-G) Hydrogel microrods had high uniformity and a wide range of AR. (H) Hydrogel microrods with AR of 1.37 ± 0.04 (CV = 0.03), 1.98 ± 0.10

(CV = 0.05), and 3.54 ± 0.37 (CV = 0.10), respectively (n>20 microrods per condition). Data are presented as mean ± standard deviation. Scale bar = 1000 μm.

3.3.3 Designs of Modified T-Junction Enable Control Over Geometric Shape.

In modulating the microspheroid geometric shape, the dimensionless capillary number (Ca) plays an important role (Xu et al. 2006). It describes the relative effect of viscous forces to surface tension at the interface of two immiscible fluids:

$$Ca = \frac{Viscous\ force}{Surface\ tension} = \frac{\mu v}{\gamma}$$

where μ is the dynamic viscosity of continuous phase (oil phase), ν is the relative velocity of continuous phase (oil phase) to discrete phase (aqueous precursor solution) at the junction, and γ is the interfacial tension (precursor solution–oil). The relationship between the microsphere diameter and Ca is described by:

$$Diameter_{Microsphere} \propto \frac{1}{Ca}$$

As the Ca increases, the microsphere diameter decreases. As the Ca decreases, the microsphere diameter increases until it is restricted by the outlet channel diameter. Based on the definition of the Ca, as the ν increases, the Ca increases. When ν decreases, Ca has a lower value. And for the relative velocity ν, it is related to the flow fraction, which is defined as:

$$Flow\ Fraction = \frac{Precursor\ flow\ rate}{Precursor\ flow\ rate + Oil\ flow\ rate}$$

The flow rate is a parameter that can be controlled during the experiment; therefore, by adjusting the flow rate, we can control the ν and Ca, eventually controlling the resulting diameter of microspheres. As the microsphere diameter increases and becomes larger than outlet channel

diameter, the droplets will elongate and become microrods because of the constraints from the outlet channel wall.

When using a light source with consistent power output, exposure time plays an important role in controlling degree of photocrosslinking, which can be reflected in hydrogel stiffness (Bonino et al. 2011). To ensure consistent photocrosslinking, the microspheroids have a similar exposure time to the visible light source when traveling through the outlet channel, which means they have a similar flow velocity in the outlet channel. As shown in the equations below, flow velocity is defined by volumetric flow rate, controlled by syringe pumps, over cross-sectional area of the outlet channel, which is proportional to the square of outlet channel diameter.

$$Flow\ velocity = \frac{Volumetric\ flow\ rate}{Cross\ sectional\ area}$$

$$Cross\ sectional\ area \propto Diameter_{Outlet}^{2}$$

Using this relationship, the total volumetric flow rate was adjusted according to the outlet channel diameter to achieve a similar velocity in the outlet channel for consistent crosslinking times. As a result, the ν is determined by not only the diameter of the junction, but also the diameter of the outlet channel. For example, for two microfluidic devices with the same junction diameter, the one with a larger outlet channel diameter will have a higher volumetric flow rate to achieve the same velocity in outlet channel, resulting with a higher velocity at the junction.

To better quantify the ν in Ca, the Narrowing Ratio (NR) is introduced to describe the relative value of junction diameter and outlet channel diameter, which helps determine the tendency of a microfluidic device to produce microspheres or microrods:

$$Narrowing\ Ratio(NR) = \frac{Diameter_{Junction}}{Diameter_{Outlet}}$$

With the same outlet channel diameter, the total volumetric flow rate remains constant to ensure similar flow velocity in the outlet channel, which is important for controlling degree of photocrosslinking as discussed previously. As the NR decreases, the junction diameter decreases, leading to a smaller cross-sectional area at the junction. As a result, the ν has a higher value, which means Ca has a higher value. When the values for NR is smaller than 0.5, the shape of the resulting droplets is typically spherical, and the size is determined by flow fraction. Similarly, as the NR increases, the ν has a lower value, decreasing the Ca. The size of the microspheroids is limited by outlet channel diameter. The shape can vary from microsphere to microrod and is determined by flow fraction. When the flow fraction increases, the AR increases. The description above is summarized in Figure 3.3. Collectively, by adjusting design parameters including junction diameter and outlet channel diameter, and experimental parameters such as the inlet flow rates of the precursor solution and mineral oil, the geometric shape of microspheroids can be adjusted.

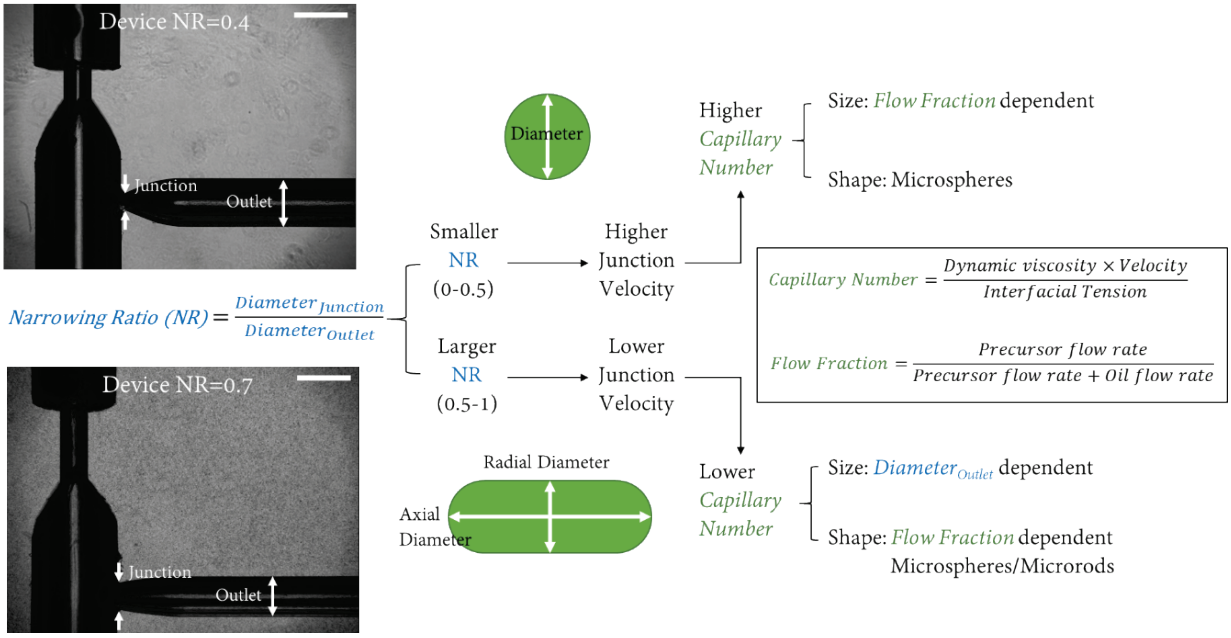

Figure 3.3 A summary of governing fundamental physical principles for the modified T-junction. By adjusting design parameters such as junction diameter and outlet diameter and experimental parameters such as inlet flow rates of precursor and oil, we can control the capillary number at the junction. As a result, the size and shape of microspheroids can be adjusted. Images of microfluidic device were modified for better visualization.

3.3.4 Control Geometric Shape by Varying Narrowing Ratio and Flow Fraction.

To demonstrate the theory summarized in the previous section, microfluidic devices with two different NRs (0.4 and 0.7) were fabricated and operated with different flow fractions. The microfluidic device with NR = 0.4 produced spherical hydrogels (Figure 3.4A-C). When increasing the flow fraction from 0.05 to 0.07, the microsphere diameter increased significantly from 680 ± 12 µm to 930 ± 16 µm (Figure 3.4D). The resulting diameter stopped increasing with increases to flow fraction once the microspheres reached the size of the outlet channel. For the microfluidic device with NR = 0.7, the radial diameter was limited to the outlet channel diameter, approximately 800 µm. With an increase of flow fraction, the axial diameter increased

significantly from 824 ± 21 μm to 3013 ± 167 μm, leading to a significant increase of AR from 1.02 ± 0.01 to 3.61 ± 0.20 (Figure 3.4E-I). Detailed information on device design parameters and experimental conditions is listed in Table 3.1. These results demonstrate that this microfluidic device provides tight control over microspheroid geometric shape by varying the NR and flow fraction.

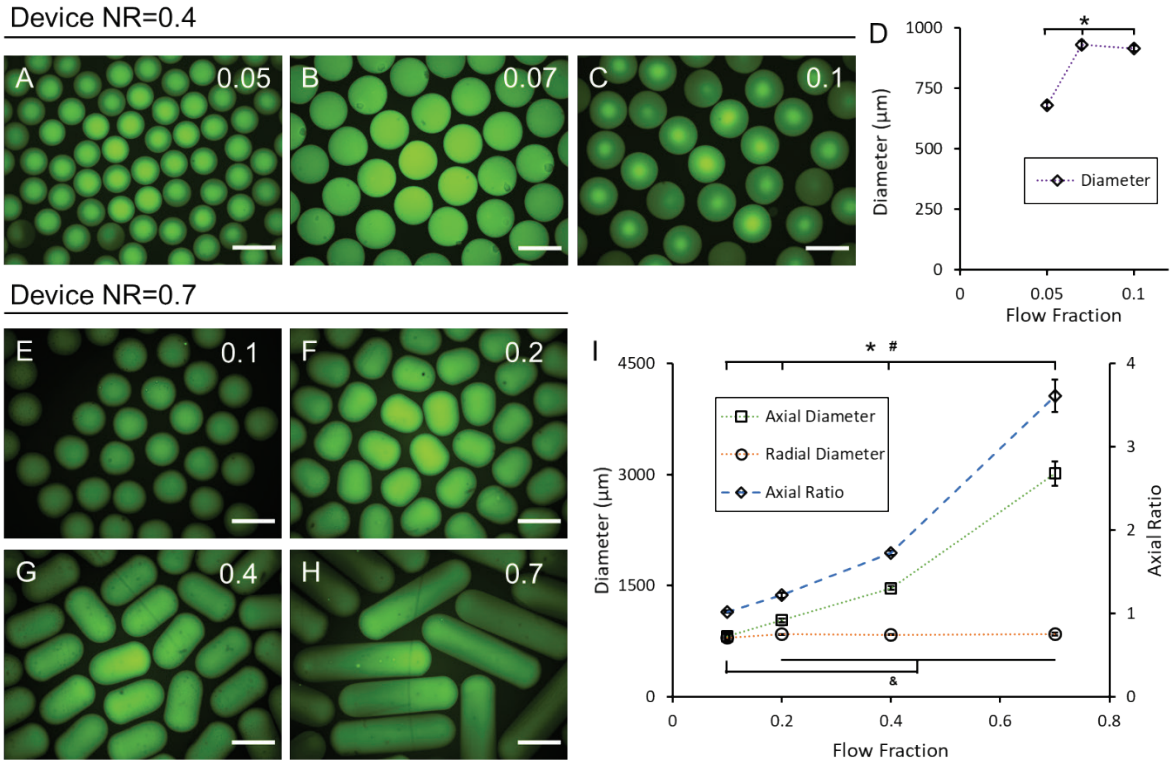

Figure 3.4 The microfluidic device provides tight control over the microspheroid geometric shape by varying the NR and flow fraction. (A-C) A microfluidic device with a small NR (NR = 0.4) produced microspheres. The diameter of microspheres changed with flow fraction. (D) When the NR = 0.4, quantitative analysis showed microsphere diameter increased with flow fraction and then stopped upon reaching the size of the outlet channel (*Significant difference between flow fractions for diameter, $p<0.05$, $n>70$ microspheroids per condition). (E-H) A microfluidic device with a large NR (NR = 0.7) produced both microspheres and microrods. By increasing the flow fraction, the radial diameter remained relatively constant while the axial diameter increased,

causing an increase in AR. (I) When NR = 0.7, quantitative analysis showed microrod AR increased along with flow fraction (*#&Significant difference between flow fractions for AR, axial diameter, and radial diameter, respectively, $p<0.05$, $n>20$ microspheroids per condition). Data are presented as mean ± standard deviation. Scale bar = 1000 μm.

Table 3.1 Microfluidic device design parameters and experimental conditions for production of microspheroids shown in Figure 3.4.

Device	NR=0.4			NR=0.7			
Junction Size (μm)	370			530			
Outlet Size (μm)	915			765			
Flow Fraction	0.05	0.07	0.1	0.1	0.2	0.4	0.7
Oil Flow Rate (mL/hr)	10	10	9	9	8	6	3
Precursor Flow Rate (mL/hr)	0.5	0.8	1	1	2	4	7
Axial Diameter (μm)	680 ± 12	930 ± 16	915 ± 12	824 ± 21	1036 ± 25	1468 ± 24	3013 ± 167
Radial Diameter (μm)	660 ± 11	905 ± 15	894 ± 13	798 ± 16	845 ± 6	843 ± 7	851 ± 18
Axial Ratio (AR)	1.01 ± 0.01	1.01 ± 0.01	1.01 ± 0.01	1.02 ± 0.01	1.22 ± 0.03	1.72 ± 0.03	3.61 ± 0.20

Note: For microspheres (AR < 1.05), the diameter reported in the text is always the axial diameter.

3.3.5 Cells Maintain Normal Function in Microspheroids

BJ-5ta fibroblasts were encapsulated in hydrogel microspheroids (13 million cells/mL) with different ARs. Geometric shape of microspheroids and viability of encapsulated cells were observed one day after encapsulation for both qualitative and quantitative assessment. As shown in Figure 3.5A, the fibroblast-laden microspheroids from both groups were highly uniform with even cell distribution. The AR for each group was 1.37 ± 0.04 and 1.98 ± 0.10, respectively (Figure 3.5B). Encapsulated cells maintained high viability (>92.7 % for both groups) one day (Figure 3.5A, C) and one month after encapsulation. The cells formed an actin filament network as shown

in Figure 3.5A. These results show that the microfluidic platform can produce cell-laden microspheroids with different ARs. The encapsulated fibroblasts maintained normal cellular activities in long-term culture.

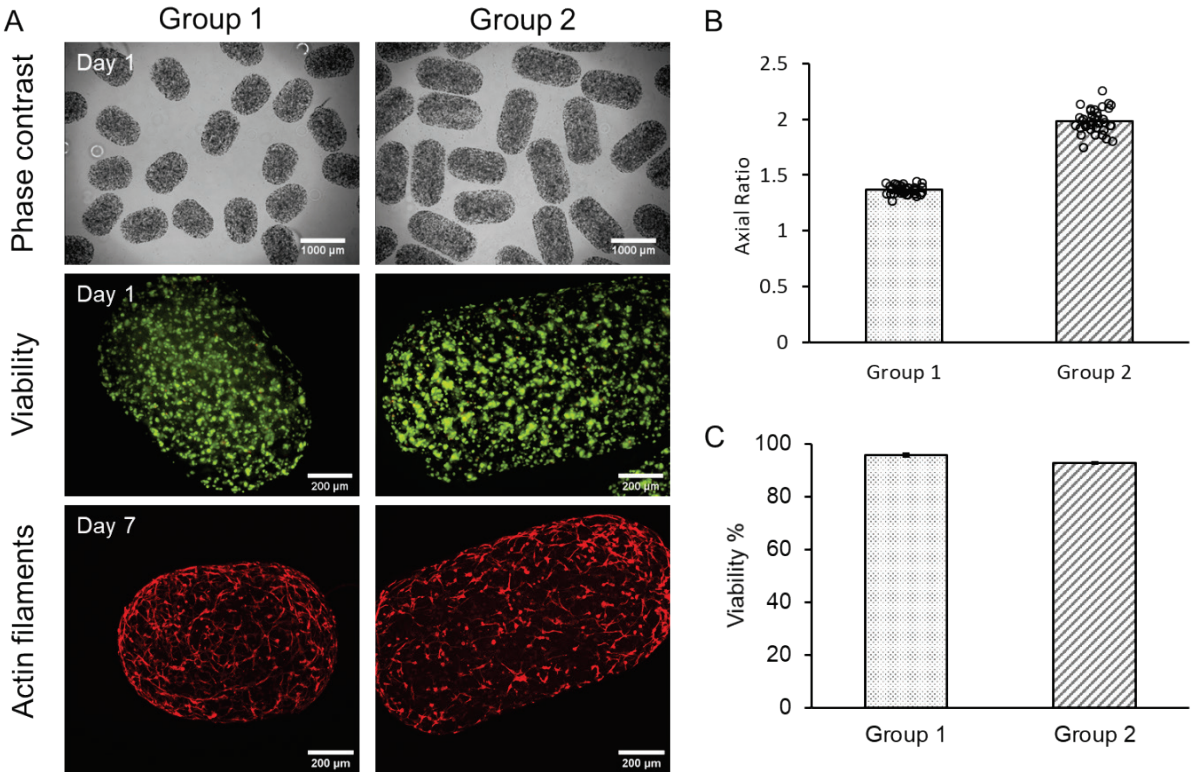

Figure 3.5 Fibroblast-laden microspheroids with different AR supported normal cellular activities post-encapsulation. (A) Fibroblast-laden microspheroids had uniform geometric shape and even cell distribution visualized using phase contrast images. Encapsulated cells maintained high viability one day after encapsulation (Live: Green, Dead: Red) and formed an actin filament network shown by fluorescence images. (B) Fibroblast-laden microspheroids had different AR of 1.37 ± 0.04 (CV = 0.03) and 1.98 ± 0.10 (CV = 0.05), respectively, for each group one day after encapsulation (n > 37 microspheroids per group). (C) Encapsulated fibroblasts maintained high viability of 95.8 ± 0.7 and 92.7 ± 0.5, respectively, for each group one day after encapsulation (n = 3 microspheroids per group).

As discussed in the introduction, the geometric shape of cell-laden hydrogels impacts their use in biomedical applications. For example, microspheres with smaller diameters can be employed as building blocks in 3D bioprinting since they can be extruded more easily through the nozzle (Highley et al. 2019, Xin et al. 2019). Cell-laden microspheres with larger diameters can be used for improving localized retention during therapeutic cell delivery (Seeto et al. 2017). Furthermore, providing certain defined geometries influences the encapsulated cellular function; controlling microspheroid shape, therefore, can guide the tissue development process. For instance, hydrogel microspheres with large diameters limit the diffusion of cell culture media, causing cell death in the center, and thereby inducing formation of a necrotic core which is desired in 3D tumor disease modeling (Pradhan, Chaudhury, and Lipke 2014). Microrods, with higher ARs compared to microspheres, can be used for culturing cells that are sensitive to spatial heterogeneity such as aligning cardiomyocytes and neurons to promote functional development of engineered cardiac or neural tissues (McCain et al. 2014, Hanson Shepherd et al. 2011). The microfluidic technology described in this study represents a promising new direction for understanding the role of ARs and diameters on tissue function, and provides opportunities for rapid production of these highly uniform microtissues for commercial use.

Geometric shape of microspheroids directly impacts their performance. Control over the diameters and ARs of microspheroids opens many exciting possibilities for various applications. Currently a number of approaches have been developed to vary geometric shape from the micro scale down to nano scale, such as molding (Rolland et al. 2005), emulsion (Franco, Price, and West 2011), electrospray (Jaworek 2007), and microfluidic techniques (Seemann et al. 2012). Compared to other methods, microfluidics can provide higher uniformity and production throughput (Khademhosseini and Langer 2007). However, most research using microfluidics to achieve

geometric shape control is done utilizing small channel sizes (Velasco, Tumarkin, and Kumacheva 2012). Whereas the small size of resulting microspheroids is necessary for purposes such as drug delivery, the upper size constraint limits their use in many other applications. Here we described a microfluidic platform with a modified T-junction design that can control the diameters and ARs of microspheroids with larger sizes (on the dimensions of hundreds to thousands of microns). We also identified and examined the mechanisms by which this junction design provides geometric control, including the role of narrowing ratio, capillary number and flow fraction. Future work will further investigate these identified relationships, as well as consider the potential influence of transition length at the tapered end. Findings from this work can potentially be used by researchers to investigate geometric control in other microfluidic devices and may also be useful for comparison with computational modeling studies of microfluidic systems.

3.4 Conclusion

In conclusion, here we have demonstrated the ability to produce hydrogel microspheroids, including microspheres and microrods, using our novel microfluidic platform. The PDMS microfluidic device used in this platform employed a modified T-junction fabricated with a molding technique instead of photolithography. This special junction design enabled production of uniform microspheroids with a wide range of diameters and ARs. We have explored the mechanism of the junction design and its control over the geometric shape of microspheroids. We show by varying the design parameter, narrowing ratio, and experimental parameter, flow fraction, we can control the tendency of the microfluidic device to make microspheres or microrods and adjust the diameters and ARs. To demonstrate maintained cellular activities, we have encapsulated fibroblasts within the hydrogel microspheroids and have kept them in long-term culture with normal cellular behavior as well as high viability. With an understanding of the governing

principles summarized from both literature and experiment, this microfluidic platform could be used for scalable production of microspheroids with desired geometric shape for various applications, such as chemical synthesis, cosmetics, bioreactor-based cell production, injectable cell delivery, disease modeling for drug discovery, and 3D bioprinting.

4. CHAPTER 4: Encapsulation of Equine Endothelial Colony Forming Cells in Highly Uniform, Injectable Hydrogel Microspheres for Local Cell Delivery

4.1 Introduction

The importance of cell-based therapies such as ECFCs for treating ischemic disease has been increasingly recognized because of studies showing improved outcomes (Wang, Chen, et al. 2008). ECFCs, a subtype of EPCs, directly participate in new blood vessel formation (Medina et al. 2017). Despite the promising results of many *in vitro* studies, the outcome of the cell-based therapies *in vivo* is often unconvincing. This is largely associated with the use of a direct cell injection method which causes insignificant cell accumulation or low retention at the targeted injection site (Qian et al. 2007, Gaffey et al. 2015). Studies have shown that as few as 1 % of the injected cells are retained after direct cell injection, with typical retention being less than 10 % (Sheikh et al. 2012, Hofmann et al. 2005, Schachinger et al. 2008, Li et al. 2009, Dow et al. 2005). In addition, exposure to ischemia and inflammation also compromises the function and fate of the injected cells (Wang et al. 2010, Laflamme et al. 2007, Robey et al. 2008).

Encapsulation of stem or progenitor cells in hydrogels has been shown to support cell proliferation and long-term survival (Rafii and Lyden 2003). In addition, hydrogels can act as semi-permeable media to protect the transplanted or delivered cells from the host immune system (Velasco, Tumarkin, and Kumacheva 2012). Cell retention at the desired location can be significantly improved by encapsulating cells in a hydrogel matrix prior to delivery (Bidarra, Barrias, and Granja 2014). Therefore, cell encapsulation in hydrogel scaffolds could advance the potential of cell-based therapies.

The natural-synthetic hybrid hydrogel PF has been shown to support a range of tissue engineering applications (Lu et al. 2015, Fuoco et al. 2012, Peled et al. 2007, Pradhan, Clary, et

al. 2017, Kerscher et al. 2016), including angiogenesis. While the acrylated-PEG enables rapid formation of a supportive structure through photocrosslinking, the fibrinogen provides adhesive anchorage and degradability for cellular activity. A wide variety of cell types including SMC, induced pluripotent stem cells, and chondrocytes have been encapsulated in PF with minimal impact on cell viability (Peyton et al. 2008, Bearzi et al. 2014, Appelman et al. 2011, Almany and Seliktar 2005, Frisman, Seliktar, and Bianco-Peled 2012). Furthermore, injection of cells encapsulated within PF has been shown to enhance cell survival and differentiation compared to injection of cells suspended in aqueous saline solution, making PF a suitable biomaterial for cell delivery.

Encapsulation of cells into hydrogel microspheres increases the flexibility of use of resulting engineered tissues for clinical applications, because of the ability to deliver microspheres by injection. However, typical cell encapsulation in microspheres using microfluidic devices is limited by low cell density which makes delivery of sufficient cell numbers in reasonable volumes for therapeutic applications challenging (Velasco, Tumarkin, and Kumacheva 2012).

In this study, we present a custom-built microfluidic device that is capable of encapsulating ECFCs in PF hydrogel microspheres at a high concentration of 10 million cells/mL. The microspheres are highly uniform in shape and size. The encapsulated ECFCs were shown to have high viability post-encapsulation and their phenotype was preserved compared to cells in typical cell culture conditions. As an initial proof of concept for utilizing microspheres produced by the microfluidic device as clinical cell delivery vehicles, an *in vivo* cell delivery study was also performed by encapsulating and injecting autologous equine ECFCs into a distal limb wound model in adult horses. The outcomes of this study demonstrate the capabilities of this cell

encapsulation platform and examine its potential for supporting therapeutic cell delivery by injection.

4.2 Methods

4.2.1 Equine cell isolation and culture

All procedures involving animals were approved by the Auburn University Animal Care and Use Committee. Isolation and culture of equine ECFCs from equine peripheral blood were performed based on a previously published method (Sharpe et al. 2016). ECFCs were cultured in Endothelial Cell Basal Medium-2 (Lonza) containing 10 % horse serum (HyClone) and SingleQuots Kit (Lonza) at 37 °C and 5 % CO_2. The SingleQuots Kit contained hydrocortisone, hFGF-β, VEGF, R3-IGF-1, ascorbic acid, hEGF, GA-1000, and heparin. The ECFCs were seeded and expanded on collagen coated tissue culture polystyrene flasks. When ECFCs reached 90 % confluency, cells were subcultured using trypsin/EDTA (Lonza) to detach the cells at 37 °C for 50s, followed by neutralization with fresh medium and centrifugation at 200 g for 5 minutes. ECFCs were resuspended in medium and then subcultured at a ratio of 1:6 or immediately used for experiments. Cells between passage 2-7 were used for all experiments.

4.2.2 PEGDA synthesis

PEG (10 kDa; Sigma) was acrylated to form PEGDA following a previously published method (DeLong, Moon, and West 2005). Briefly, PEG was first lyophilized and then reacted with 0.4 M acryloyl chloride (Alfa Aesar) and 0.2 M triethyl amine (TEA, Sigma) in anhydrous dichloromethane (Acros) under argon overnight. 1.5 M K_2CO_3 (Fisher) was added, and then the solution was separated into aqueous and organic phases. The organic phase was collected and dried with anhydrous $MgSO_4$ (Fisher). The PEGDA was then precipitated by cold ethyl ether, filtered,

dried, and stored under argon at 20 °C. The degree of acrylation was estimated to be 96 % by NMR.

4.2.3 PEG-Fibrinogen synthesis

PF was synthesized by following a previously published method (Almany and Seliktar 2005). In brief, fibrinogen (Type I-S; Sigma) was dissolved in 8 M urea (Sigma) in PBS (Lonza) solution to a final concentration of 7 mg/mL with pH of 7.4. Tris (2-carboxyethyl) phosphine (Acros Organics) was added to the solution and reacted at pH of 8. PEGDA was dissolved in urea-PBS to a final concentration of 280 mg/mL and then slowly added to the fibrinogen solution and allowed to react for 3 hours in the dark at room temperature. After reaction, PEGylated fibrinogen was extracted with acetone, then centrifuged to remove acetone, and finally dissolved in urea-PBS again for dialysis. The product was dialyzed in sterile PBS over 24 hours in the dark at 4 °C and then stored at 80 °C. Protein content was determined to be 12.5 mg/mL using a BCA protein assay kit (Thermo Fisher). PEGylation yield was calculated to be 98 %.

4.2.4 Cell encapsulation in PEG fibrinogen microspheres

Cell encapsulation in PF hydrogel microspheres was achieved through a custom developed microfluidic polydimethylsiloxane (PDMS) system. The PDMS mold was created with Sylgard 184 silicone elastomer kit (Dow Corning) by pouring the mixture of base and cure component into a polystyrene dish containing the pre-assembled microfluidic channel mold. The mixture was subsequently degassed and heat-cured at 60 °C for 2 hours. After curing, the microfluidic channel mold was disassembled. The microfluidic PDMS mold was sonicated in 70 % ethanol before and after each use.

Before cell encapsulation, hydrogel precursor solution was prepared including PF solution with the addition of 1 % (v/v) of 10 % (w/v) Pluronic F68 (Sigma) in PBS, 1 % (v/v) of 10 mM of

EosinY photoinitiator (Fisher Scientific) in PBS, 1.5 % (v/v) triethanolamine (Acros Organics), and 0.39 % (v/v) of N-vinylpyrrolidone (Sigma). Pluronic F68 is an amphiphilic block copolymer that is commonly used as a surfactant to stabilize the emulsion of microencapsulation which narrows the size distribution of the microspheres. It was also confirmed that the addition of low concentration of Pluronic will have negligible effect on the hydrogel degradation profile (Franco, Price, and West 2011). ECFCs were detached by trypsinization as described above, centrifuged, and resuspended in hydrogel precursor solution to a cell density of 10 million cells/mL.

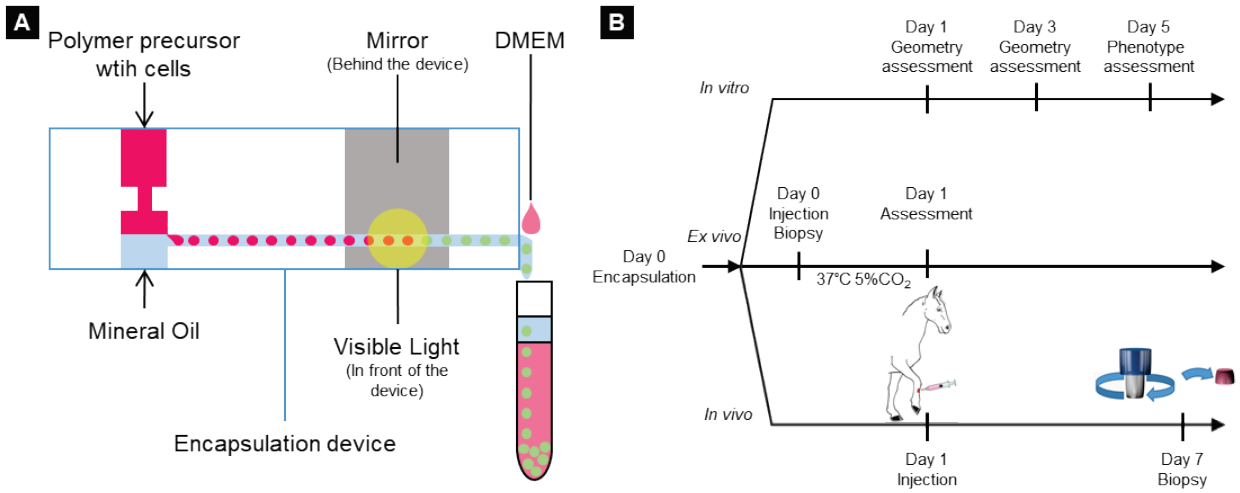

Figure 4.1 (A) Schematic of ECFC encapsulation in PF microspheres. (B) Timeline for *in vitro*, *ex vivo*, and *in vivo* study.

Cells encapsulation and hydrogel photo-crosslinking (Figure 4.1) were conducted in a biosafety cabinet. The microfluidic device had two inlets and one outlet; the PF hydrogel precursor with suspended cells flowed from the top inlet, and mineral oil flowed from the bottom inlet using syringe pumps. When the two streams met at the junction, microspheres were formed due to emulsification, and the cell-encapsulated microspheres were crosslinked by a 2.7 W full spectrum visible light (Prior Lumen 200). A mirror was placed behind the microfluidic device near the outlet to aid the crosslinking by reflecting the light that passed through the device. The microspheres

were washed down from the outlet with pre-warmed Dulbecco's Modified Eagle Medium (DMEM) by using a third syringe pump setting at 22 mL/hr. The microspheres were then washed twice with DMEM by centrifugation at 200 g for 3 minutes to remove the residual mineral oil and cultured in endothelial growth medium on a collagen coated well plate at 37 °C with 5 % CO_2.

4.2.5 Post-cell encapsulation cell viability assay

Cell viability after encapsulation was assessed using Live/Dead viability/cytotoxicity (Invitrogen) kits for Live/Dead staining. Microspheres collected immediately after encapsulation were incubated for 30 minutes with calcein AM and ethidium homodimer-1, and then Z-stack-images were acquired with fluorescence microscopy. Three regions with same size (250 × 250 μm) were randomly selected on each microsphere using ImageJ and viability was then assessed by counting Live/Dead stained cells through the optical slices along the z-axis for the depth about 550 μm.

4.2.6 Microsphere geometry characterization

The uniformity of the microspheres was evaluated by measuring their maximum diameter and roundness 1 and 3 days after cell encapsulation. Three batches of microspheres with at least 30 microspheres per batch were measured, and the measurements were performed using ImageJ.

4.2.7 Microsphere stiffness

In order to measure the Young's modulus of the hydrogel microspheres, they were subjected to compression testing under physiological conditions using the MicroSquisher (CellScale). Briefly, ECFCs encapsulated in microspheres were cultured for 1 or 3 days prior to mechanical testing. These microspheres were then loaded onto the MicroSquisher platform, maintained at 37 °C in PBS, preconditioned for compression testing and made to undergo cycles of compression and relaxation at a rate of 2.5 μm/s with a minimum of 15 % strain. The force-displacement data

obtained from the stress were converted to stress-strain curves, and the lower portion of the curve (5-15 % strain) was used to estimate the Young's moduli of microspheres.

4.2.8 Outgrowth cells phenotypic characterization

To assess the phenotype of the encapsulated cells, microspheres were cultured on collagen coated well-plates, and cells growing out from microspheres onto the well-plate were harvested and sub-cultured once to obtain sufficient cells for characterization. In order to ensure the ECFC phenotype was not impacted by the number of subcultures, ECFCs that had the same passage number in culture but did not go through encapsulation were used for comparison.

Uptake of DiI-Ac-LDL

The ability of ECFCs to take up 1,1'-Dioctadecyl-3,3,3',3'-tetramethylindocarbocyanine perchlorate-labeled acetylated low-density lipoprotein (DiI-Ac-LDL) was evaluated. 10 μg/mL of DiI-Ac-LDL (Biomedical Technologies) in pre-warmed medium was added to the ECFCs followed by incubation for 6 hours at 37 °C and 5 % CO_2. After incubation, uptake of DiI-Ac-LDL by ECFCs was imaged using fluorescent microscopy.

***In vitro* tubule formation assay**

ECFCs were seeded onto a 96-well plate (30,000 cells/well) containing Matrigel (Corning, 50 μL/well), which had been incubated for 15 minutes before cell seeding. Tubule formation was assessed after 5 hours of incubation at 37 °C and 5 % CO_2 by light microscopy.

Immunofluorescence analysis

Equine ECFCs pre- and post-encapsulation were evaluated for the expression of cell markers von Willebrand Factor (vWF), CD14, and CD105 with indirect immunofluorescence assay (IFA) as previously published (Salter et al. 2015). ECFCs were fixed with 4 % paraformaldehyde (PFA) solution and rinsed with PBS solution. For analysis of expression of the intracellular protein vWF,

ECFCs were permeabilized with PBS-T containing 0.2 % Triton X 100 (Sigma) in PBS for 30 minutes, and then blocked with 3 % horse serum at 4 °C overnight. The fixed cells were then incubated at room temperature for 1 hour with primary antibodies diluted in 3 % horse serum as follows: rabbit anti-human vWF (Dako) at 1:100, mouse anti-horse CD14 at 1:200 (Wagner Laboratory, Cornell University, (Kabithe et al. 2010)), mouse anti-human CD105 at 1:200 (AbD Serotec). After incubation, cells were washed with PBS-T before the application of secondary antibodies. Secondary antibodies were diluted in 3 % horse serum and incubated with cells at room temperature in the dark for 1 hour as follows: Alexa Fluor 488-conjugated goat anti-rabbit IgG at 1:400 for vWF and Alexa Fluor 488-conjugated goat anti-mouse IgG at 1:400 for CD14 and CD105. Cells were counter stained with DAPI, washed with PBS, mounted on glass slides with ProLong Gold antifade reagent (Life Technologies), and imaged with fluorescent microscopy.

Flow cytometry

To assess the influence of the encapsulation process on ECFC phenotype, flow cytometry was used to quantify expression of vWF, CD14, CD105, and uptake of DiI-Ac-LDL. For DiI-Ac-LDL uptake, cells were incubated with medium containing 10 μg/mL of DiI-Ac-LDL at 37 °C for 6 hours. After incubation, cells were rinsed with medium and PBS, detached, centrifuged, and fixed in suspension with 4 % PFA for 20 minutes at room temperature, followed by a rinse with PBS. The cells were then stored in 3 % horse serum in PBS.

For vWF staining, detached cells were fixed, permeabilized, and blocked with 10 % horse serum at 4 °C overnight. Then cells were incubated with primary antibodies at room temperature for 1 hour, rinsed with blocking solution, and incubated in secondary antibodies at room temperature for 1 hour in the dark. For CD14 and CD105 staining, detached cells were incubated with primary antibodies at 4 °C for 1 hour, rinsed with blocking solution, incubated in secondary

antibodies at room temperature for 1 hour in the dark, rinsed with blocking solution, and then fixed. The same concentrations of the primary and secondary antibodies were used as for IFA. Cells that were incubated with the secondary antibody only were used to measure the background staining. Cells were resuspended in 3 % horse serum in PBS and filtered using Flowmi tip strainers (Bel-Art) before flow analysis. A total of 10,000 events were collected for each sample which were analyzed using a BD Accuri C6 flow cytometer (BD Biosciences).

4.2.9 Cell viability after injection through a syringe and needle

To further assess the potential of the microspheres as vehicles for injectable cell delivery, the effect of shear stress during injection on cell viability was studied. Microspheres were suspended in cold equine serum, with a viscosity of 1.909 cP at 14 °C, loaded into 1 mL luer lock syringes, and sheared through 18 gauge, 20 gauge, and 23 gauge needles respectively at 1 mL/minute (Aguado et al. 2012). The XTT Cell Viability Assay Kit (Biotium) was then used to evaluate cell viability and proliferation. Following the injection simulation, microspheres containing ECFCs were aliquoted into a 96-well-plate with one microsphere per well. 100 µL of pre-warmed medium and 25 µL of XTT working solution were then added to each well. After incubation for 18 hours at 37 °C, absorbance signal of the sample was measured with a microplate reader (BioTek). Four separate trials were performed; viability was assessed for five microspheres per condition per trial and data for each trial normalized with respect to control optical density.

4.2.10 Microspheres for subcutaneous injection

Ex vivo cell delivery and survival of encapsulated ECFCs

A cadaver limb from an adult horse collected immediately after euthanasia (for reasons unrelated to this study) was used to evaluate cell delivery *ex vivo*. The hair of the dorsomedial aspect of the metacarpus was clipped and two 6.25 cm^2 square, full-thickness wounds were created

using a surgical template. Trypan blue stained PEGDA microspheres in saline or ECFCs encapsulated into PF microspheres in serum were injected (600 μL) subcutaneously at the wound edge. Injections were made through an 18-gauge x 1" needle on a 1 mL luer lock syringe. Trypan blue stained PEGDA microspheres were directly visualized. A full thickness section of skin and subcutaneous tissue surrounding the area of injection was removed using a scalpel blade and placed in cell culture media and incubated over night at 37 °C. Subcutaneous tissue was bluntly dissected at 24 hours and visualized with fluorescent and phase contrast microscopy.

***In vivo* injection and cell tracking of autologous ECFCs encapsulated in PF microspheres**

Three adult horses were used to evaluate delivery of encapsulated, autologous ECFCs labeled with Qtracker 655 (Invitrogen) to full thickness wounds created on the distal limb. Autologous ECFCs were labeled with 4 μM Qtracker 655 according to the manufacturer's instructions prior to encapsulation. The equine distal limb wound model was created in a similar manner to previous studies (Celeste et al. 2013, Celeste et al. 2011, Deschene et al. 2011). Horses were kept free in individual box stalls for the duration of the study and allowed ad libitum access to grass hay and water. For the surgical procedure, analgesia and sedation were provided with detomidine hydrocholoride (0.01 mg/kg; IV) and butorphanol tartrate (0.04 mg/kg; IV), and local anesthesia was performed using 2 % mepivacaine hydrochloride. The surgical sites were clipped and aseptically prepared, and two 6.25 cm^2 square, full thickness wounds were created on the dorsal aspect of each metacarpus and metatarsus using a sterile wound template and a #15 scalpel blade. 24 hours after surgery, the edges of 2 wounds per horse were injected subcutaneously using 18 gauge 1" needles on 1 mL luer lock syringes with autologous ECFCs encapsulated in PF microspheres diluted into equine serum (600 μL). Each injection of cell-laden microspheres contained approximately 2 x 10^6 ECFCs in PF microspheres. All 4 edges of the wound were

injected for a total of 8 x 10^6 ECFCs in PF microspheres per wound. As the wound model was also being utilized for a larger, ongoing treatment trial with ECFCs, the remaining wounds were treated in duplicate with autologous ECFCs (2 x 10^6), PF microspheres, and equine serum only and evaluated weekly until complete healing (approximately 6 weeks). One week after injection, the horses were sedated, local anesthesia performed, and then the lateral leading edge of each was biopsied using a 6 mm punch biopsy instrument. One biopsy sample was placed in optimal cutting temperature (OCT) freezing media and snap frozen in liquid N_2 cooled isopentane and the other sample was formalin fixed and paraffin embedded for immunohistochemical analysis as part of the wound healing study. Frozen tissues were cryosectioned (20 μm), placed on glass slides, fixed in 4 % PFA, stained with DAPI, and imaged with confocal microscopy.

4.2.11 Statistical analysis

Data are represented as means ± SD. All statistical analysis was performed using Minitab 17 Statistical Software (Minitab Inc.). After verifying equal variances using the F-test, the Student's t-test was used for comparisons between two groups. After checking for normality of distribution, one-way ANOVA followed by the Tukey-Kramer HSD test for multiple comparisons was used to evaluate statistical significance between multiple groups. Unless otherwise indicated, $p < 0.05$ was considered statistically significant.

4.3 Results

4.3.1 High cell viability and uniform microsphere geometry post-encapsulation

Microspheres formed using the custom-built PDMS molded microfluidic device were highly uniform and provided a suitable microenvironment for cell proliferation and survival. Following microsphere encapsulation, ECFC viability was very high (96.8 ± 1.4 %) as shown in Figure 4.2A-D. The microspheres produced were highly uniform in both size and roundness. The diameters

were 598 ± 45 µm on Day 1 and 584 ± 22 µm on Day 3; while the roundness was 0.95 ± 0.001 on Day 1 and 0.91 ± 0.001 on Day 3 as shown in Figure 4.2E-H.

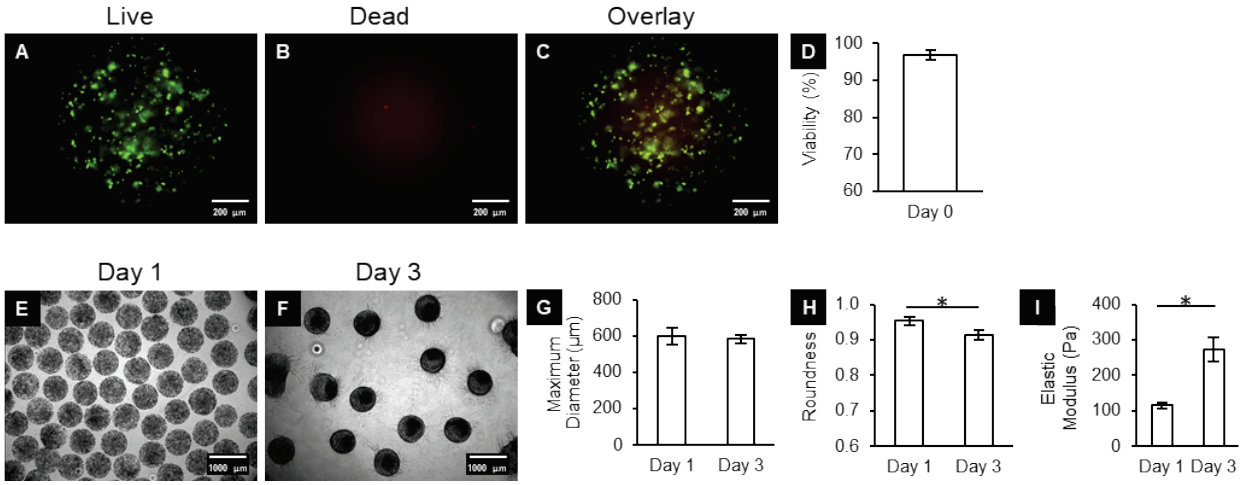

Figure 4.2 High microsphere uniformity and cell viability post-encapsulation. (A–D) Immediately post-encapsulation (day 0), ECFC viability was 96.8 % as quantified using Live (green)/Dead (red) staining (n = 3 separate encapsulations with >3 microspheres evaluated per encapsulation). (E, F) Phase-contrast images showing ECFC-encapsulated microspheres on days 1 and 3. Similar maximum diameter (G) and high roundness (H) of the microspheres on days 1 and 3 (n = 3 separate encapsulations with 30–100 microspheres evaluated per encapsulation). Roundness significantly decreased by day 3 (*$p < 0.05$). (I) Elastic modulus of microspheres significantly increased from days 1 to 3 (*$p < 0.01$, $n \geq 4$ microspheres per condition).

4.3.2 Increased elastic modulus and outgrowth from microspheres indicating cell proliferation post-encapsulation in PEG fibrinogen microspheres

The stiffness of the microspheres was assessed in terms of elastic modulus. The elastic modulus of the microspheres with encapsulated ECFCs increased significantly from 141 ± 10 Pa on Day 1 to 354 ± 62 Pa on Day 3 (Figure 4.2I). This increase was potentially a result of increased ECFC density and re-organization within the microspheres (Figure 4.2F).

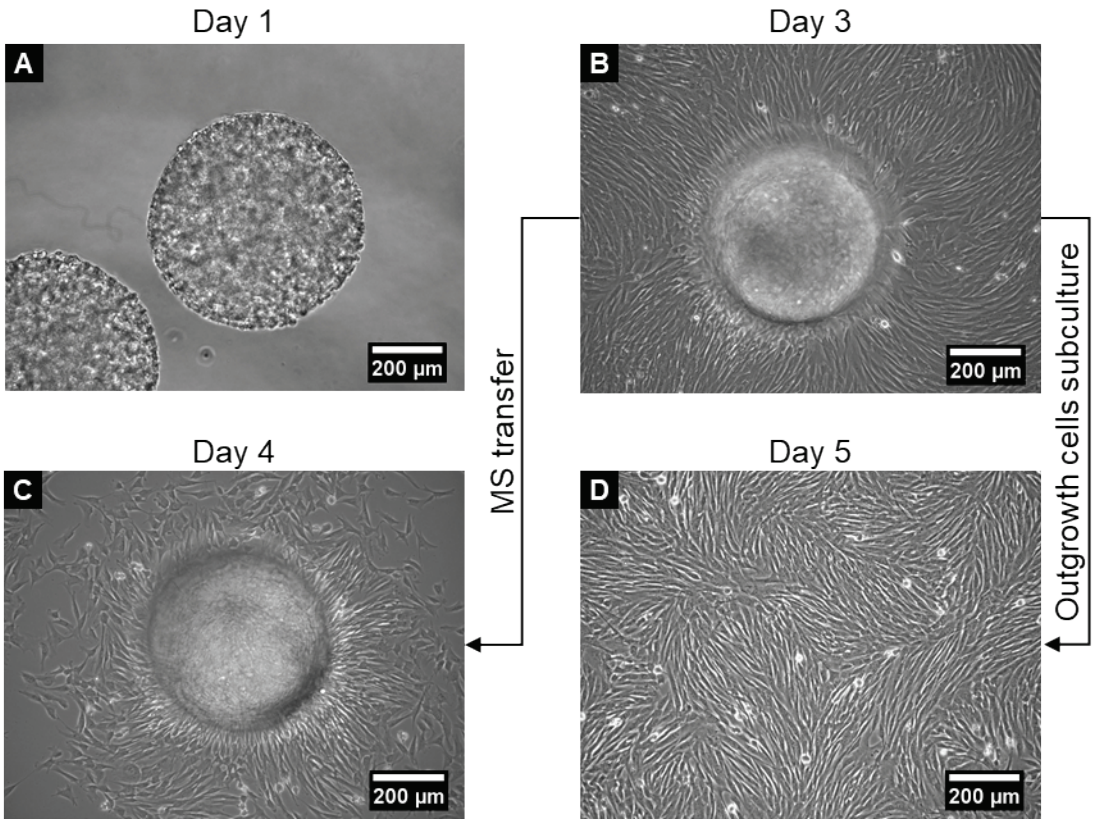

Figure 4.3 Phase-contrast images showing ECFC migration, and proliferation phenotypes were maintained post-encapsulation. (A) By day 1, cells are aligning and covering the surface of the MS. (B) Outgrowth ECFCs from the MS forming a confluent monolayer on day 3. (C) Outgrowth ECFCs proliferating 1 day after transfer of MS to a new well plate. (D) ECFCs subcultured from the confluent monolayer of outgrowth ECFCs maintain a characteristic high proliferation rate. MS, microsphere.

In addition to maintaining a high level of viability, the ECFCs also remained highly proliferative post-encapsulation. On Day 1, the encapsulated ECFCs were observed to align and cover the surface of the microspheres (Figure 4.3A). As ECFCs continued to remodel the microspheres, a confluent monolayer of ECFCs was observed on the bottom of the well plate by Day 3 indicating active cell migration and proliferation (Figure 4.3B). After the ECFCs and

microspheres were trypsinized and transferred to a new well plate, ECFCs were again observed on the bottom of the well plate around the re-plated microspheres after just one day (Figure 4.3C). In addition, the confluent monolayer of outgrowth ECFCs observed on Day 3 was passaged, and the passaged outgrowth ECFCs again formed a confluent monolayer at an equivalent rate to encapsulated control ECFCs, indicating that the ECFCs maintained their highly proliferative nature following microsphere encapsulation of the ECFCs (Figure 4.3D).

4.3.3 Outgrowth ECFCs maintain their phenotype

ECFCs have the same phenotypic characteristics pre- and post-encapsulation. Both outgrowth ECFCs and non-encapsulated ECFCs (only cultured on tissue culture polystyrene (TCPS) flasks) were able to form tubular networks on Matrigel, take up DiI-Ac-LDL, and express vWF as shown in Figure 4.4A-H. Endothelial function and expression of markers previously used to characterize equine ECFCs (Salter et al. 2015) were evaluated quantitatively in both groups of ECFCs using flow cytometry. For ECFCs that were only cultured on TCPS flasks (non-encapsulated), 98.6 ± 1.4 % of cells demonstrated uptake of DiI-Ac-LDL, 99.8 ± 0.2 % of cells expressed vWF, 99.8 ± 0.2 % expressed CD105, and 98.1 ± 1.5 % expressed CD14 (Figure 4.4I). In outgrowth ECFCs from the microspheres, 99.0 ± 1.6 % of cells demonstrated uptake of DiI-Ac-LDL, 99.3 ± 0.6 % of cells expressed vWF, 98.5 ± 1.7 % expressed CD105, and 98.4 ± 1.0 % expressed CD14 (Figure 4.4I). No significant differences were found between the two groups.

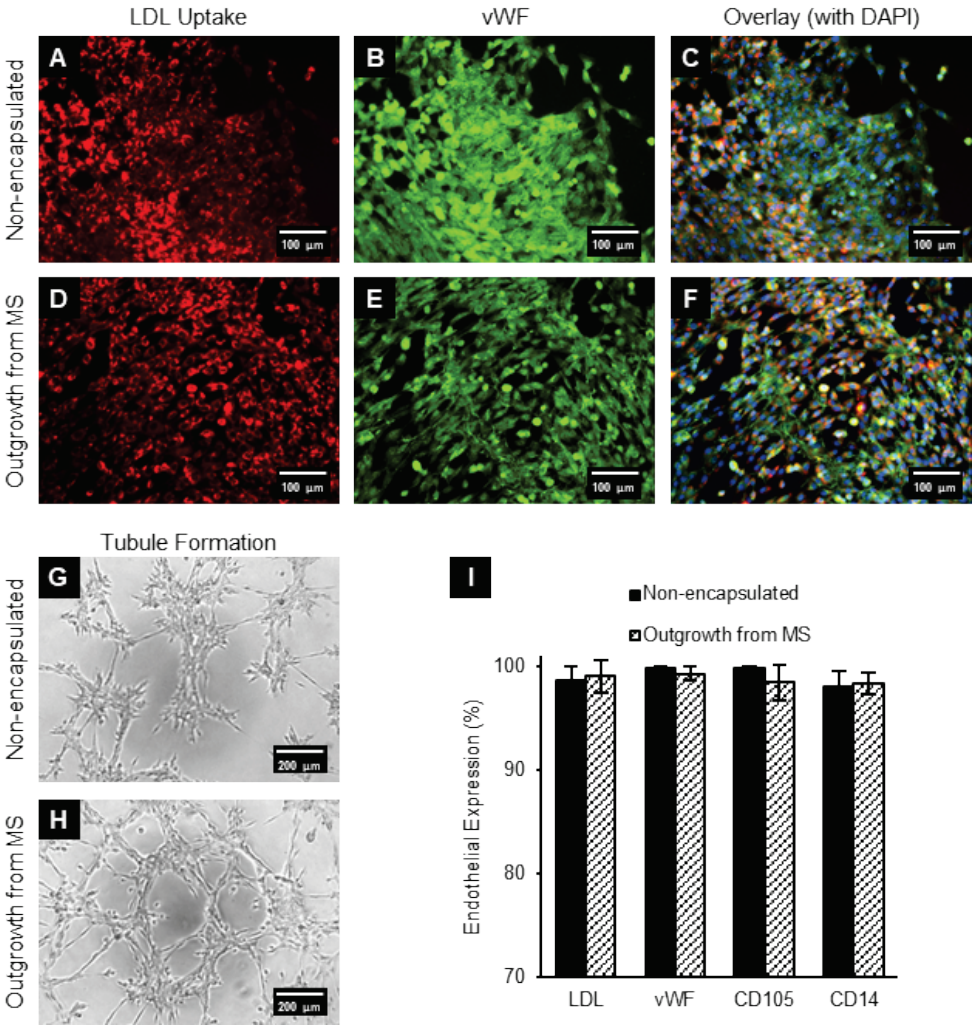

Figure 4.4 ECFCs maintained their endothelial phenotype after encapsulation and culture in PF microspheres. Outgrowth ECFCs from microspheres showed similar endothelial phenotype compared to nonencapsulated ECFCs in terms of DiI-Ac-LDL uptake, vWF expression (A–F), and tubule formation (G, H). (I) No difference was found in expression of markers (vWF, CD105, and CD14) or DiI-Ac-LDL uptake between the outgrowth ECFCs from microspheres and nonencapsulated ECFCs (flow cytometry, n = 3 separate encapsulations).

4.3.4 Microspheres are retained and encapsulated cells are viable in tissue after subcutaneous injection and shear through different gauge needles

To evaluate the potential of using hydrogel microspheres for cell injection therapy, the retention of microspheres in tissue and the viability of encapsulated ECFCs after shear through different needle gauges was examined ex vivo. There was no statistical difference in the viability of encapsulated ECFCs as quantified by XTT assay after shear through 18, 20, and 23 gauge needles (Figure 4.5A). Cell-free microspheres that were created with PEGDA and stained with trypan blue were injected subcutaneously into the edge of a wound created on an equine cadaver limb using 18 gauge 1" needles. The injected microspheres remained in the subcutaneous tissue at the wound edge without any visually obvious breakdown or deformation of the microspheres (Figure 4.5B).

An *ex vivo* experiment was then performed to evaluate viability and migration from the microspheres of the encapsulated cells when injected into and surrounded by host tissue. After one day of *ex vivo* culture at 37 °C, subcutaneously injected microspheres remained present as a group within the tissue as indicated by the green autofluorescence of eosin Y (Figure 4.5C). Furthermore, encapsulated ECFCs became elongated and formed tubules along the surface of the microspheres (Figure 4.5D). This observation was similar compared to the *in vitro* study shown in Figure 4.3.

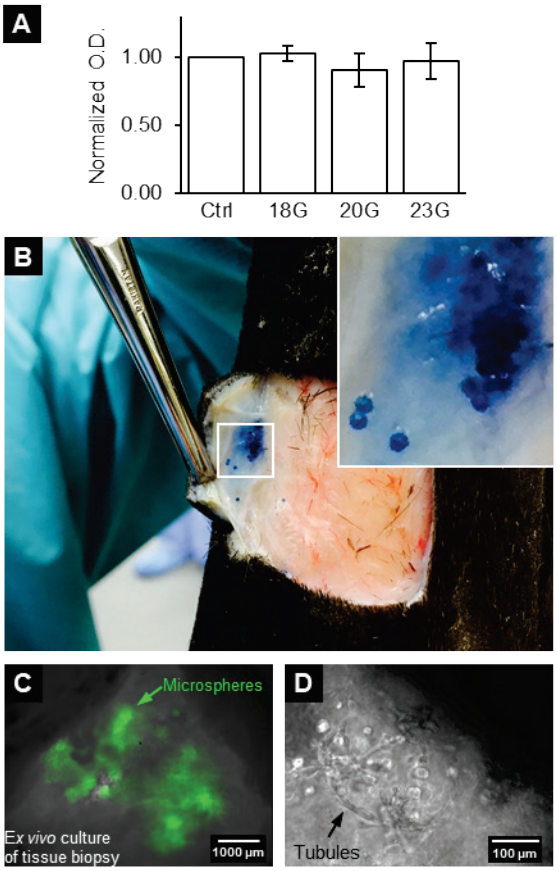

Figure 4.5 Injected microspheres supported cell delivery. (A) XTT assay indicated the encapsulated ECFCs (day 1) remained viable after shearing through different sizes of needles (n = 4 separate encapsulations normalized to control). There is no statistical difference between conditions. (B) PEGDA microspheres (stained with trypan blue) remained localized in the tissues after subcutaneous injection at the edge of a wound in a cadaver limb from a horse. (C) Overlay image of the autofluorescence of ECFC-laden PF microspheres (green) in a horse subcutaneous tissue 1 day after ex vivo culture. (D) Phase-contrast image showing tubule formation (black arrow) of the encapsulated ECFCs on the surface of the microspheres in subcutaneous tissue 1 day after ex vivo culture.

4.3.5 PEG Fibrinogen encapsulated ECFCs are retained at the injection site and beginning to migrate out of PF 7 days after *in vivo* subcutaneous injection

An *in vivo* study was performed in 3 horses to evaluate cell retention and outgrowth of the encapsulated ECFCs to the surrounding host tissue. Autologous ECFCs were labeled with Qtracker 655 (red, Figure 4.6A) and then encapsulated at a concentration of 10 million cells per mL of PF precursor solution, which was necessary to achieve the desired dose of 2 million cells for each injection. For each horse, ECFCs were encapsulated for 4 injections per wound with two wounds per animal plus an *in vitro* control, meaning that 24 million cells were encapsulated. After microfluidic system setup, encapsulation took approximately 12 minutes per 2 million cell injection.

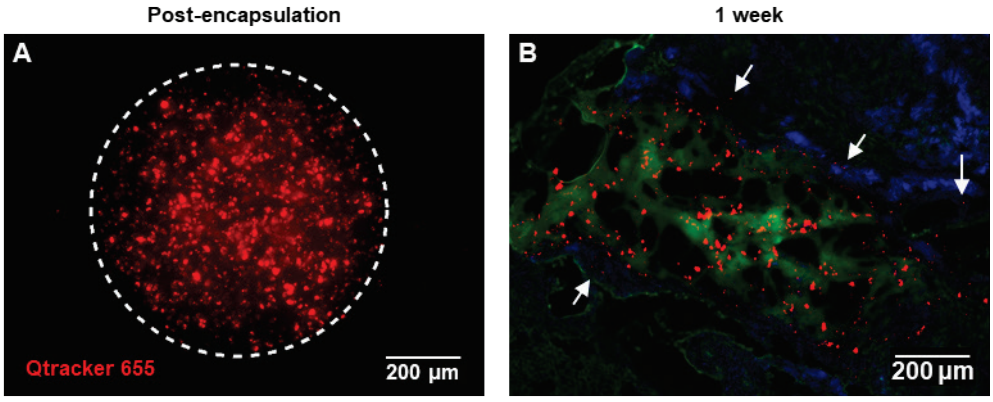

Figure 4.6 Qtracker-labeled ECFCs remained visible for cell tracking post-encapsulation and 1 week after *in vivo* injection. (A) Fluorescent microscopy showed the presence of Qtracker-labeled ECFCs (fluorescent red in color) encapsulated in microspheres before injection. (B) Encapsulated ECFCs (red) were found in cryosectioned biopsy 1 week after injection. Migration of ECFCs to host tissue was observed (white arrows).

Following rinsing and resuspension, cell-laden microspheres were injected into the edges of distal limb wounds in 3 adult horses. One week post-injection of the microspheres into the edge of

a wound, the Qtracker labeled ECFCs (red) were identified in the biopsy of all 3 horses as shown in a representative biopsy sample in Figure 4.6B. The injected microspheres were still present in 1 horse as shown by the green autofluorescence. There was evidence of migration of some ECFCs from the microspheres to the surrounding host tissue suggesting viable cells as indicated by the white arrows. The PF encapsulated ECFCs were verified to be retained at the injection site and demonstrating outgrowth 1 week after subcutaneous injection.

4.4 Discussion

For veterinary and human clinical applications, delivery of therapeutic cells by injection has the advantage of being minimally invasive. Here we demonstrate the rapid encapsulation of equine ECFCs in PF microspheres using a custom-built microfluidic encapsulation system, verify the uniformity of resulting microspheres and maintenance of cell viability, proliferative capacity, and phenotype, and establish the ability of these microspheres to be used for delivery of cells by injection for autologous cell therapy.

Having employed the equine wound healing model, we have tested the ability of our cell encapsulation system to be used for the large numbers of cells (2 million cells per injection, 8 million cells per wound) that are likely necessary to achieve therapeutic benefit. The achieved cell concentration of 10 million cells per mL of hydrogel precursor solution is substantially higher than what has been reported for other microencapsulation systems, which was necessary to maintain a reasonable injection volume (200 μL of microspheres suspended in serum for a total of 600 μL). Also, the time required for encapsulation is short, which was necessary to produce sufficient numbers of encapsulated cells within a reasonable timeframe for this large animal model and eventual clinical use.

Utilization of hydrogel technologies has received much attention for regeneration of vasculature and ultimately healing of a range of vascular diseases and disorders (Rufaihah and Seliktar 2016). Previous work has primarily focused on the formation of macroscopic tissues and polymerization of the cell/hydrogel precursor in situ, both of which would frequently require a surgical approach for many clinical applications (Klouda 2015, Hacker and Nawaz 2015). As an alternative approach, cell microencapsulation for the purpose of therapeutic cell delivery has been investigated as recently reviewed (Olabisi 2015, Barron and He 2017, Jiang et al. 2016). While technically challenging to produce, hydrogel microspheres have many advantages for use in cell delivery compared to cell/scaffold implantation methods. Microspheres are able to be more widely distributed across a wound or tissue than cell-supporting scaffolds with other geometries, while maintaining short diffusion distances from the host tissue, and microspheres can be injected at one or more sites which increases their flexibility for clinical use and reduce surgical trauma from implantation (Williams et al. 2005). Microfluidic systems have better control in producing microspheres with a narrow size distribution compared to traditional methods including bulk emulsification, electrostatic dripping, extrusion methods, and hydrodynamic dripping (Velasco, Tumarkin, and Kumacheva 2012). By utilizing an emulsification technique in microfluidic systems, hydrogel microspheres can be fabricated with various stream geometries, including flow-focusing, T-junction, terrace-like, and co-flowing (Tumarkin and Kumacheva 2009). However, typical cell encapsulation in microspheres using microfluidic devices has been limited by low cell density which makes delivery of sufficient cell numbers in reasonable volumes for therapeutic applications challenging (Velasco, Tumarkin, and Kumacheva 2012). The microfluidic device presented here is capable of encapsulating ECFCs at a high cell density of 10 million cells/mL, which is essential for delivering a reasonable volume of microspheres while having an effective

number of cells for cell therapy. Besides, microfluidic devices are generally fabricated using photolithography which requires expensive microfabrication facilities. The channel height of the microfluidic devices is also restricted due to the limited thickness of the photoresist on wafer. In this study, the microfluidic device does not require expensive facilities for photolithography and can be used for encapsulating cells in hydrogel microspheres that are larger in size. In addition, the use of emulsification and the microfluidic system together achieved highly reproducible and tightly controllable microsphere size and geometry.

We used an equine wound model to study *in vivo* cell delivery for this study. There are only a few studies using biomaterial scaffolds to optimize the function of stem cells in equine regenerative medicine, most of which have involved musculoskeletal disease (Ferris et al. 2012, Youngstrom et al. 2013, Watts, Ackerman-Yost, and Nixon 2013). This is the first study to use PF hydrogels for cell delivery/tissue healing/regenerative studies in veterinary medicine. The potential benefit of EPC treatment in other models of poor wound healing due to poor vascularization (Drela et al. 2012, Asai et al. 2013) prompted the use of autologous equine ECFCs for use in the current study.

Promoting rapid vascularization is one of the biggest challenges in using engineered tissues for enhancing wound healing and treating disease (Moon et al. 2010). While ECFCs, or late EPCs, have been described in the literature as the only subtype of EPC that is responsible for building vessels, evidence has also shown that early EPCs promote angiogenesis through a paracrine mechanism (Urbich et al. 2005, Medina et al. 2017). Recent studies have also suggested that adult stem cell therapy provides a majority of benefits through paracrine effect rather than direct tissue replacement (Luo et al. 2017, Tang et al. 2017). Although assessing the use of ECFC alone to achieve rapid wound healing is beyond the scope of this study, the presented method of combining

ECFCs with engineered biomaterials allows the direct delivery and retention of ECFCs, as well as the appropriate growth factors and signaling molecules needed, in the area of interest.

Encapsulation of ECFCs in PF hydrogels has great potential in tissue engineering and clinical applications. PF was developed to create a controllable, degradable, and biofunctional 3D scaffold for cell culture (Almany and Seliktar 2005). While PEG provides high biocompatibility and versatile physical structure, fibrinogen provides biological functionality including protease degradation capability (Werb 1997) and cell-adhesion motifs (Herrick et al. 1999). It is to our best knowledge that this is the first study of encapsulating autologous ECFC in PF that support ECFC survival, proliferation, and outgrowth migration for tissue regeneration application. Encapsulated ECFCs were observed to cover the surface of the microspheres by Day 3 showing that they are able to migrate through and remodel the PF hydrogel microsphere. Whereas microsphere size remained the same through Day 3, the modulus increased, indicating the microspheres supported cell growth.

One of the most common challenges in cell therapy is the inability to benefit from all the injected therapeutic cells. Direct injection of cells alone is commonly used in human and veterinary regenerative medicine and may minimize the complexity of the delivery; however, the cells are not retained or do not migrate to the area of interest. Studies have shown that intracoronary delivery of cardiomyocytes by saline injection caused cells to appear in lung, liver, and spleen (Dow et al. 2005). The loss of cells to other organs through the vascular system may also impose other complications. For instance, intravenous delivery of ECFCs may contribute to tumorigenesis, atherosclerosis or retinopathy, so this strategy should be followed clinically with the utmost caution (Rafii and Lyden 2003). In addition, ischemic areas may have a low blood supply, so intravenous delivery of ECFCs may not reach the site of injury. Therefore, local delivery of cells

that results in high retention is critical. By injecting the microspheres with labeled cells directly at the site of injury, we were able to verify the presence of cells 1 week after injection.

4.5 Conclusions

We developed a unique microfluidic system to encapsulate ECFCs in PF hydrogel microspheres. High concentrations of cells could be rapidly encapsulated making the system practical for use in cell encapsulation for large animal therapeutic cell delivery. The resulting cell-laden microspheres were highly uniform in size and geometry with strong consistency between batches. The ECFCs had high viability and proliferation post-encapsulation. Outgrowth ECFCs from microspheres exhibited the same phenotype as ECFCs maintained in traditional monolayer culture. As a proof of concept, microspheres encapsulated with Qtracker labeled ECFCs were injected into an equine distal limb wound model, and cell retention at the injection site and migration of outgrowth ECFCs into the host tissue was observed one week after injection confirming that this is a feasible system for injectable cell delivery.

5. CHAPTER 5: Induction of Endothelial Colony Forming Cell Dynamic Adhesion Using Peptides

5.1 Introduction

A major cause of cardiovascular disease is atherosclerosis, where a plaque is formed within the artery wall. When severe atherosclerosis has developed, surgical treatments including coronary artery bypass graft or angioplasty are normally performed to restore blood flow to the ischemic region of heart. However, restenosis either on synthetic vascular graft or at the stent implantation region is one of the main long-term causes of failed surgery. Much research has been done on prevention of restenosis using strategies such as pharmacotherapy (Walter et al. 2002), growth factors (Asahara et al. 1995), and nitric oxide (Lipke and West 2005, Taite et al. 2008). Despite substantial progress made in artificial biocompatible surface technologies, the endothelium remains the ideal surface to prevent thrombogenesis and neointimal hyperplasia.

The endothelium, which is the lining of the blood vessel, consists of a monolayer of ECs. ECFCs, a subtype of EPCs, are unipotent stem cells carrying a high proliferative capability and are able to differentiate into ECs, making them a promising cell source for rapid reendothelialization of vasculature (Medina et al. 2017). Much research is done to promote reendothelialization by capturing circulating ECFCs using various strategies, including cytokines (Kong et al. 2004), antibodies (Aoki et al. 2005), peptides (Jun and West 2004, Seeto, Tian, and Lipke 2013), magnetic molecules, oligosaccharides, and aptamers (Avci-Adali, Ziemer, and Wendel 2010).

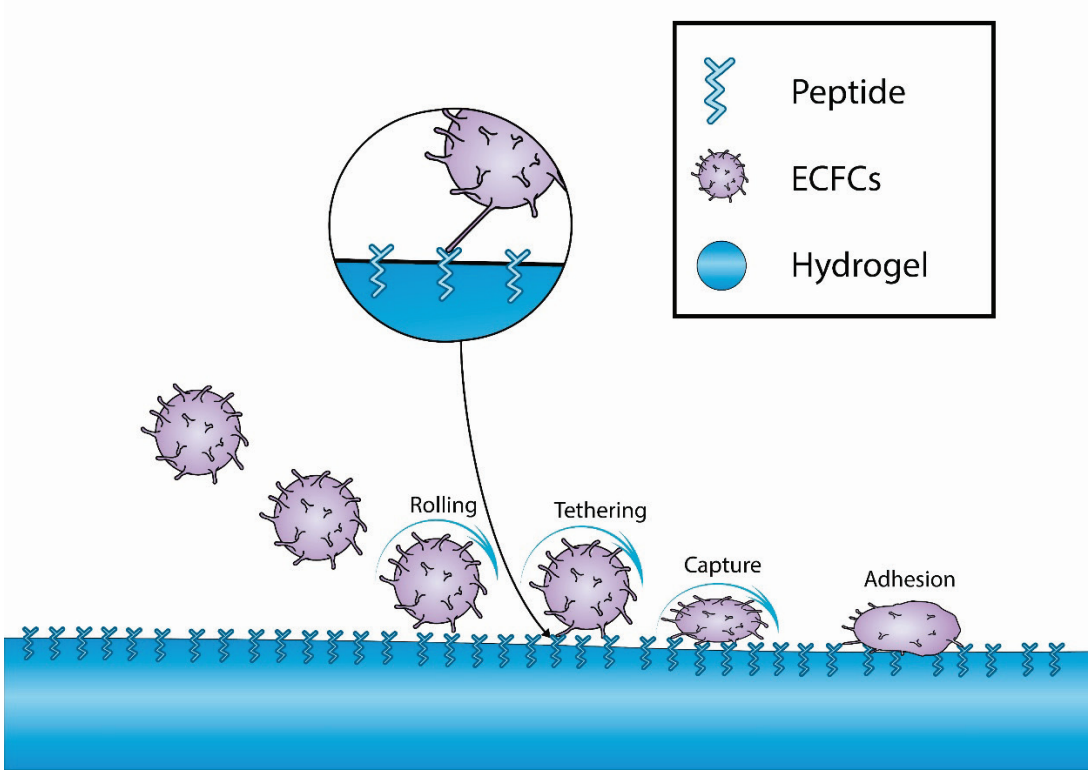

Figure 5.1 Schematic of ECFC dynamic adhesion on a peptide grafted-hydrogel surface.

Adhesion of cells to other cells and to extracellular matrix is a dynamic process and is crucial to biological functions such as immune response and tissue healing or remodeling (Springer 1995). During the rolling adhesion process, leukocytes, hematopoietic progenitors, and platelets are recruited to the site of infection or injury on the vascular surface under blood flow. Cells tether and roll along the vessel wall, decelerate, arrest, and migrate (McEver and Zhu 2010). Integrins are among the cell surface receptors that participate in the rolling process and mediate firm adhesion. They specifically bind to ligands represented on the vessel surface. By forming and breaking the bond rapidly, the cells will roll along the vessel wall. The dynamic adhesion of leukocytes mediated by cell surface receptors has been previously investigated (Ley et al. 2007, Vergnolle 1999, Chang, Tees, and Hammer 2000, Sperandio et al. 2003); however, relatively little

work has been done to study cell surface receptor-mediated, especially integrin-mediated, dynamic adhesion of ECFCs for reendothelialization (Angelos et al. 2010).

In this study, novel peptides and peptide combinations containing integrin-binding sequences were designed to support dynamic adhesion of ECFCs (Figure 5.1). Compared to natural components like protein, peptides have advantages including the rapid synthesis process, minimal batch to batch variability, and precise structural control. To eliminate non-specific interactions, PEGDA hydrogels, which have been shown to resist protein adsorption and cell adhesion (Gombotz et al. 1991), have been used as substrate. Peptides are then grafted onto PEGDA hydrogels through photocrosslinking for assessment. The peptide REDV, which can bind specifically to $\alpha_4\beta_1$ integrin (Massia and Hubbell 1992), has been demonstrated to reduce the velocity of the ECFCs while rolling but cannot support ECFCs adhesion (Seeto, Tian, and Lipke 2013). Some other peptide sequences are able to support ECFCs adhesion, such as peptide RGDS (Koivunen, Wang, and Ruoslahti 1994, Mardilovich et al. 2006). The peptide RGDS has been found in various ECM proteins including fibronectin, vitronectin, laminin, and collagen. RGDS-grafted PEGDA hydrogel has been shown to support ECFC rolling *in vitro* using a parallel flow chamber (Seeto, Tian, and Lipke 2013). Based on the mechanism of ECFCs dynamic adhesion, a combination of peptides might be more efficient in capturing the cells under shear flow. To verify this assumption, both novel peptides and their combinations were assessed on their ability to support ECFC tethering, rolling, and adhesion.

5.2 Materials and Methods

5.2.1 ECFC culture

Human ECFCs were kindly provided by Dr. Mervin Yoder, School of Medicine, Indiana University. Cells were cultured on collagen (Type I; Corning)-coated polystyrene flasks (Greiner

Bio One) in EGM™-2 media (Lonza) supplemented with 10 % (v/v) fetal bovine serum (Atlanta Biologicals) and 1.5 % (v/v) Antibiotic-Antimycotic (100x; Gibco). When ECFCs reached 90 % confluency, TrypLE™ Express Enzyme (1x; Gibco) was added to detach the cells at 37 °C for 2.5 minutes and then neutralized by ECFC media. Cells were collected by centrifugation at 200 g for 5 minutes, resuspended in ECFC media, and subcultured at a ratio of 1:3 or used for experiments immediately. Cells between passage 6-13 were used for experiments.

5.2.2 PEGDA synthesis and characterization

PEGDA was synthesized through acrylation of PEG (6 kDa; Sigma) by following a method reported previously (DeLong, Moon, and West 2005). Briefly, lyophilized PEG was dissolved in anhydrous dichloromethane (Acros) and reacted with acryloyl chloride (0.4 M; Alfa Aesar) and triethylamine (0.2 M; Sigma) under argon overnight. After the reaction, K_2CO_3 solution (1.5 M; Fisher) was added and fully mixed with the product through vigorous shaking, and the mixture was allowed to separate. The organic phase was collected, and anhydrous $MgSO_4$ (Fisher) was added to remove excess water and filtered out through vacuum filtration. PEGDA was precipitated with cold ethyl ether (J.T.Baker), collected through vacuum filtration, desiccated, and stored under argon at -20 °C. The acrylation percentage was quantified to be 96 % by nuclear magnetic resonance.

5.2.3 PEGDA hydrogel formation

The hydrogel precursor solution was prepared by dissolving PEGDA in phosphate buffer saline (PBS) to 200 mg mL^{-1}. The photoinitiator solution was prepared by dissolving 2,2-dimethoxy-2-phenylacetophenone (Acros) in N-vinylpyrrolidinone (Sigma) at 300 mg mL^{-1} and added to PEGDA solution at 10 µl mL^{-1}.

To form PEGDA hydrogels, the precursor solution was sandwiched in between two pieces of clean glass slides separated by a 500-μm thick spacer and held together using binder clips. The hydrogels were then photocrosslinked under a 365 nm UV lamp (3 mW cm^{-2}; Cole-Parmer) for 5 minutes. After the PEGDA hydrogels were formed, they were either stored in sterile PBS to be used as control groups or grafted with peptides as described below.

5.2.4 Peptide-grafting to PEGDA hydrogels

Peptides, either synthesized or purchased (American Peptide), were first conjugated onto acryloyl-PEG-succinimidyl valerate (acryloyl-PEG-SVA, 3400Da; Laysan Bio) and then grafted onto PEGDA hydrogels. Peptides were dissolved in sodium bicarbonate buffer (50 mM, pH 8.5). Acryloyl-PEG-SVA was dissolved in 1 mL of sodium bicarbonate buffer in a brown vial for every 10 mg of peptide. The molar ratio of peptide to acryloyl-PEG-SVA for reaction was 1.2:1. The peptide solution was then added dropwise to acryloyl-PEG-SVA solution. The mixture was reacted for at least 8 hours at room temperature. After the reaction, acryloyl-PEG-peptide was dialyzed (molecular weight cutoff 500-1,000; Spectrum Labs), lyophilized, and stored at -80 °C under argon.

To prepare peptide-grafted PEGDA hydrogels, the acryloyl-PEG-peptide was dissolved in PBS to 0.7 mM, and the photoinitiator solution was added to 10 μl mL^{-1}. After completion of PEGDA hydrogel photocrosslinking, the top glass slide was removed, and the 500-μm thick spacer was replaced by a 700-μm thick spacer. Peptide grafting solution was added on top of the PEGDA hydrogel, covered with a clean glass slide, and photocrosslinked under UV lamp for 7 minutes. The peptide-grafted hydrogels were stored in PBS overnight in fridge for swelling before experiments.

5.2.5 ECFC adhesion on peptide-grafted hydrogels

The capability of peptide-grafted hydrogels to support cell adhesion under static conditions was tested. The pre-swelled peptide-grafted hydrogels were placed in a 6-well plate. ECFCs were seeded on the hydrogels at 15,000 cells cm^{-2} and incubated for 1 hour at 37 °C and 5 % CO_2. After incubation, the hydrogels were gently rinsed with PBS, and the cell adhesion was assessed using microscopy.

5.2.6 Dynamic adhesion of ECFC under shear condition

The ECFC dynamic adhesion experiment was conducted using a parallel plate flow chamber system reported previously (Seeto, Tian, and Lipke 2013). ECFCs with 90 % confluency were detached from tissue culture flask and resuspended in pre-warmed media at 1 x 10^6 cells mL^{-1}. The cell suspension was kept in a reservoir, which had a 37 °C water jacket, and stirred at 150 rpm between each run to diminish cell aggregation. The shear flow was created by withdrawing cell suspension from the cell reservoir through the parallel plate flow chamber (Glycotech), placed on top of the peptide-grafted hydrogel, with a syringe pump (KD Scientific). Movement of ECFCs on hydrogels was recorded using a 20x microscope objective (Nikon) and a high-speed camera (Andor Luca S) at 73 fps for 2 minutes. A custom-developed data analysis system was employed to track ECFCs and analyze ECFC velocity (Seeto and Lipke 2016).

5.2.7 Statistical analysis

All data were presented as mean ± standard deviation (SD). All statistical analysis was performed using Minitab 19 Statistical Software (Minitab Inc.) After checking for normality of distribution, one-way analysis of variance (ANOVA) followed by Tukey-Kramer honest significant difference (HSD) test was performed to evaluate statistical significance between multiple groups. Statistical significance was declared if $p < 0.05$.

5.3 Results and Discussion

5.3.1 Set cutoff velocity for identifying tether event

PEGDA hydrogels are used to set the cutoff velocity for identifying tether events during the cell rolling process. When rolling on peptide-grafted hydrogels, the cells experience rapid velocity fluctuation, including deceleration and acceleration. The deceleration is mainly a result of a tether force applied through the bond formed between cell surface receptors and the peptides, which is defined as the tether event here. During this process, the force from the flowing fluid also exerted on the cells, leading to the dissociation of the bond, resulting in cell acceleration. Besides the specific interaction, non-specific interactions such as friction can also contribute the deceleration. To eliminate the instantaneous velocity resulting from non-specific interaction, PEGDA hydrogels which have been shown to resist protein adsorption and cell adhesion were used as substrates (Gombotz et al. 1991). The velocity of ECFCs on PEGDA hydrogels in the absence of grafted peptides was first assessed.

The average velocity of ECFCs on PEGDA hydrogels is shown in Figure 5.2A. The velocity increases as the shear rate increases from 20 s^{-1} to 120 s^{-1}. For each shear rate, the instantaneous velocity of cells was plotted, and the average instantaneous velocity was calculated to be 208, 411, 836, and 1165 μm/s, respectively (Figure 5.2B-E). The upper velocity limit for tether event was set as two standard deviations below the average instantaneous velocity (Ave-2SD), which was below the 95 % confidence interval. The cutoff velocity for identifying tether events was 168, 330, 669, and 917 μm/s, respectively for each shear rate. When ECFC rolling on peptide-grafted hydrogels, instantaneous velocities lower than the cutoff velocity were defined as tether events which are shown in Figure 5.2F. The percentage of tether events in the whole rolling process is defined as the tether percentage.

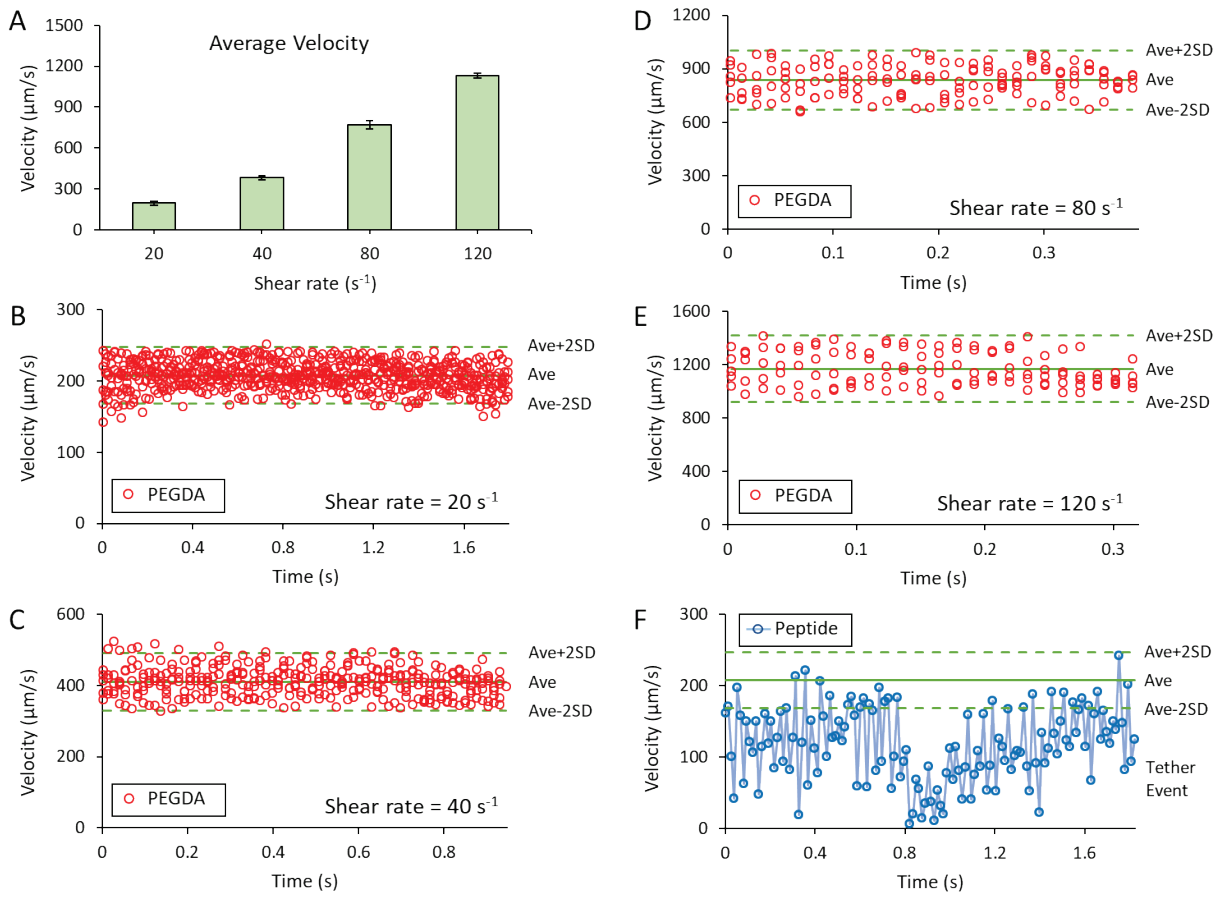

Figure 5.2 Cutoff velocity for identifying tether events. (A) The average velocity of ECFCs on PEGDA hydrogels under different shear rates. Data represent Mean ± SD (n = 3 separately prepared experiments per shear rate). (B-E) Cutoff velocity for identifying tether event was set as two standard deviations below the average instantaneous velocity of ECFCs on PEGDA hydrogels (n = 5 cells per shear rate). (F) An example showing when ECFC rolling on peptide-grafted hydrogels at shear rate = 20 s^{-1}, instantaneous velocities lower than the cutoff velocity were defined as tether events.

5.3.2 Tether events on peptide-grafted hydrogels

The dynamic adhesion of ECFCs consists of decelerating the cells through rolling and capture of the slow-downed cells. Peptides containing the REDV sequence can bind to $\alpha_4\beta_1$ integrin and

have been shown to have the ability to slow down the rolling ECFCs but cannot support ECFCs adhesion (Seeto, Tian, and Lipke 2013). The peptide RGDS has also been shown to support ECFC adhesion and rolling (Seeto, Tian, and Lipke 2013). Besides REDV and RGDS peptides, other peptides were also assessed including PHSRNSGSGSGSGSGRGDSG (P_RGDS), CRRETAWAC, PHSRNSGSGSGSGSGREDVG (P_REDV), and KSSPHSRNSGSGSGSGSGREDVG (KSSP_REDV) as listed in Table 5.1.

The peptide P_RGDS included RGDS and PHSRN sequences, which mimic the binding ligands of fibronectin for $\alpha_5\beta_1$ integrin. The RGDS sequence worked as the primary binding ligand and the PHSRN sequence worked as synergy binding ligand (Kauf, Hough, and Bowditch 2001). In between these two peptide sequences was the $(SG)_5$ sequence, whose role was as a linker to simulate the distance and the hydrophobicity/hydrophilicity between the PHSRN and RGDS sequences in the fibronectin molecule (Mardilovich et al. 2006, Mardilovich and Kokkoli 2004). The peptide P_RGDS has been demonstrated to support HUVECs adhesion and spreading. Having a high binding affinity and selectivity with $\alpha_5\beta_1$ integrin, the peptide CRRETAWAC has the capability of supporting ECFCs adhesion (Koivunen, Wang, and Ruoslahti 1994). The cysteines on each side of the peptide were designed to form a disulfide bond, making the peptide cyclic. The REDV-containing peptides including P_REDV and KSSP_REDV were synthesized to match the length of P_RGDS peptide.

Table 5.1 Peptide sequences and their abbreviations.

Integrin	Peptide	Abbreviation
$\alpha_5\beta_1$	RGDSG	RGDS
	PHSRNSGSGSGSGSGRGDSG	P_RGDS
	CRRETAWAC	CRRETAWAC
$\alpha_4\beta_1$	REDVG	REDV
	PHSRNSGSGSGSGSGREDVG	P_REDV
	KSSPHSRNSGSGSGSGSGREDVG	KSSP_REDV

Based on the mechanism of ECFCs dynamic adhesion, peptide combinations were also tested as listed in Table 5.2. Unless mentioned otherwise, in order to maintain consistent grafting of peptides, the combination of acryloyl-PEG-peptides was mixed with an equal molar ratio to a final concentration of 0.7 μmol/mL, which was the same concentration for single peptide grafting. The tether percentage of all tested peptides are shown in Figure 5.3 and Figure 5.4.

Table 5.2 List of peptide combinations.

$\alpha_5\beta_1$	$\alpha_4\beta_1$
RGDS	REDV
CRRETAWAC	REDV
P_RGDS	REDV
P_RGDS	P_REDV
P_RGDS	KSSP_REDV

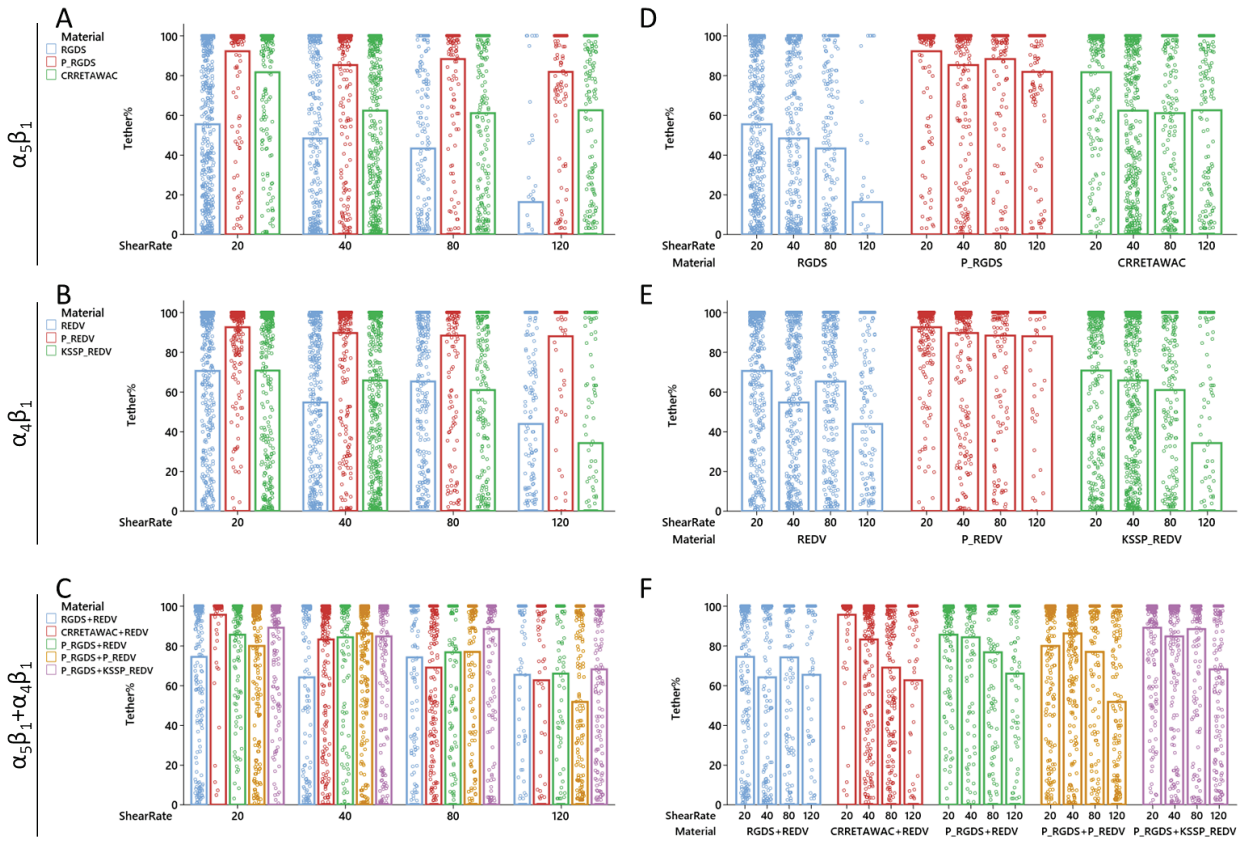

Figure 5.3 Tether percentage of peptide-grafted hydrogels. Peptides interacting with A) $\alpha_5\beta_1$ integrins and B) $\alpha_4\beta_1$ integrins, and C) peptide combinations interacting with both integrins were assessed and compared at different shear rates. (D-F) The effect of different shear rates was compared for the same peptides and peptide combinations. Each dot represents the result of a single cell, and the bar stands for the average of all cells assessed under the same condition. (n > 60 cells per condition)

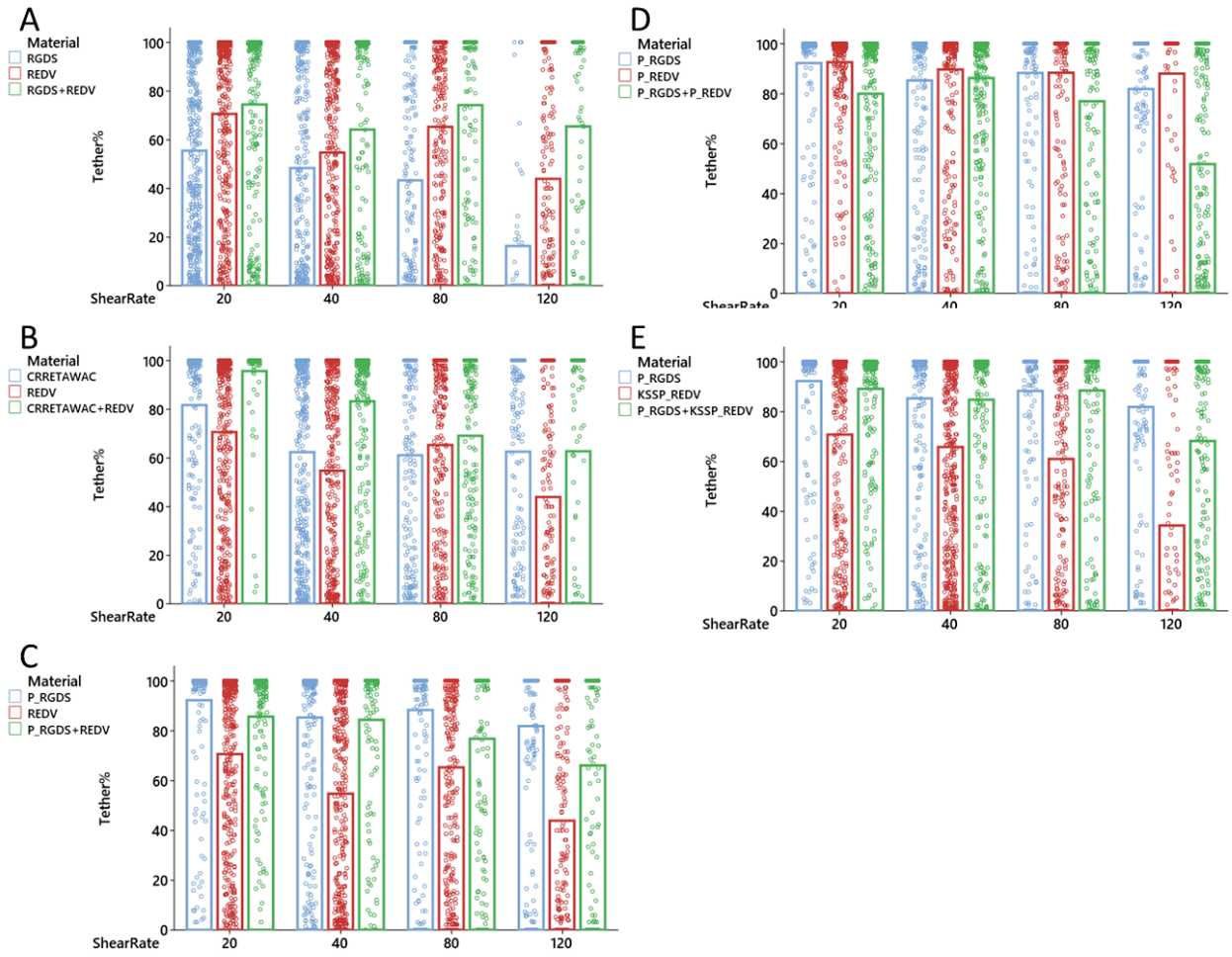

Figure 5.4 Tether percentage of peptide-grafted hydrogels. (A-E) Single peptides (shown in blue and red) were compared to peptide combinations (shown in green) at different shear rates. Each dot represents the result of a single cell, and the bar stands for the average of all cells assessed under the same condition. (n > 60 cells per condition)

5.3.3 Quantitative analysis of velocity fluctuation

As mentioned previously, the homing of circulating ECFCs is a dynamic process consisting of tethering, rolling, and adhesion. The bond between cell surface receptors and peptides form and break rapidly, leading to velocity fluctuation. The level of fluctuation may vary with peptide type

as shown in Figure 5.5A. In order to better quantify and assess the velocity fluctuation, the Velocity Increase Rate (r) is calculated as shown below.

$$V_2 = V_1(1 + r)$$

Where:

V_2 is the final instantaneous velocity;

V_1 is the original instantaneous velocity;

r is the velocity increase rate.

Then similar to calculating compound interest:

$$V_2 = V_1(1 + \frac{r}{n})^n$$

Where:

n is the compounding frequency.

When the frequency of compounding n gets to infinitely large, the formula will converge to a function as shown below.

$$\lim_{n\to\infty} \left(1 + \frac{r}{n}\right)^n = e^r$$

Then:

$$\frac{V_2}{V_1} = e^r$$

$$\ln V_2 - \ln V_1 = r$$

Where:

$\ln V_2$ and $\ln V_1$ is the natural log-transformed instantaneous velocity;

r is the log difference for instantaneous velocity.

The standard deviation of velocity increase rate, which indicates severity of velocity fluctuation, for all tested peptides are shown in Figure 5.5 and Figure 5.6.

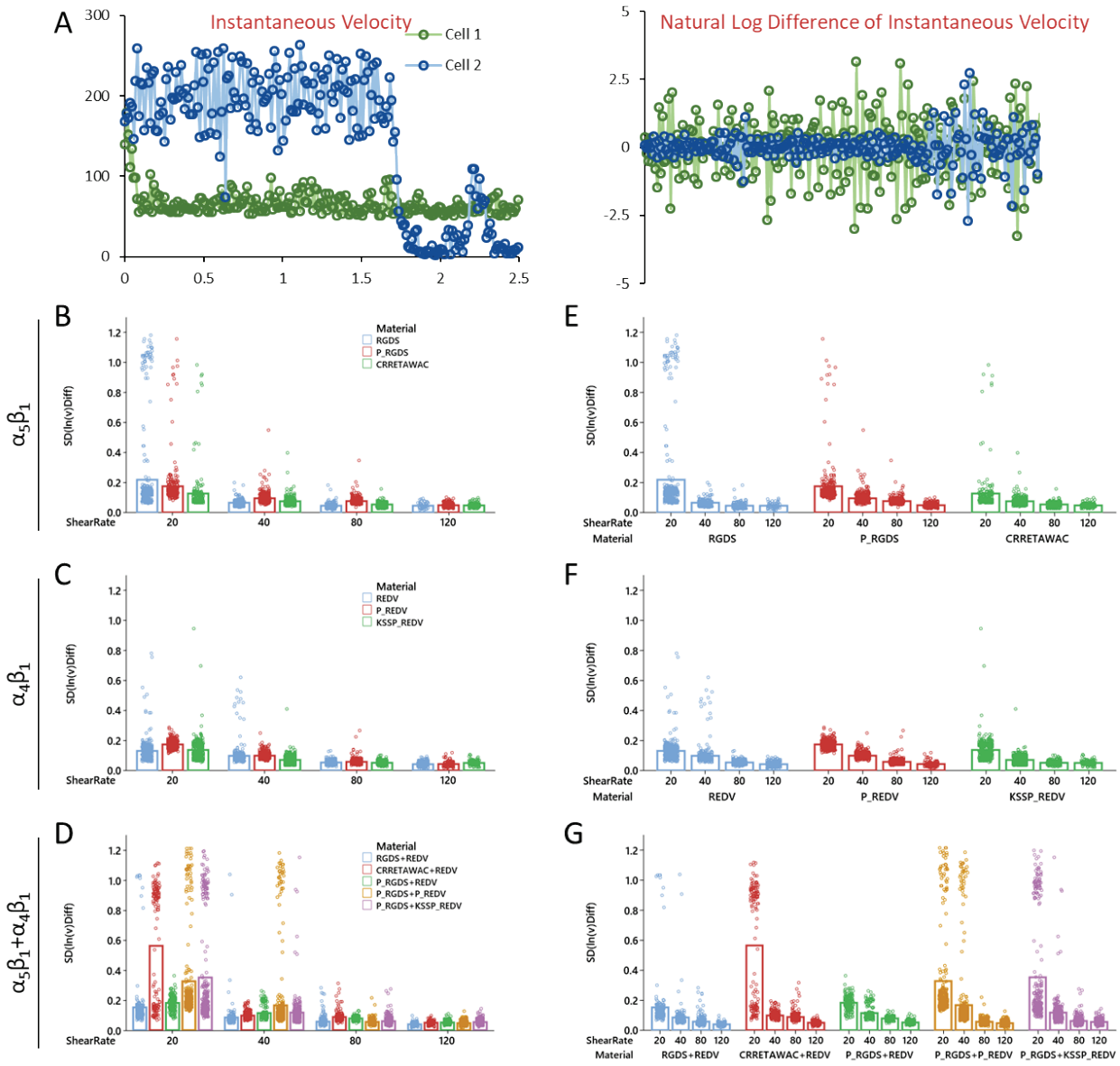

Figure 5.5 Evaluating velocity fluctuation using the standard deviation of velocity increase rate, which is calculated by the SD(ln(velocity) difference). (A) Instantaneous velocities and the corresponding ln(velocity) difference from two different rolling ECFCs with different velocity profiles. Peptides interacting with B) $\alpha_5\beta_1$ integrins and C) $\alpha_4\beta_1$ integrins, and D) peptide combinations interacting with both integrins were assessed and compared at different shear rates. (E-G) The effect of different shear rates was compared for the same peptides and peptide

combinations. Each dot represents the result of a single cell, and the bar stands for the average of all cells assessed under the same condition. (n > 60 cells per condition)

The result shows that when ECFCs were rolling under a higher shear rate, the cells would experience a less severe velocity fluctuation. One possible explanation is that when the shear rate was high, the cells would move faster. Faster cell velocity would shorten the contact time between peptides and cell surface receptors, thus affecting the efficiency of tethering (McEver and Zhu 2010). When the shear rate was 20 s^{-1}, the ECFCs had a relatively low rolling velocity and would experience a more efficient interaction with the peptides. It is found that the velocity fluctuated more severe for ECFCs rolling on the RGD-containing peptides, including peptide P_RGDS and RGDS. This is probably because the RGD-containing peptides could support both ECFC deceleration and adhesion, which could lead to pauses of cells during the rolling process. The pauses of cells would cause quick changes in rolling velocity. Besides the RGD-containing peptides, peptide P_REDV also produced a more severe velocity fluctuation, which indicated a stronger interaction between the peptides and cell surface receptors. So, peptide P_REDV might be a better option for tethering ECFCs compared to other REDV-containing peptides, including peptide REDV and KSSP_REDV.

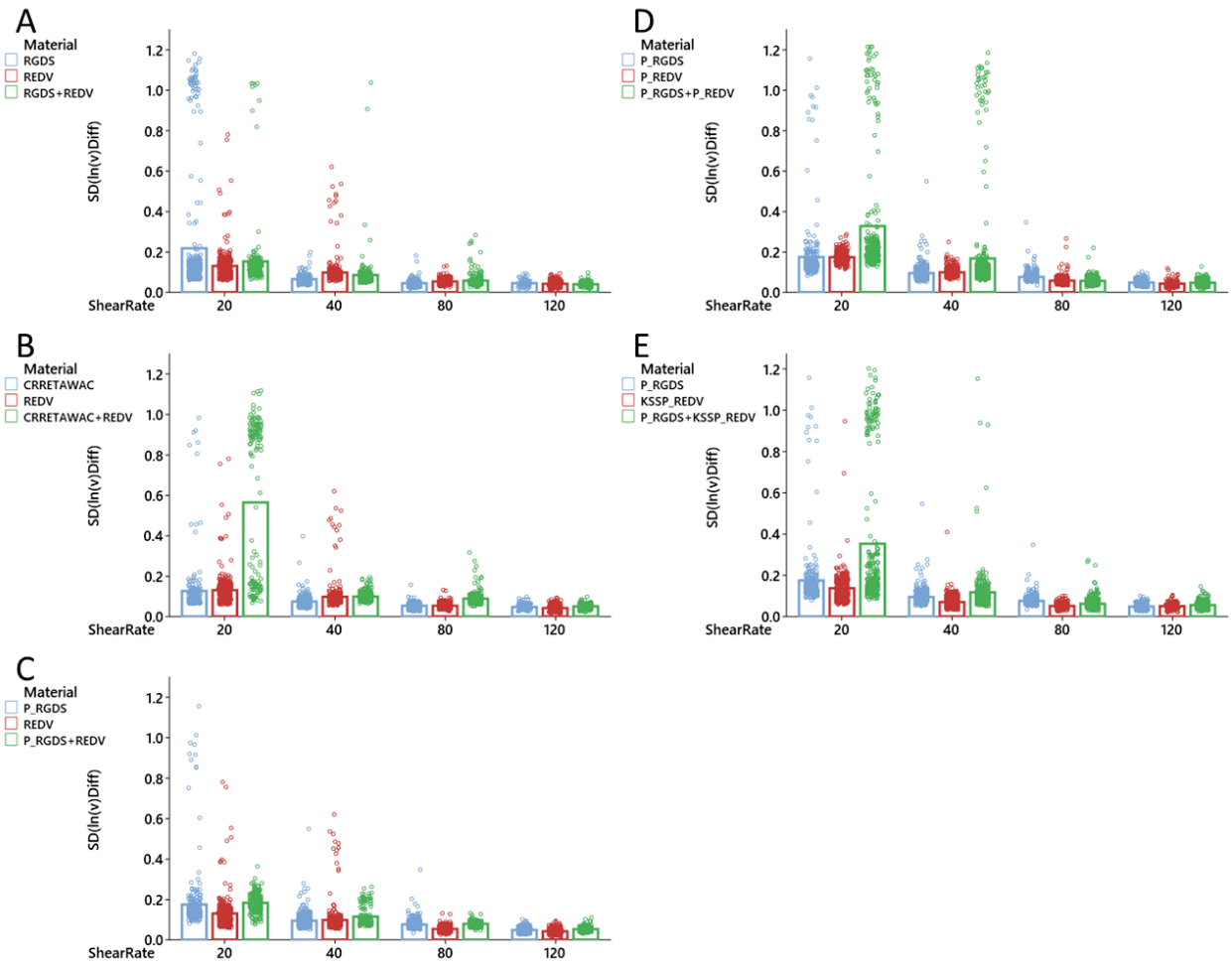

Figure 5.6 Quantitative analysis of velocity fluctuation. (A-E) Single peptides (shown in blue and red) were compared to peptide combinations (shown in green) at different shear rates. Each dot represents the result of a single cell, and the bar stands for the average of all cells assessed under the same condition. (n > 60 cells per condition)

Indicated by a higher level of velocity fluctuation, the combination of peptide CRRETAWAC and REDV showed a stronger interaction with ECFCs at the shear rate of 20 s^{-1} compared to other peptide combinations. Also, the CRRETAWAC+REDV combination had a better performance compared to peptide CRRETAWAC or REDV alone. For other combinations, P_RGDS+P_REDV

and P_RGDS+KSSP_REDV showed improved performance compared to the corresponding single peptides at the shear rate of 20 s^{-1} and 40 s^{-1}, whereas other peptide combinations didn't show the improvement.

5.3.4 Cell capture on peptide-grafted hydrogels

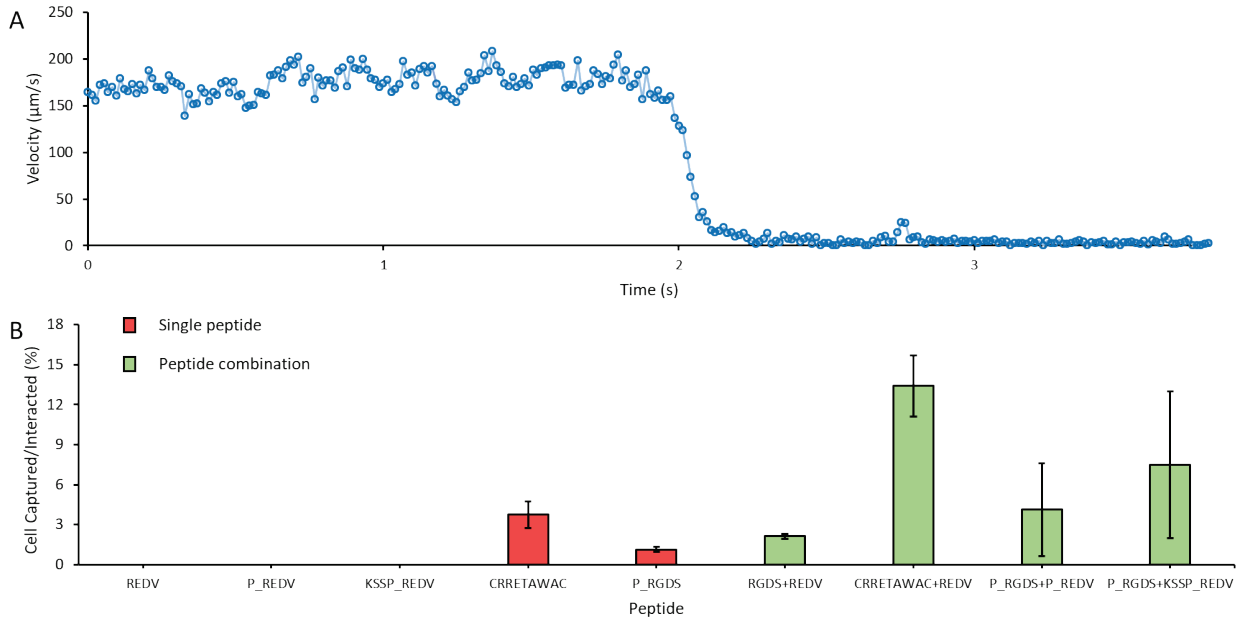

Figure 5.7 Cell capture on peptide-grafted hydrogels. (A) Velocity profile of cell capture. (B) Percentage of captured ECFCs with different peptide-grafted hydrogels under shear flow. All conditions were assessed at shear rate 20 s^{-1}. The total concentration of peptides for grafting in each condition was 0.7 μmol/mL. Data represent mean ± SD (n=3).

An instantaneous velocity profile of cell capture was found to be similar to the "landing state" previously reported by Caputo et al as shown in Figure 5.7A (Caputo and Hammer 2005). The cell started out rolling very fast but suddenly experienced a velocity drop and became firmly bound. This is different from the leukocyte rolling velocity profile, which is mediated by selectin (Ramachandran et al. 2004, Alon et al. 1997).

By using the peptide combination of CRRETAWAC and REDV, the percentage of captured ECFCs under shear increased significantly compared to CRRETAWAC and REDV along. This increased ECFC capture may be due to the contribution from REDV which has shown that it significantly reduces the rolling velocity. This theory is supported by the observation of lowering rolling velocity on REDV/CRRETAWAC-grafted hydrogels, although no significant difference was found between the rolling velocities on CRRETAWAC and REDV/CRRETAWAC at all tested shear rates.

Compared to the low ECFC capture percentage on P_RGDS along, the peptide combination P_RGDS+P_REDV and P_RGDS+KSSP_REDV enhanced the capability of capturing ECFCs under shear flow. Also, they showed an increase in the percentage of captured ECFCs compared to the combination RGDS+REDV. But no significant difference was found.

5.4 Conclusions

Novel peptides and peptide combinations were evaluated for their ability in supporting ECFC tether and capture under shear condition. The velocity increase rate was defined to quantify the severity of velocity fluctuation on different peptide-grafted hydrogels. Peptide combinations CRRETAWAC+REDV, P_RGDS+REDV, and P_RGDS+KSSP_REDV showed improved ECFC capture at the shear rate of 20 s^{-1} compared to the corresponding single peptides.

6. Chapter 6: Summary and Conclusions

This research focuses on the development of approaches for more efficient subcutaneous and intravascular ECFCs delivery with the aid of biomimetic PEG-based hydrogels. The findings of these studies can potentially be used for restoring blood flow to the ischemic tissues for CVD patients and can also be beneficial for other tissue engineering applications. The first part of the studies includes three projects: 1) development of a microfluidic encapsulation platform for rapid production of cell-laden hydrogel microspheres; 2) investigation of the underlying mechanism for controlling microspheroid geometric shape using the microfluidic platform; 3) a large animal study of injectable cell delivery using the ECFC-laden hydrogel microspheres produced by the microfluidic platform. The second part of the studies includes one project and focuses on delivery of ECFCs inside the blood vessel under a shear condition.

This first project established a novel microfluidic platform for rapid encapsulation of cells at high densities in photocrosslinkable microspherical hydrogels including PEGDA, PF, and GelMA, enabled by a new molding technique for microfluidic device fabrication. Cell-laden hydrogel microspheres are advantageous for many applications from high-throughput drug screening to regenerative medicine. Employing microfluidic systems is considered the most efficient method for scale-up production of uniform microspheres. However, existing platforms have been constrained by traditional microfabrication techniques for microfluidic device fabrication, restricting microsphere diameter to below 200 μm and making iterative design changes time-consuming and costly. Using the new molding technique, the microfluidic device employs a modified T-junction design with readily adjustable channel sizes, enabling production of highly uniform microspheres with high cell densities (10-60 million cells mL^{-1}) and a wide range of diameters (300-1100 μm), which are critical for realizing downstream applications, through rapid

photocrosslinking (approximately 1 second per microsphere). Multiple cell types were encapsulated, were evenly distributed throughout the microspheres, and maintained high viability and appropriate cellular activities in long-term culture. This microfluidic encapsulation platform is a valuable and readily adoptable tool for numerous applications, including supporting injectable cell therapy, bioreactor-based cell expansion and differentiation, and high throughput tissue sphere-based drug testing assays.

In the second project, the primary objective was to provide control over the geometric shape of microspheroids, such as diameter and axial ratio, for it is critical for their use in multiple applications. Building on the first project establishing a microfluidic platform for spherical hydrogel production, here the capabilities of this system to produce microspheroids with varying axial ratio (microrods) was extended and the underlying mechanisms controlling microspheroidal geometry were elucidated. This system produced microspheroids with radial diameters ranging from 300 to over 1000 μm and axial ratios from 1.3 to 3.6. This microfluidic platform employed a modified T-junction design fabricated using molding rather than photolithography, thereby overcoming the microspheroid upper size limitation imposed by traditional microfluidic devices, while maintaining high uniformity of geometric shape and high production throughput. The governing fundamental principles of this junction design for microspheroid geometric control was also explored. Two parameters including narrowing ratio (junction diameter over outlet diameter) and flow fraction (discrete phase flow rate over total flow rate) were found critical in adjusting the capillary number, enabling control over microspheroid diameter and axial ratio. This understanding of the relationships enhanced the ability to modulate microspheroid geometric shape by changing device design and experimental parameters. Finally, the applicability to tissue engineering was demonstrated through encapsulation of fibroblasts in hydrogel microspheroids

with different axial ratios. The microspheroids were highly uniform, and the encapsulated cells were able to maintain high viability for over one month. This microfluidic platform represents a new approach for scalable production of large microspheroids with desired geometric shape for various chemical and biomedical applications.

In the third project, a large animal study was conducted. A common challenge in cell therapy is the inability to routinely maintain survival and localization of injected therapeutic cells. Delivering cells by direct injection increases the flexibility of clinical applications, but may cause low cell viability and retention rates due to the high shear force by the needle and mechanical wash out. In this project, the custom-built microfluidic device that was capable of encapsulating high numbers of ECFCs in PF hydrogel microspheres that were highly uniform in shape and size was used. The encapsulated ECFCs were shown to have >95 % viability and maintain a high proliferation rate. Expression of cell markers (vonWillebrand factor, CD105, and CD14), the ability to form tubules on basement membrane matrix, and the ability to take up low-density lipoprotein were similar between pre- and post-encapsulated cells. Viability of encapsulated ECFCs was maintained after shear through 18-23 gauge needles. *Ex vivo* and *in vivo* cell delivery studies were performed by encapsulating and injecting autologous equine ECFCs subcutaneously into distal limb full thickness wounds of adult horses. Injected ECFCs were visualized by labeling with fluorescent nanodots prior to encapsulation. One week after injection, confocal microscopy analysis of biopsies of the leading edges of the wounds showed that the encapsulated ECFCs migrated into the surrounding host tissue indicating successful retention and survival of the delivered ECFCs. Rapid, scalable cell encapsulation into PF microspheres is a clinically relevant method to maintain cell retention and survival after local injection. However, future work is needed to investigate the functionality of delivered ECFCs to form new vasculature.

The last project focused on delivery of ECFCs inside the blood vessel under a shear condition. For patients with coronary artery disease, restenosis is one of the main long-term causes of failed surgery. It is mainly due to thrombogenesis and neointimal hyperplasia within synthetic vascular grafts or at site of stent implantation. Despite substantial progress in the development of biocompatible surface technologies, endothelialization remains the single truly effective long-term means of preventing this undesirable narrowing of the vessel lumen. ECFCs are unipotent stem cells that carry high proliferative capability and can differentiate into ECs, making them a promising cell source for rapid reendothelialization of injured vasculature. Generally, recruitment of circulating ECFCs to a site of injury occurs through a dynamic adhesion process consisting of cell tethering, rolling, and firm adhesion. Bonds between certain cell surface receptors and their corresponding ligands rapidly form and then are broken. Currently only limited work has been done to study individual cell surface receptor-mediated, especially integrin-mediated, dynamic adhesion of ECFCs for endothelialization of biomaterials. This study investigated the ability of novel peptides, which work as the ligands here, to support dynamic adhesion of ECFCs under shear flow. Both single peptides and peptide combinations were tethered to PEGDA hydrogels and assessed for their capabilities to support deceleration, as well as firm adhesion of ECFCs. A parallel plate flow chamber was used to mimic the physiological fluid shear. The interaction of ECFCs with different peptides was recorded using a high-speed camera and assessed by an optical cell tracking analysis system. This study investigated the dynamic adhesion process of ECFCs on peptide-grafted hydrogels. In addition to this, future work is needed to study the functionality of captured ECFCs to form an endothelial layer under shear condition.

Taken together, new approaches were developed for more efficient delivery of ECFCs by using knowledge in engineering and biology. A novel microfluidic encapsulation platform was

developed and investigated for its ability to rapidly produce engineered tissues. The results of this work provide great potential for minimally invasive delivery of not only ECFCs but also other therapeutic cell types, such as mesenchymal stem cells and hiPSCs for regeneration of cartilage, bone, heart, and neural tissue. When using non-degrading hydrogels for encapsulation, the delivered cells may remain at the site of injection, secreting therapeutic extracellular vesicles under the protection of the hydrogel scaffolds. Besides injectable cell delivery, the microspheroidal engineered tissues can also be used for disease modeling and drug discovery, such as high throughput and high content screening for testing the efficacy and cardiotoxicity of anticancer drugs. In addition, the hydrogel microspheroids can be a promising tool for 3D bioprinting and bioreactor-based cell production and differentiation. For the second part of the studies, novel peptides and peptide combinations were designed and examined for their capabilities to support dynamic adhesion of ECFCs, and findings of this project contribute to our knowledge of ECFC-peptide interaction under shear condition and may assist in developing novel vascular grafts and stents.

References

1. Aguado, B. A., W. Mulyasasmita, J. Su, K. J. Lampe, and S. C. Heilshorn. 2012. "Improving viability of stem cells during syringe needle flow through the design of hydrogel cell carriers." *Tissue Eng Part A* 18 (7-8):806-15. doi: 10.1089/ten.TEA.2011.0391.

2. Almany, L., and D. Seliktar. 2005. "Biosynthetic hydrogel scaffolds made from fibrinogen and polyethylene glycol for 3D cell cultures." *Biomaterials* 26 (15):2467-77. doi: 10.1016/j.biomaterials.2004.06.047.

3. Alon, R., S. Chen, K. D. Puri, E. B. Finger, and T. A. Springer. 1997. "The kinetics of L-selectin tethers and the mechanics of selectin-mediated rolling." *J Cell Biol* 138 (5):1169-80. doi: 10.1083/jcb.138.5.1169.

4. An, D., A. Chiu, J. A. Flanders, W. Song, D. Shou, Y. C. Lu, L. G. Grunnet, L. Winkel, C. Ingvorsen, N. S. Christophersen, J. J. Fels, F. W. Sand, Y. Ji, L. Qi, Y. Pardo, D. Luo, M. Silberstein, J. Fan, and M. Ma. 2018. "Designing a retrievable and scalable cell encapsulation device for potential treatment of type 1 diabetes." *Proc Natl Acad Sci U S A* 115 (2):E263-E272. doi: 10.1073/pnas.1708806115.

5. Angelos, M. G., M. A. Brown, L. L. Satterwhite, V. W. Levering, N. T. Shaked, and G. A. Truskey. 2010. "Dynamic adhesion of umbilical cord blood endothelial progenitor cells under laminar shear stress." *Biophys J* 99 (11):3545-54. doi: 10.1016/j.bpj.2010.10.004.

6. Anna, S. L., N. Bontoux, and H. A. Stone. 2003. "Formation of dispersions using "flow focusing" in microchannels." *Applied Physics Letters* 82 (3):364-366. doi: 10.1063/1.1537519.

7. Annabi, N., J. W. Nichol, X. Zhong, C. Ji, S. Koshy, A. Khademhosseini, and F. Dehghani. 2010. "Controlling the porosity and microarchitecture of hydrogels for tissue engineering." *Tissue Eng Part B Rev* 16 (4):371-83. doi: 10.1089/ten.TEB.2009.0639.

8. Aoki, J., P. W. Serruys, H. van Beusekom, A. T. Ong, E. P. McFadden, G. Sianos, W. J. van der Giessen, E. Regar, P. J. de Feyter, H. R. Davis, S. Rowland, and M. J. Kutryk. 2005. "Endothelial progenitor cell capture by stents coated with antibody against CD34: the HEALING-FIM (Healthy Endothelial Accelerated Lining Inhibits Neointimal Growth-First In Man) Registry." *J Am Coll Cardiol* 45 (10):1574-9. doi: 10.1016/j.jacc.2005.01.048.

9. Appelman, T. P., J. Mizrahi, J. H. Elisseeff, and D. Seliktar. 2011. "The influence of biological motifs and dynamic mechanical stimulation in hydrogel scaffold systems on the phenotype of chondrocytes." *Biomaterials* 32 (6):1508-16. doi: 10.1016/j.biomaterials.2010.10.017.

10. Asahara, T., C. Bauters, C. Pastore, M. Kearney, S. Rossow, S. Bunting, N. Ferrara, J. F. Symes, and J. M. Isner. 1995. "Local delivery of vascular endothelial growth factor accelerates reendothelialization and attenuates intimal hyperplasia in balloon-injured rat carotid artery." *Circulation* 91 (11):2793-801. doi: 10.1161/01.cir.91.11.2793.

11. Asai, J., H. Takenaka, M. Ii, M. Asahi, S. Kishimoto, N. Katoh, and D. W. Losordo. 2013. "Topical application of ex vivo expanded endothelial progenitor cells promotes vascularisation and wound healing in diabetic mice." *Int Wound J* 10 (5):527-33. doi: 10.1111/j.1742-481X.2012.01010.x.

12. Avci-Adali, M., G. Ziemer, and H. P. Wendel. 2010. "Induction of EPC homing on biofunctionalized vascular grafts for rapid in vivo self-endothelialization--a review of current strategies." *Biotechnol Adv* 28 (1):119-29. doi: 10.1016/j.biotechadv.2009.10.005.

13. Baah, D., and T. Floyd-Smith. 2014. "Microfluidics for particle synthesis from photocrosslinkable materials." *Microfluidics and Nanofluidics* 17 (3):431-455. doi: 10.1007/s10404-014-1333-y.

14. Baeyens, N., C. Bandyopadhyay, B. G. Coon, S. Yun, and M. A. Schwartz. 2016. "Endothelial fluid shear stress sensing in vascular health and disease." *J Clin Invest* 126 (3):821-8. doi: 10.1172/JCI83083.

15. Barron, C., and J. Q. He. 2017. "Alginate-based microcapsules generated with the coaxial electrospray method for clinical application." *J Biomater Sci Polym Ed* 28 (13):1245-1255. doi: 10.1080/09205063.2017.1318030.

16. Baudin, B., A. Bruneel, N. Bosselut, and M. Vaubourdolle. 2007. "A protocol for isolation and culture of human umbilical vein endothelial cells." *Nat Protoc* 2 (3):481-5. doi: 10.1038/nprot.2007.54.

17. Bearzi, C., C. Gargioli, D. Baci, O. Fortunato, K. Shapira-Schweitzer, O. Kossover, M. V. Latronico, D. Seliktar, G. Condorelli, and R. Rizzi. 2014. "PlGF-MMP9-engineered iPS cells supported on a PEG-fibrinogen hydrogel scaffold possess an enhanced capacity to repair damaged myocardium." *Cell Death Dis* 5 (2):e1053. doi: 10.1038/cddis.2014.12.

18. Belair, D. G., J. A. Whisler, J. Valdez, J. Velazquez, J. A. Molenda, V. Vickerman, R. Lewis, C. Daigh, T. D. Hansen, D. A. Mann, J. A. Thomson, L. G. Griffith, R. D. Kamm, M. P. Schwartz, and W. L. Murphy. 2015. "Human vascular tissue models formed from human induced pluripotent stem cell derived endothelial cells." *Stem Cell Rev Rep* 11 (3):511-25. doi: 10.1007/s12015-014-9549-5.

19. Bidarra, S. J., C. C. Barrias, M. A. Barbosa, R. Soares, and P. L. Granja. 2010. "Immobilization of human mesenchymal stem cells within RGD-grafted alginate microspheres and assessment of their angiogenic potential." *Biomacromolecules* 11 (8):1956-64. doi: 10.1021/bm100264a.

20. Bidarra, S. J., C. C. Barrias, and P. L. Granja. 2014. "Injectable alginate hydrogels for cell delivery in tissue engineering." *Acta Biomater* 10 (4):1646-62. doi: 10.1016/j.actbio.2013.12.006.

21. Bompais, H., J. Chagraoui, X. Canron, M. Crisan, X. H. Liu, A. Anjo, C. Tolla-Le Port, M. Leboeuf, P. Charbord, A. Bikfalvi, and G. Uzan. 2004. "Human endothelial cells derived

from circulating progenitors display specific functional properties compared with mature vessel wall endothelial cells." *Blood* 103 (7):2577-84. doi: 10.1182/blood-2003-08-2770.

22. Bonino, C. A., J. E. Samorezov, O. Jeon, E. Alsberg, and S. A. Khan. 2011. "Real-time in situ rheology of alginate hydrogel photocrosslinking." *Soft Matter* 7 (24):11510-11517. doi: 10.1039/c1sm06109g.

23. Boura, C., P. Menu, E. Payan, C. Picart, J. C. Voegel, S. Muller, and J. F. Stoltz. 2003. "Endothelial cells grown on thin polyelectrolyte mutlilayered films: an evaluation of a new versatile surface modification." *Biomaterials* 24 (20):3521-30. doi: 10.1016/s0142-9612(03)00214-x.

24. Brouzes, E., M. Medkova, N. Savenelli, D. Marran, M. Twardowski, J. B. Hutchison, J. M. Rothberg, D. R. Link, N. Perrimon, and M. L. Samuels. 2009. "Droplet microfluidic technology for single-cell high-throughput screening." *Proc Natl Acad Sci U S A* 106 (34):14195-200. doi: 10.1073/pnas.0903542106.

25. Caliari, S. R., and J. A. Burdick. 2016. "A practical guide to hydrogels for cell culture." *Nat Methods* 13 (5):405-14. doi: 10.1038/nmeth.3839.

26. Capretto, L., S. Mazzitelli, G. Luca, and C. Nastruzzi. 2010. "Preparation and characterization of polysaccharidic microbeads by a microfluidic technique: application to the encapsulation of Sertoli cells." *Acta Biomater* 6 (2):429-35. doi: 10.1016/j.actbio.2009.08.023.

27. Caputo, K. E., and D. A. Hammer. 2005. "Effect of microvillus deformability on leukocyte adhesion explored using adhesive dynamics simulations." *Biophys J* 89 (1):187-200. doi: 10.1529/biophysj.104.054171.

28. Celeste, C. J., K. Deschene, C. B. Riley, and C. L. Theoret. 2011. "Regional differences in wound oxygenation during normal healing in an equine model of cutaneous fibroproliferative disorder." *Wound Repair Regen* 19 (1):89-97. doi: 10.1111/j.1524-475X.2010.00639.x.

29. Celeste, C. J., K. Deschesne, C. B. Riley, and C. L. Theoret. 2013. "Skin temperature during cutaneous wound healing in an equine model of cutaneous fibroproliferative disorder: kinetics and anatomic-site differences." *Vet Surg* 42 (2):147-53. doi: 10.1111/j.1532-950X.2012.00966.x.

30. Champion, J. A., and S. Mitragotri. 2006. "Role of target geometry in phagocytosis." *Proc Natl Acad Sci U S A* 103 (13):4930-4. doi: 10.1073/pnas.0600997103.

31. Chang, K. C., D. F. Tees, and D. A. Hammer. 2000. "The state diagram for cell adhesion under flow: leukocyte rolling and firm adhesion." *Proc Natl Acad Sci U S A* 97 (21):11262-7. doi: 10.1073/pnas.200240897.

32. Chen, Q. Z., S. L. Liang, and G. A. Thouas. 2013. "Elastomeric biomaterials for tissue engineering." *Progress in Polymer Science* 38 (3-4):584-671. doi: 10.1016/j.progpolymsci.2012.05.003.

33. Choi, C. H., J. H. Jung, Y. W. Rhee, D. P. Kim, S. E. Shim, and C. S. Lee. 2007. "Generation of monodisperse alginate microbeads and in situ encapsulation of cell in microfluidic device." *Biomedical Microdevices* 9 (6):855-862. doi: 10.1007/s10544-007-9098-7.

34. Choi, C. H., H. Wang, H. Lee, J. H. Kim, L. Zhang, A. Mao, D. J. Mooney, and D. A. Weitz. 2016. "One-step generation of cell-laden microgels using double emulsion drops with a sacrificial ultra-thin oil shell." *Lab Chip* 16 (9):1549-55. doi: 10.1039/c6lc00261g.

35. Choi, K. D., J. Yu, K. Smuga-Otto, G. Salvagiotto, W. Rehrauer, M. Vodyanik, J. Thomson, and I. Slukvin. 2009. "Hematopoietic and endothelial differentiation of human induced pluripotent stem cells." *Stem Cells* 27 (3):559-67. doi: 10.1634/stemcells.2008-0922.

36. Christopher, G. F., and S. L. Anna. 2007. "Microfluidic methods for generating continuous droplet streams." *Journal of Physics D-Applied Physics* 40 (19):R319-R336. doi: 10.1088/0022-3727/40/19/R01.

37. Clausell-Tormos, J., D. Lieber, J. C. Baret, A. El-Harrak, O. J. Miller, L. Frenz, J. Blouwolff, K. J. Humphry, S. Koster, H. Duan, C. Holtze, D. A. Weitz, A. D. Griffiths, and C. A. Merten. 2008. "Droplet-based microfluidic platforms for the encapsulation and screening of mammalian cells and multicellular organisms." *Chemistry & Biology* 15 (5):427-437. doi: 10.1016/j.chembiol.2008.04.004.

38. Davis, Jaeger, Steve P Crampton, and Christopher CW Hughes. 2007. "Isolation of human umbilical vein endothelial cells (HUVEC)." *JoVE (Journal of Visualized Experiments)* (3):e183.

39. de Vicente, J., J. P. Segovia-Gutierrez, E. Andablo-Reyes, F. Vereda, and R. Hidalgo-Alvarez. 2009. "Dynamic rheology of sphere- and rod-based magnetorheological fluids." *Journal of Chemical Physics* 131 (19). doi: 10.1063/1.3259358.

40. DeLong, S. A., J. J. Moon, and J. L. West. 2005. "Covalently immobilized gradients of bFGF on hydrogel scaffolds for directed cell migration." *Biomaterials* 26 (16):3227-34. doi: 10.1016/j.biomaterials.2004.09.021.

41. Deschene, K., C. Celeste, D. Boerboom, and C. L. Theoret. 2011. "Constitutive expression of hypoxia-inducible factor-1 alpha in keratinocytes during the repair of skin wounds in horses." *Wound Repair Regen* 19 (2):250-9. doi: 10.1111/j.1524-475X.2010.00663.x.

42. Dikovsky, D., H. Bianco-Peled, and D. Seliktar. 2006. "The effect of structural alterations of PEG-fibrinogen hydrogel scaffolds on 3-D cellular morphology and cellular migration." *Biomaterials* 27 (8):1496-1506. doi: 10.1016/j.biomaterials.2005.09.038.

43. Dini, E., S. Alexandridou, and C. Kiparissides. 2003. "Synthesis and characterization of cross-linked chitosan microspheres for drug delivery applications." *J Microencapsul* 20 (3):375-85. doi: 10.1080/0265204031000093078.

44. Dow, J., B. Z. Simkhovich, L. Kedes, and R. A. Kloner. 2005. "Washout of transplanted cells from the heart: a potential new hurdle for cell transplantation therapy." *Cardiovasc Res* 67 (2):301-7. doi: 10.1016/j.cardiores.2005.04.011.

45. Drela, E., K. Stankowska, A. Kulwas, and D. Rosc. 2012. "Endothelial progenitor cells in diabetic foot syndrome." *Adv Clin Exp Med* 21 (2):249-54.

46. Dupin, M. M., I. Halliday, and C. M. Care. 2006. "Simulation of a microfluidic flow-focusing device." *Phys Rev E Stat Nonlin Soft Matter Phys* 73 (5 Pt 2):055701. doi: 10.1103/PhysRevE.73.055701.

47. Farooq, V., B. D. Gogas, and P. W. Serruys. 2011. "Restenosis: delineating the numerous causes of drug-eluting stent restenosis." *Circ Cardiovasc Interv* 4 (2):195-205. doi: 10.1161/CIRCINTERVENTIONS.110.959882.

48. Faxon, D. P., T. A. Sanborn, and C. C. Haudenschild. 1987. "Mechanism of angioplasty and its relation to restenosis." *Am J Cardiol* 60 (3):5B-9B. doi: 10.1016/0002-9149(87)90476-0.

49. Ferris, D., D. Frisbie, J. Kisiday, and C. W. McIlwraith. 2012. "In vivo healing of meniscal lacerations using bone marrow-derived mesenchymal stem cells and fibrin glue." *Stem Cells Int* 2012:691605. doi: 10.1155/2012/691605.

50. Franco, C. L., J. Price, and J. L. West. 2011. "Development and optimization of a dual-photoinitiator, emulsion-based technique for rapid generation of cell-laden hydrogel microspheres." *Acta Biomater* 7 (9):3267-76. doi: 10.1016/j.actbio.2011.06.011.

51. Frisman, I., D. Seliktar, and H. Bianco-Peled. 2012. "Nanostructuring biosynthetic hydrogels for tissue engineering: a cellular and structural analysis." *Acta Biomater* 8 (1):51-60. doi: 10.1016/j.actbio.2011.07.030.

52. Fuoco, C., M. L. Salvatori, A. Biondo, K. Shapira-Schweitzer, S. Santoleri, S. Antonini, S. Bernardini, F. S. Tedesco, S. Cannata, D. Seliktar, G. Cossu, and C. Gargioli. 2012. "Injectable polyethylene glycol-fibrinogen hydrogel adjuvant improves survival and differentiation of transplanted mesoangioblasts in acute and chronic skeletal-muscle degeneration." *Skelet Muscle* 2 (1):24. doi: 10.1186/2044-5040-2-24.

53. Furchgott, R. F., and P. M. Vanhoutte. 1989. "Endothelium-derived relaxing and contracting factors." *FASEB J* 3 (9):2007-18.

54. Gaffey, A. C., M. H. Chen, C. M. Venkataraman, A. Trubelja, C. B. Rodell, P. V. Dinh, G. Hung, J. W. MacArthur, R. V. Soopan, J. A. Burdick, and P. Atluri. 2015. "Injectable shear-thinning hydrogels used to deliver endothelial progenitor cells, enhance cell engraftment,

and improve ischemic myocardium." *J Thorac Cardiovasc Surg* 150 (5):1268-76. doi: 10.1016/j.jtcvs.2015.07.035.

55. Garg, U. C., and A. Hassid. 1989. "Nitric oxide-generating vasodilators and 8-bromo-cyclic guanosine monophosphate inhibit mitogenesis and proliferation of cultured rat vascular smooth muscle cells." *J Clin Invest* 83 (5):1774-7. doi: 10.1172/JCI114081.

56. Garstecki, P., M. J. Fuerstman, H. A. Stone, and G. M. Whitesides. 2006. "Formation of droplets and bubbles in a microfluidic T-junction-scaling and mechanism of break-up." *Lab Chip* 6 (3):437-46. doi: 10.1039/b510841a.

57. Gombotz, W. R., G. H. Wang, T. A. Horbett, and A. S. Hoffman. 1991. "Protein adsorption to poly(ethylene oxide) surfaces." *J Biomed Mater Res* 25 (12):1547-62. doi: 10.1002/jbm.820251211.

58. Greenberg, D., A. Bakhai, and D. J. Cohen. 2004. "Can we afford to eliminate restenosis? Can we afford not to?" *J Am Coll Cardiol* 43 (4):513-8. doi: 10.1016/j.jacc.2003.11.020.

59. Hacker, M. C., and H. A. Nawaz. 2015. "Multi-Functional Macromers for Hydrogel Design in Biomedical Engineering and Regenerative Medicine." *Int J Mol Sci* 16 (11):27677-706. doi: 10.3390/ijms161126056.

60. Hanson Shepherd, J. N., S. T. Parker, R. F. Shepherd, M. U. Gillette, J. A. Lewis, and R. G. Nuzzo. 2011. "3D Microperiodic Hydrogel Scaffolds for Robust Neuronal Cultures." *Adv Funct Mater* 21 (1):47-54. doi: 10.1002/adfm.201001746.

61. Hawkes, A. L., M. Nowak, B. Bidstrup, and R. Speare. 2006. "Outcomes of coronary artery bypass graft surgery." *Vasc Health Risk Manag* 2 (4):477-84. doi: 10.2147/vhrm.2006.2.4.477.

62. He, W., Z. Ma, T. Yong, W. E. Teo, and S. Ramakrishna. 2005. "Fabrication of collagen-coated biodegradable polymer nanofiber mesh and its potential for endothelial cells growth." *Biomaterials* 26 (36):7606-15. doi: 10.1016/j.biomaterials.2005.05.049.

63. Headen, D. M., G. Aubry, H. Lu, and A. J. Garcia. 2014. "Microfluidic-based generation of size-controlled, biofunctionalized synthetic polymer microgels for cell encapsulation." *Adv Mater* 26 (19):3003-8. doi: 10.1002/adma.201304880.

64. Herrick, S., O. Blanc-Brude, A. Gray, and G. Laurent. 1999. "Fibrinogen." *Int J Biochem Cell Biol* 31 (7):741-6. doi: 10.1016/s1357-2725(99)00032-1.

65. Hidalgo San Jose, L., P. Stephens, B. Song, and D. Barrow. 2018. "Microfluidic Encapsulation Supports Stem Cell Viability, Proliferation, and Neuronal Differentiation." *Tissue Eng Part C Methods* 24 (3):158-170. doi: 10.1089/ten.TEC.2017.0368.

66. Highley, C. B., K. H. Song, A. C. Daly, and J. A. Burdick. 2019. "Jammed Microgel Inks for 3D Printing Applications." *Adv Sci (Weinh)* 6 (1):1801076. doi: 10.1002/advs.201801076.

67. Hindson, B. J., K. D. Ness, D. A. Masquelier, P. Belgrader, N. J. Heredia, A. J. Makarewicz, I. J. Bright, M. Y. Lucero, A. L. Hiddessen, T. C. Legler, T. K. Kitano, M. R. Hodel, J. F. Petersen, P. W. Wyatt, E. R. Steenblock, P. H. Shah, L. J. Bousse, C. B. Troup, J. C. Mellen, D. K. Wittmann, N. G. Erndt, T. H. Cauley, R. T. Koehler, A. P. So, S. Dube, K. A. Rose, L. Montesclaros, S. Wang, D. P. Stumbo, S. P. Hodges, S. Romine, F. P. Milanovich, H. E. White, J. F. Regan, G. A. Karlin-Neumann, C. M. Hindson, S. Saxonov, and B. W. Colston. 2011. "High-throughput droplet digital PCR system for absolute quantitation of DNA copy number." *Anal Chem* 83 (22):8604-10. doi: 10.1021/ac202028g.

68. Hofmann, M., K. C. Wollert, G. P. Meyer, A. Menke, L. Arseniev, B. Hertenstein, A. Ganser, W. H. Knapp, and H. Drexler. 2005. "Monitoring of bone marrow cell homing into the infarcted human myocardium." *Circulation* 111 (17):2198-202. doi: 10.1161/01.CIR.0000163546.27639.AA.

69. Hong, S., D. Sycks, H. F. Chan, S. Lin, G. P. Lopez, F. Guilak, K. W. Leong, and X. Zhao. 2015. "3D Printing of Highly Stretchable and Tough Hydrogels into Complex, Cellularized Structures." *Adv Mater* 27 (27):4035-40. doi: 10.1002/adma.201501099.

70. Hong, Y. P., and F. J. Wang. 2007. "Flow rate effect on droplet control in a co-flowing microfluidic device." *Microfluidics and Nanofluidics* 3 (3):341-346. doi: 10.1007/s10404-006-0134-3.

71. Horning, Jayme L., Sanjeeb K. Sahoo, Sivakumar Vijayaraghavalu, Sanja Dimitrijevic, Jaspreet K. Vasir, Tapan K. Jain, Amulya K. Panda, and Vinod Labhasetwar. 2008. "3-D tumor model for in vitro evaluation of anticancer drugs." *Molecular Pharmaceutics* 5 (5):849-862. doi: 10.1021/mp800047v.

72. Hur, J., C. H. Yoon, H. S. Kim, J. H. Choi, H. J. Kang, K. K. Hwang, B. H. Oh, M. M. Lee, and Y. B. Park. 2004. "Characterization of two types of endothelial progenitor cells and their different contributions to neovasculogenesis." *Arterioscler Thromb Vasc Biol* 24 (2):288-93. doi: 10.1161/01.ATV.0000114236.77009.06.

73. Ingram, D. A., L. E. Mead, D. B. Moore, W. Woodard, A. Fenoglio, and M. C. Yoder. 2005. "Vessel wall-derived endothelial cells rapidly proliferate because they contain a complete hierarchy of endothelial progenitor cells." *Blood* 105 (7):2783-6. doi: 10.1182/blood-2004-08-3057.

74. Ingram, D. A., L. E. Mead, H. Tanaka, V. Meade, A. Fenoglio, K. Mortell, K. Pollok, M. J. Ferkowicz, D. Gilley, and M. C. Yoder. 2004. "Identification of a novel hierarchy of endothelial progenitor cells using human peripheral and umbilical cord blood." *Blood* 104 (9):2752-60. doi: 10.1182/blood-2004-04-1396.

75. Iyer, S. R., and B. H. Annex. 2017. "Therapeutic Angiogenesis for Peripheral Artery Disease: Lessons Learned in Translational Science." *JACC Basic Transl Sci* 2 (5):503-512. doi: 10.1016/j.jacbts.2017.07.012.

76. Jadhav, S., C. D. Eggleton, and K. Konstantopoulos. 2005. "A 3-D computational model predicts that cell deformation affects selectin-mediated leukocyte rolling." *Biophys J* 88 (1):96-104. doi: 10.1529/biophysj.104.051029.

77. Jaworek, A. 2007. "Electrospray droplet sources for thin film deposition." *Journal of Materials Science* 42 (1):266-297. doi: 10.1007/s10853-006-0842-9.

78. Jiang, W., M. Li, Z. Chen, and K. W. Leong. 2016. "Cell-laden microfluidic microgels for tissue regeneration." *Lab Chip* 16 (23):4482-4506. doi: 10.1039/c6lc01193d.

79. Jiang, Z., B. Xia, R. McBride, and J. Oakey. 2017. "A microfluidic-based cell encapsulation platform to achieve high long-term cell viability in photopolymerized PEGNB hydrogel microspheres." *J Mater Chem B* 5 (1):173-180. doi: 10.1039/C6TB02551J.

80. Jun, H. W., and J. West. 2004. "Development of a YIGSR-peptide-modified polyurethaneurea to enhance endothelialization." *J Biomater Sci Polym Ed* 15 (1):73-94. doi: 10.1163/156856204322752246.

81. Kabithe, E., J. Hillegas, T. Stokol, J. Moore, and B. Wagner. 2010. "Monoclonal antibodies to equine CD14." *Vet Immunol Immunopathol* 138 (1-2):149-53. doi: 10.1016/j.vetimm.2010.07.003.

82. Karp, J. M., J. Yeh, G. Eng, J. Fukuda, J. Blumling, K. Y. Suh, J. Cheng, A. Mahdavi, J. Borenstein, R. Langer, and A. Khademhosseini. 2007. "Controlling size, shape and homogeneity of embryoid bodies using poly(ethylene glycol) microwells." *Lab on a Chip* 7 (6):786-794. doi: 10.1039/b705085m.

83. Kauf, Adam CW, Scott M Hough, and Ron D Bowditch. 2001. "Recognition of fibronectin by the platelet integrin αIIbβ3 involves an extended interface with multiple electrostatic interactions." *Biochemistry* 40 (31):9159-9166.

84. Kerscher, P., J. A. Kaczmarek, S. E. Head, M. E. Ellis, W. J. Seeto, J. Kim, S. Bhattacharya, V. Suppiramaniam, and E. A. Lipke. 2017. "Direct Production of Human Cardiac Tissues by Pluripotent Stem Cell Encapsulation in Gelatin Methacryloyl." *Acs Biomaterials Science & Engineering* 3 (8):1499-1509. doi: 10.1021/acsbiomaterials.6b00226.

85. Kerscher, P., I. C. Turnbull, A. J. Hodge, J. Kim, D. Seliktar, C. J. Easley, K. D. Costa, and E. A. Lipke. 2016. "Direct hydrogel encapsulation of pluripotent stem cells enables ontomimetic differentiation and growth of engineered human heart tissues." *Biomaterials* 83:383-95. doi: 10.1016/j.biomaterials.2015.12.011.

86. Khademhosseini, A., and R. Langer. 2007. "Microengineered hydrogels for tissue engineering." *Biomaterials* 28 (34):5087-92. doi: 10.1016/j.biomaterials.2007.07.021.

87. Kim, H., D. W. Luo, D. Link, D. A. Weitz, M. Marquez, and Z. D. Cheng. 2007. "Controlled production of emulsion drops using an electric field in a flow-focusing microfluidic device." *Applied Physics Letters* 91 (13). doi: 10.1063/1.2790785.

88. King, T. W., and C. W. Patrick. 2000. "Development and in vitro characterization of vascular endothelial growth factor (VEGF)-loaded poly(DL-lactic-co-glycolic acid)/poly(ethylene glycol) microspheres using a solid encapsulation/single emulsion/solvent extraction technique." *Journal of Biomedical Materials Research* 51 (3):383-390. doi: Doi 10.1002/1097-4636(20000905)51:3<383::Aid-Jbm12>3.0.Co;2-D.

89. Klouda, L. 2015. "Thermoresponsive hydrogels in biomedical applications: A seven-year update." *Eur J Pharm Biopharm* 97 (Pt B):338-49. doi: 10.1016/j.ejpb.2015.05.017.

90. Koivunen, E., B. Wang, and E. Ruoslahti. 1994. "Isolation of a highly specific ligand for the alpha 5 beta 1 integrin from a phage display library." *J Cell Biol* 124 (3):373-80. doi: 10.1083/jcb.124.3.373.

91. Kolesky, D. B., R. L. Truby, A. S. Gladman, T. A. Busbee, K. A. Homan, and J. A. Lewis. 2014. "3D bioprinting of vascularized, heterogeneous cell-laden tissue constructs." *Adv Mater* 26 (19):3124-30. doi: 10.1002/adma.201305506.

92. Kong, D., L. G. Melo, M. Gnecchi, L. Zhang, G. Mostoslavsky, C. C. Liew, R. E. Pratt, and V. J. Dzau. 2004. "Cytokine-induced mobilization of circulating endothelial progenitor cells enhances repair of injured arteries." *Circulation* 110 (14):2039-46. doi: 10.1161/01.CIR.0000143161.01901.BD.

93. Koster, S., F. E. Angile, H. Duan, J. J. Agresti, A. Wintner, C. Schmitz, A. C. Rowat, C. A. Merten, D. Pisignano, A. D. Griffiths, and D. A. Weitz. 2008. "Drop-based microfluidic devices for encapsulation of single cells." *Lab on a Chip* 8 (7):1110-1115. doi: 10.1039/b802941e.

94. Kropp, C., D. Massai, and R. Zweigerdt. 2017. "Progress and challenges in large-scale expansion of human pluripotent stem cells." *Process Biochemistry* 59:244-254. doi: 10.1016/j.procbio.2016.09.032.

95. Kumachev, A., J. Greener, E. Tumarkin, E. Eiser, P. W. Zandstra, and E. Kumacheva. 2011. "High-throughput generation of hydrogel microbeads with varying elasticity for cell encapsulation." *Biomaterials* 32 (6):1477-83. doi: 10.1016/j.biomaterials.2010.10.033.

96. Laflamme, M. A., K. Y. Chen, A. V. Naumova, V. Muskheli, J. A. Fugate, S. K. Dupras, H. Reinecke, C. Xu, M. Hassanipour, S. Police, C. O'Sullivan, L. Collins, Y. Chen, E. Minami, E. A. Gill, S. Ueno, C. Yuan, J. Gold, and C. E. Murry. 2007. "Cardiomyocytes derived from human embryonic stem cells in pro-survival factors enhance function of infarcted rat hearts." *Nat Biotechnol* 25 (9):1015-24. doi: 10.1038/nbt1327.

97. Lasic, D. D., F. J. Martin, A. Gabizon, S. K. Huang, and D. Papahadjopoulos. 1991. "Sterically stabilized liposomes: a hypothesis on the molecular origin of the extended circulation times." *Biochim Biophys Acta* 1070 (1):187-92. doi: 10.1016/0005-2736(91)90162-2.

98. Lee, W., V. Lee, S. Polio, P. Keegan, J. H. Lee, K. Fischer, J. K. Park, and S. S. Yoo. 2010. "On-demand three-dimensional freeform fabrication of multi-layered hydrogel scaffold with fluidic channels." *Biotechnol Bioeng* 105 (6):1178-86. doi: 10.1002/bit.22613.

99. Leong, W., and D. A. Wang. 2015. "Cell-laden Polymeric Microspheres for Biomedical Applications." *Trends Biotechnol* 33 (11):653-666. doi: 10.1016/j.tibtech.2015.09.003.

100. Ley, K., C. Laudanna, M. I. Cybulsky, and S. Nourshargh. 2007. "Getting to the site of inflammation: the leukocyte adhesion cascade updated." *Nat Rev Immunol* 7 (9):678-89. doi: 10.1038/nri2156.

101. Li, S. H., T. Y. Lai, Z. Sun, M. Han, E. Moriyama, B. Wilson, S. Fazel, R. D. Weisel, T. Yau, J. C. Wu, and R. K. Li. 2009. "Tracking cardiac engraftment and distribution of implanted bone marrow cells: Comparing intra-aortic, intravenous, and intramyocardial delivery." *J Thorac Cardiovasc Surg* 137 (5):1225-33 e1. doi: 10.1016/j.jtcvs.2008.11.001.

102. Lipke, E. A., and J. L. West. 2005. "Localized delivery of nitric oxide from hydrogels inhibits neointima formation in a rat carotid balloon injury model." *Acta Biomater* 1 (6):597-606. doi: 10.1016/j.actbio.2005.07.010.

103. Liu, H. H., and Y. H. Zhang. 2009. "Droplet formation in a T-shaped microfluidic junction." *Journal of Applied Physics* 106 (3). doi: 10.1063/1.3187831.

104. Lloyd-Jones, D., R. Adams, M. Carnethon, G. De Simone, T. B. Ferguson, K. Flegal, E. Ford, K. Furie, A. Go, K. Greenlund, N. Haase, S. Hailpern, M. Ho, V. Howard, B. Kissela, S. Kittner, D. Lackland, L. Lisabeth, A. Marelli, M. McDermott, J. Meigs, D. Mozaffarian, G. Nichol, C. O'Donnell, V. Roger, W. Rosamond, R. Sacco, P. Sorlie, R. Stafford, J. Steinberger, T. Thom, S. Wasserthiel-Smoller, N. Wong, J. Wylie-Rosett, Y. Hong, Committee American Heart Association Statistics, and Subcommittee Stroke Statistics. 2009. "Heart disease and stroke statistics--2009 update: a report from the American Heart Association Statistics Committee and Stroke Statistics Subcommittee." *Circulation* 119 (3):e21-181. doi: 10.1161/CIRCULATIONAHA.108.191261.

105. Lu, Y. C., W. Song, D. An, B. J. Kim, R. Schwartz, M. M. Wu, and M. L. Ma. 2015. "Designing compartmentalized hydrogel microparticles for cell encapsulation and scalable 3D cell culture." *Journal of Materials Chemistry B* 3 (3):353-360. doi: 10.1039/c4tb01735h.

106. Luo, L., J. Tang, K. Nishi, C. Yan, P. U. Dinh, J. Cores, T. Kudo, J. Zhang, T. S. Li, and K. Cheng. 2017. "Fabrication of Synthetic Mesenchymal Stem Cells for the Treatment of Acute Myocardial Infarction in Mice." *Circ Res* 120 (11):1768-1775. doi: 10.1161/CIRCRESAHA.116.310374.

107. Lutolf, M. P., and J. A. Hubbell. 2005. "Synthetic biomaterials as instructive extracellular microenvironments for morphogenesis in tissue engineering." *Nat Biotechnol* 23 (1):47-55. doi: 10.1038/nbt1055.

108. Ma, Z., M. Kotaki, T. Yong, W. He, and S. Ramakrishna. 2005. "Surface engineering of electrospun polyethylene terephthalate (PET) nanofibers towards development of a new

material for blood vessel engineering." *Biomaterials* 26 (15):2527-36. doi: 10.1016/j.biomaterials.2004.07.026.

109. Macaya, C., P. W. Serruys, P. Ruygrok, H. Suryapranata, G. Mast, S. Klugmann, P. Urban, P. den Heijer, K. Koch, R. Simon, M. C. Morice, P. Crean, H. Bonnier, W. Wijns, N. Danchin, C. Bourdonnec, and M. A. Morel. 1996. "Continued benefit of coronary stenting versus balloon angioplasty: one-year clinical follow-up of Benestent trial. Benestent Study Group." *J Am Coll Cardiol* 27 (2):255-61. doi: 10.1016/0735-1097(95)00473-4.

110. Mardilovich, A., J. A. Craig, M. Q. McCammon, A. Garg, and E. Kokkoli. 2006. "Design of a novel fibronectin-mimetic peptide-amphiphile for functionalized biomaterials." *Langmuir* 22 (7):3259-64. doi: 10.1021/la052756n.

111. Mardilovich, A., and E. Kokkoli. 2004. "Biomimetic peptide-amphiphiles for functional biomaterials: the role of GRGDSP and PHSRN." *Biomacromolecules* 5 (3):950-7. doi: 10.1021/bm0344351.

112. Massia, S. P., and J. A. Hubbell. 1992. "Vascular Endothelial-Cell Adhesion and Spreading Promoted by the Peptide Redv of the Iiics Region of Plasma Fibronectin Is Mediated by Integrin Alpha-4-Beta-1." *Journal of Biological Chemistry* 267 (20):14019-14026.

113. McCain, M. L., A. Agarwal, H. W. Nesmith, A. P. Nesmith, and K. K. Parker. 2014. "Micromolded gelatin hydrogels for extended culture of engineered cardiac tissues." *Biomaterials* 35 (21):5462-71. doi: 10.1016/j.biomaterials.2014.03.052.

114. McDonald, J. C., D. C. Duffy, J. R. Anderson, D. T. Chiu, H. Wu, O. J. Schueller, and G. M. Whitesides. 2000. "Fabrication of microfluidic systems in poly(dimethylsiloxane)." *Electrophoresis* 21 (1):27-40. doi: 10.1002/(SICI)1522-2683(20000101)21:1<27::AID-ELPS27>3.0.CO;2-C.

115. McEver, R. P., and C. Zhu. 2010. "Rolling cell adhesion." *Annu Rev Cell Dev Biol* 26 (1):363-96. doi: 10.1146/annurev.cellbio.042308.113238.

116. Medina, R. J., C. L. Barber, F. Sabatier, F. Dignat-George, J. M. Melero-Martin, K. Khosrotehrani, O. Ohneda, A. M. Randi, J. K. Y. Chan, T. Yamaguchi, V. W. M. Van Hinsbergh, M. C. Yoder, and A. W. Stitt. 2017. "Endothelial Progenitors: A Consensus Statement on Nomenclature." *Stem Cells Transl Med* 6 (5):1316-1320. doi: 10.1002/sctm.16-0360.

117. Mendis, Shanthi, Pekka Puska, Bo Norrving, and World Health Organization. 2011. *Global atlas on cardiovascular disease prevention and control*: Geneva: World Health Organization.

118. Mironov, V., R. P. Visconti, V. Kasyanov, G. Forgacs, C. J. Drake, and R. R. Markwald. 2009. "Organ printing: tissue spheroids as building blocks." *Biomaterials* 30 (12):2164-74. doi: 10.1016/j.biomaterials.2008.12.084.

119. Mitra, A. K., and D. K. Agrawal. 2006. "In stent restenosis: bane of the stent era." *J Clin Pathol* 59 (3):232-9. doi: 10.1136/jcp.2005.025742.

120. Moon, J. J., J. E. Saik, R. A. Poche, J. E. Leslie-Barbick, S. H. Lee, A. A. Smith, M. E. Dickinson, and J. L. West. 2010. "Biomimetic hydrogels with pro-angiogenic properties." *Biomaterials* 31 (14):3840-7. doi: 10.1016/j.biomaterials.2010.01.104.

121. Mozaffarian, D., E. J. Benjamin, A. S. Go, D. K. Arnett, M. J. Blaha, M. Cushman, S. R. Das, S. de Ferranti, J. P. Despres, H. J. Fullerton, V. J. Howard, M. D. Huffman, C. R. Isasi, M. C. Jimenez, S. E. Judd, B. M. Kissela, J. H. Lichtman, L. D. Lisabeth, S. Liu, R. H. Mackey, D. J. Magid, D. K. McGuire, E. R. Mohler, 3rd, C. S. Moy, P. Muntner, M. E. Mussolino, K. Nasir, R. W. Neumar, G. Nichol, L. Palaniappan, D. K. Pandey, M. J. Reeves, C. J. Rodriguez, W. Rosamond, P. D. Sorlie, J. Stein, A. Towfighi, T. N. Turan, S. S. Virani, D. Woo, R. W. Yeh, M. B. Turner, Committee American Heart Association Statistics, and Subcommittee Stroke Statistics. 2016. "Heart Disease and Stroke Statistics-2016 Update: A Report From the American Heart Association." *Circulation* 133 (4):e38-360. doi: 10.1161/CIR.0000000000000350.

122. Nguyen, K. T., and J. L. West. 2002. "Photopolymerizable hydrogels for tissue engineering applications." *Biomaterials* 23 (22):4307-14. doi: 10.1016/s0142-9612(02)00175-8.

123. Nichol, J. W., S. T. Koshy, H. Bae, C. M. Hwang, S. Yamanlar, and A. Khademhosseini. 2010. "Cell-laden microengineered gelatin methacrylate hydrogels." *Biomaterials* 31 (21):5536-44. doi: 10.1016/j.biomaterials.2010.03.064.

124. Nicodemus, G. D., and S. J. Bryant. 2008. "Cell encapsulation in biodegradable hydrogels for tissue engineering applications." *Tissue Eng Part B Rev* 14 (2):149-65. doi: 10.1089/ten.teb.2007.0332.

125. Odian, George G. 2004. *Principles of polymerization*. 4th ed ed. Hoboken, N.J: Wiley-Interscience.

126. Olabisi, R. M. 2015. "Cell microencapsulation with synthetic polymers." *J Biomed Mater Res A* 103 (2):846-59. doi: 10.1002/jbm.a.35205.

127. Oliveira, M. B., O. Kossover, J. F. Mano, and D. Seliktar. 2015. "Injectable PEGylated fibrinogen cell-laden microparticles made with a continuous solvent- and oil-free preparation method." *Acta Biomater* 13:78-87. doi: 10.1016/j.actbio.2014.11.013.

128. Orive, G., M. De Castro, S. Ponce, R. M. Hernandez, A. R. Gascon, M. Bosch, J. Alberch, and J. L. Pedraz. 2005. "Long-term expression of erythropoietin from myoblasts immobilized in biocompatible and neovascularized microcapsules." *Molecular Therapy* 12 (2):283-289. doi: 10.1016/j.ymthe.2005.04.002.

129. Peled, E., J. Boss, J. Bejar, C. Zinman, and D. Seliktar. 2007. "A novel poly(ethylene glycol)-fibrinogen hydrogel for tibial segmental defect repair in a rat model." *J Biomed Mater Res A* 80 (4):874-84. doi: 10.1002/jbm.a.30928.

130. Peyton, S. R., P. D. Kim, C. M. Ghajar, D. Seliktar, and A. J. Putnam. 2008. "The effects of matrix stiffness and RhoA on the phenotypic plasticity of smooth muscle cells in a 3-D biosynthetic hydrogel system." *Biomaterials* 29 (17):2597-607. doi: 10.1016/j.biomaterials.2008.02.005.

131. Pradhan, S., C. S. Chaudhury, and E. A. Lipke. 2014. "Dual-phase, surface tension-based fabrication method for generation of tumor millibeads." *Langmuir* 30 (13):3817-25. doi: 10.1021/la500402m.

132. Pradhan, S., J. M. Clary, D. Seliktar, and E. A. Lipke. 2017. "A three-dimensional spheroidal cancer model based on PEG-fibrinogen hydrogel microspheres." *Biomaterials* 115:141-154. doi: 10.1016/j.biomaterials.2016.10.052.

133. Pradhan, S., I. Hassani, W. J. Seeto, and E. A. Lipke. 2017. "PEG-fibrinogen hydrogels for three-dimensional breast cancer cell culture." *J Biomed Mater Res A* 105 (1):236-252. doi: 10.1002/jbm.a.35899.

134. Puranik, A. S., E. R. Dawson, and N. A. Peppas. 2013. "Recent advances in drug eluting stents." *Int J Pharm* 441 (1-2):665-79. doi: 10.1016/j.ijpharm.2012.10.029.

135. Qian, H., Y. Yang, J. Huang, R. Gao, K. Dou, G. Yang, J. Li, R. Shen, Z. He, M. Lu, and S. Zhao. 2007. "Intracoronary delivery of autologous bone marrow mononuclear cells radiolabeled by 18F-fluoro-deoxy-glucose: tissue distribution and impact on post-infarct swine hearts." *J Cell Biochem* 102 (1):64-74. doi: 10.1002/jcb.21277.

136. Rafii, S., and D. Lyden. 2003. "Therapeutic stem and progenitor cell transplantation for organ vascularization and regeneration." *Nat Med* 9 (6):702-12. doi: 10.1038/nm0603-702.

137. Ramachandran, V., M. Williams, T. Yago, D. W. Schmidtke, and R. P. McEver. 2004. "Dynamic alterations of membrane tethers stabilize leukocyte rolling on P-selectin." *Proc Natl Acad Sci U S A* 101 (37):13519-24. doi: 10.1073/pnas.0403608101.

138. Robey, T. E., M. K. Saiget, H. Reinecke, and C. E. Murry. 2008. "Systems approaches to preventing transplanted cell death in cardiac repair." *J Mol Cell Cardiol* 45 (4):567-81. doi: 10.1016/j.yjmcc.2008.03.009.

139. Rolland, J. P., B. W. Maynor, L. E. Euliss, A. E. Exner, G. M. Denison, and J. M. DeSimone. 2005. "Direct fabrication and harvesting of monodisperse, shape-specific nanobiomaterials." *J Am Chem Soc* 127 (28):10096-100. doi: 10.1021/ja051977c.

140. Roudsari, L. C., S. E. Jeffs, A. S. Witt, B. J. Gill, and J. L. West. 2016. "A 3D Poly(ethylene glycol)-based Tumor Angiogenesis Model to Study the Influence of Vascular Cells on Lung Tumor Cell Behavior." *Sci Rep* 6:32726. doi: 10.1038/srep32726.

141. Rufaihah, A. J., N. F. Huang, S. Jame, J. C. Lee, H. N. Nguyen, B. Byers, A. De, J. Okogbaa, M. Rollins, R. Reijo-Pera, S. S. Gambhir, and J. P. Cooke. 2011. "Endothelial cells derived from human iPSCS increase capillary density and improve perfusion in a mouse model of

peripheral arterial disease." *Arterioscler Thromb Vasc Biol* 31 (11):e72-9. doi: 10.1161/ATVBAHA.111.230938.

142. Rufaihah, A. J., N. F. Huang, J. Kim, J. Herold, K. S. Volz, T. S. Park, J. C. Lee, E. T. Zambidis, R. Reijo-Pera, and J. P. Cooke. 2013. "Human induced pluripotent stem cell-derived endothelial cells exhibit functional heterogeneity." *Am J Transl Res* 5 (1):21-35.

143. Rufaihah, A. J., and D. Seliktar. 2016. "Hydrogels for therapeutic cardiovascular angiogenesis." *Adv Drug Deliv Rev* 96:31-9. doi: 10.1016/j.addr.2015.07.003.

144. Sakai, S., S. Ito, H. Inagaki, K. Hirose, T. Matsuyama, M. Taya, and K. Kawakami. 2011. "Cell-enclosing gelatin-based microcapsule production for tissue engineering using a microfluidic flow-focusing system." *Biomicrofluidics* 5 (1):13402. doi: 10.1063/1.3516657.

145. Salter, M. M., W. J. Seeto, B. B. DeWitt, S. A. Hashimi, D. D. Schwartz, E. A. Lipke, and A. A. Wooldridge. 2015. "Characterization of endothelial colony-forming cells from peripheral blood samples of adult horses." *Am J Vet Res* 76 (2):174-87. doi: 10.2460/ajvr.76.2.174.

146. Schachinger, V., A. Aicher, N. Dobert, R. Rover, J. Diener, S. Fichtlscherer, B. Assmus, F. H. Seeger, C. Menzel, W. Brenner, S. Dimmeler, and A. M. Zeiher. 2008. "Pilot trial on determinants of progenitor cell recruitment to the infarcted human myocardium." *Circulation* 118 (14):1425-32. doi: 10.1161/CIRCULATIONAHA.108.777102.

147. Schwartz, S. M. 1978. "Selection and characterization of bovine aortic endothelial cells." *In Vitro* 14 (12):966-80. doi: 10.1007/bf02616210.

148. Seemann, R., M. Brinkmann, T. Pfohl, and S. Herminghaus. 2012. "Droplet based microfluidics." *Rep Prog Phys* 75 (1):016601. doi: 10.1088/0034-4885/75/1/016601.

149. Seeto, W. J., and E. A. Lipke. 2016. "Optical cell tracking analysis using a straight-forward approach to minimize processing time for high frame rate data." *Rev Sci Instrum* 87 (3):033705. doi: 10.1063/1.4943420.

150. Seeto, W. J., Y. Tian, and E. A. Lipke. 2013. "Peptide-grafted poly(ethylene glycol) hydrogels support dynamic adhesion of endothelial progenitor cells." *Acta Biomater* 9 (9):8279-89. doi: 10.1016/j.actbio.2013.05.023.

151. Seeto, W. J., Y. Tian, S. Pradhan, P. Kerscher, and E. A. Lipke. 2019. "Rapid Production of Cell-Laden Microspheres Using a Flexible Microfluidic Encapsulation Platform." *Small*:e1902058. doi: 10.1002/smll.201902058.

152. Seeto, W. J., Y. Tian, R. L. Winter, F. J. Caldwell, A. A. Wooldridge, and E. A. Lipke. 2017. "Encapsulation of Equine Endothelial Colony Forming Cells in Highly Uniform, Injectable Hydrogel Microspheres for Local Cell Delivery." *Tissue Eng Part C Methods* 23 (11):815-825. doi: 10.1089/ten.TEC.2017.0233.

153. Seliktar, D. 2012. "Designing cell-compatible hydrogels for biomedical applications." *Science* 336 (6085):1124-8. doi: 10.1126/science.1214804.

154. Serruys, P. W., P. de Jaegere, F. Kiemeneij, C. Macaya, W. Rutsch, G. Heyndrickx, H. Emanuelsson, J. Marco, V. Legrand, P. Materne, and et al. 1994. "A comparison of balloon-expandable-stent implantation with balloon angioplasty in patients with coronary artery disease. Benestent Study Group." *N Engl J Med* 331 (8):489-95. doi: 10.1056/NEJM199408253310801.

155. Sharpe, A. N., W. J. Seeto, R. L. Winter, Q. Zhong, E. A. Lipke, and A. A. Wooldridge. 2016. "Isolation of endothelial colony-forming cells from blood samples collected from the jugular and cephalic veins of healthy adult horses." *Am J Vet Res* 77 (10):1157-65. doi: 10.2460/ajvr.77.10.1157.

156. Sheikh, A. Y., B. C. Huber, K. H. Narsinh, J. M. Spin, K. van der Bogt, P. E. de Almeida, K. J. Ransohoff, D. L. Kraft, G. Fajardo, D. Ardigo, J. Ransohoff, D. Bernstein, M. P. Fischbein, R. C. Robbins, and J. C. Wu. 2012. "In vivo functional and transcriptional profiling of bone marrow stem cells after transplantation into ischemic myocardium." *Arterioscler Thromb Vasc Biol* 32 (1):92-102. doi: 10.1161/ATVBAHA.111.238618.

157. Shin, S. R., C. Zihlmann, M. Akbari, P. Assawes, L. Cheung, K. Zhang, V. Manoharan, Y. S. Zhang, M. Yuksekkaya, K. T. Wan, M. Nikkhah, M. R. Dokmeci, X. S. Tang, and A. Khademhosseini. 2016. "Reduced Graphene Oxide-GelMA Hybrid Hydrogels as Scaffolds for Cardiac Tissue Engineering." *Small* 12 (27):3677-89. doi: 10.1002/smll.201600178.

158. Shofuda, T., H. Fukusumi, D. Kanematsu, A. Yamamoto, M. Yamasaki, N. Arita, and Y. Kanemura. 2013. "A method for efficiently generating neurospheres from human-induced pluripotent stem cells using microsphere arrays." *Neuroreport* 24 (2):84-90. doi: 10.1097/WNR.0b013e32835cb677.

159. Sonnet, C., C. L. Simpson, R. M. Olabisi, K. Sullivan, Z. Lazard, Z. Gugala, J. F. Peroni, J. M. Weh, A. R. Davis, J. L. West, and E. A. Olmsted-Davis. 2013. "Rapid healing of femoral defects in rats with low dose sustained BMP2 expression from PEGDA hydrogel microspheres." *Journal of Orthopaedic Research* 31 (10):1597-1604. doi: 10.1002/jor.22407.

160. Sousa, J. E., P. W. Serruys, and M. A. Costa. 2003. "New frontiers in cardiology - Drug-eluting stents: Part I." *Circulation* 107 (17):2274-2279. doi: 10.1161/01.Cir.0000069330.41022.90.

161. Sperandio, M., M. L. Smith, S. B. Forlow, T. S. Olson, L. Xia, R. P. McEver, and K. Ley. 2003. "P-selectin glycoprotein ligand-1 mediates L-selectin-dependent leukocyte rolling in venules." *J Exp Med* 197 (10):1355-63. doi: 10.1084/jem.20021854.

162. Springer, T. A. 1995. "Traffic signals on endothelium for lymphocyte recirculation and leukocyte emigration." *Annu Rev Physiol* 57 (1):827-72. doi: 10.1146/annurev.ph.57.030195.004143.

163. Taite, L. J., P. Yang, H. W. Jun, and J. L. West. 2008. "Nitric oxide-releasing polyurethane-PEG copolymer containing the YIGSR peptide promotes endothelialization with decreased platelet adhesion." *J Biomed Mater Res B Appl Biomater* 84 (1):108-16. doi: 10.1002/jbm.b.30850.

164. Takahashi, K., and S. Yamanaka. 2006. "Induction of pluripotent stem cells from mouse embryonic and adult fibroblast cultures by defined factors." *Cell* 126 (4):663-76. doi: 10.1016/j.cell.2006.07.024.

165. Tan, W. H., and S. Takeuchi. 2007. "Monodisperse alginate hydrogel microbeads for cell encapsulation." *Advanced Materials* 19 (18):2696-+. doi: 10.1002/adma.200700433.

166. Tang, J., X. Cui, T. G. Caranasos, M. T. Hensley, A. C. Vandergriff, Y. Hartanto, D. Shen, H. Zhang, J. Zhang, and K. Cheng. 2017. "Heart Repair Using Nanogel-Encapsulated Human Cardiac Stem Cells in Mice and Pigs with Myocardial Infarction." *ACS Nano* 11 (10):9738-9749. doi: 10.1021/acsnano.7b01008.

167. Tashiro, S., K. Tsumoto, and E. Sano. 2012. "Establishment of a microcarrier culture system with serial sub-cultivation for functionally active human endothelial cells." *J Biotechnol* 160 (3-4):202-13. doi: 10.1016/j.jbiotec.2012.02.022.

168. Tice, J. D., H. Song, A. D. Lyon, and R. F. Ismagilov. 2003. "Formation of droplets and mixing in multiphase microfluidics at low values of the Reynolds and the capillary numbers." *Langmuir* 19 (22):9127-9133. doi: 10.1021/la030090w.

169. Tree, J. A., C. Richardson, A. R. Fooks, J. C. Clegg, and D. Looby. 2001. "Comparison of large-scale mammalian cell culture systems with egg culture for the production of influenza virus A vaccine strains." *Vaccine* 19 (25-26):3444-50. doi: 10.1016/s0264-410x(01)00053-6.

170. Tumarkin, E., and E. Kumacheva. 2009. "Microfluidic generation of microgels from synthetic and natural polymers." *Chem Soc Rev* 38 (8):2161-8. doi: 10.1039/b809915b.

171. Urbich, C., A. Aicher, C. Heeschen, E. Dernbach, W. K. Hofmann, A. M. Zeiher, and S. Dimmeler. 2005. "Soluble factors released by endothelial progenitor cells promote migration of endothelial cells and cardiac resident progenitor cells." *J Mol Cell Cardiol* 39 (5):733-42. doi: 10.1016/j.yjmcc.2005.07.003.

172. Van Den Bulcke, A. I., B. Bogdanov, N. De Rooze, E. H. Schacht, M. Cornelissen, and H. Berghmans. 2000. "Structural and rheological properties of methacrylamide modified gelatin hydrogels." *Biomacromolecules* 1 (1):31-8. doi: 10.1021/bm990017d.

173. Velasco, D., E. Tumarkin, and E. Kumacheva. 2012. "Microfluidic encapsulation of cells in polymer microgels." *Small* 8 (11):1633-42. doi: 10.1002/smll.201102464.

174. Vergnolle, N. 1999. "Proteinase-activated receptor-2-activating peptides induce leukocyte rolling, adhesion, and extravasation in vivo." *J Immunol* 163 (9):5064-9.

175. von Maltzahn, G., J. H. Park, A. Agrawal, N. K. Bandaru, S. K. Das, M. J. Sailor, and S. N. Bhatia. 2009. "Computationally guided photothermal tumor therapy using long-circulating gold nanorod antennas." *Cancer Res* 69 (9):3892-900. doi: 10.1158/0008-5472.CAN-08-4242.

176. Voyta, J. C., D. P. Via, C. E. Butterfield, and B. R. Zetter. 1984. "Identification and isolation of endothelial cells based on their increased uptake of acetylated-low density lipoprotein." *J Cell Biol* 99 (6):2034-40. doi: 10.1083/jcb.99.6.2034.

177. Walter, D. H., K. Rittig, F. H. Bahlmann, R. Kirchmair, M. Silver, T. Murayama, H. Nishimura, D. W. Losordo, T. Asahara, and J. M. Isner. 2002. "Statin therapy accelerates reendothelialization: a novel effect involving mobilization and incorporation of bone marrow-derived endothelial progenitor cells." *Circulation* 105 (25):3017-24. doi: 10.1161/01.cir.0000018166.84319.55.

178. Wan, J., L. Shi, B. Benson, M. J. Bruzek, J. E. Anthony, P. J. Sinko, R. K. Prudhomme, and H. A. Stone. 2012. "Microfluidic generation of droplets with a high loading of nanoparticles." *Langmuir* 28 (37):13143-8. doi: 10.1021/la3025952.

179. Wang, C. C., C. H. Chen, W. W. Lin, S. M. Hwang, P. C. Hsieh, P. H. Lai, Y. C. Yeh, Y. Chang, and H. W. Sung. 2008. "Direct intramyocardial injection of mesenchymal stem cell sheet fragments improves cardiac functions after infarction." *Cardiovasc Res* 77 (3):515-24. doi: 10.1093/cvr/cvm046.

180. Wang, C. H., W. J. Cherng, N. I. Yang, L. T. Kuo, C. M. Hsu, H. I. Yeh, Y. J. Lan, C. H. Yeh, and W. L. Stanford. 2008. "Late-outgrowth endothelial cells attenuate intimal hyperplasia contributed by mesenchymal stem cells after vascular injury." *Arterioscler Thromb Vasc Biol* 28 (1):54-60. doi: 10.1161/ATVBAHA.107.147256.

181. Wang, H., J. Zhou, Z. Liu, and C. Wang. 2010. "Injectable cardiac tissue engineering for the treatment of myocardial infarction." *J Cell Mol Med* 14 (5):1044-55. doi: 10.1111/j.1582-4934.2010.01046.x.

182. Wang, S., A. Bruning, O. Jeon, F. Long, E. Alsberg, and C. K. Choi. 2018. "An in-situ photocrosslinking microfluidic technique to generate non-spherical, cytocompatible, degradable, monodisperse alginate microgels for chondrocyte encapsulation." *Biomicrofluidics* 12 (1). doi: 10.1063/1.5017644.

183. Watts, A. E., J. C. Ackerman-Yost, and A. J. Nixon. 2013. "A comparison of three-dimensional culture systems to evaluate in vitro chondrogenesis of equine bone marrow-derived mesenchymal stem cells." *Tissue Eng Part A* 19 (19-20):2275-83. doi: 10.1089/ten.TEA.2012.0479.

184. Werb, Z. 1997. "ECM and cell surface proteolysis: regulating cellular ecology." *Cell* 91 (4):439-42. doi: 10.1016/s0092-8674(00)80429-8.

185. Williams, C. G., A. N. Malik, T. K. Kim, P. N. Manson, and J. H. Elisseeff. 2005. "Variable cytocompatibility of six cell lines with photoinitiators used for polymerizing hydrogels and cell encapsulation." *Biomaterials* 26 (11):1211-8. doi: 10.1016/j.biomaterials.2004.04.024.

186. Workman, V. L., L. B. Tezera, P. T. Elkington, and S. N. Jayasinghe. 2014. "Controlled Generation of Microspheres Incorporating Extracellular Matrix Fibrils for Three-Dimensional Cell Culture." *Adv Funct Mater* 24 (18):2648-2657. doi: 10.1002/adfm.201303891.

187. Xia, Z. H., K. W. Connington, S. Rapaka, P. T. Yue, J. J. Feng, and S. Y. Chen. 2009. "Flow patterns in the sedimentation of an elliptical particle." *Journal of Fluid Mechanics* 625:249-272. doi: 10.1017/S0022112008005521.

188. Xin, S., D. Chimene, J. E. Garza, A. K. Gaharwar, and D. L. Alge. 2019. "Clickable PEG hydrogel microspheres as building blocks for 3D bioprinting." *Biomater Sci* 7 (3):1179-1187. doi: 10.1039/c8bm01286e.

189. Xu, J. H., S. W. Li, J. Tan, and G. S. Luo. 2008. "Correlations of droplet formation in T-junction microfluidic devices: from squeezing to dripping." *Microfluidics and Nanofluidics* 5 (6):711-717. doi: 10.1007/s10404-008-0306-4.

190. Xu, J. H., S. W. Li, J. Tan, Y. J. Wang, and G. S. Luo. 2006. "Preparation of highly monodisperse droplet in a T-junction microfluidic device." *Aiche Journal* 52 (9):3005-3010. doi: 10.1002/aic.10924.

191. Xu, Q., M. Hashimoto, T. T. Dang, T. Hoare, D. S. Kohane, G. M. Whitesides, R. Langer, and D. G. Anderson. 2009. "Preparation of monodisperse biodegradable polymer microparticles using a microfluidic flow-focusing device for controlled drug delivery." *Small* 5 (13):1575-81. doi: 10.1002/smll.200801855.

192. Yang, Y. Y., T. S. Chung, and N. P. Ng. 2001. "Morphology, drug distribution, and in vitro release profiles of biodegradable polymeric microspheres containing protein fabricated by double-emulsion solvent extraction/evaporation method." *Biomaterials* 22 (3):231-41. doi: 10.1016/s0142-9612(00)00178-2.

193. Yao, R., R. Zhang, F. Lin, and J. Luan. 2012. "Injectable cell/hydrogel microspheres induce the formation of fat lobule-like microtissues and vascularized adipose tissue regeneration." *Biofabrication* 4 (4):045003. doi: 10.1088/1758-5082/4/4/045003.

194. Yao, R., R. Zhang, F. Lin, and J. Luan. 2013. "Biomimetic injectable HUVEC-adipocytes/collagen/alginate microsphere co-cultures for adipose tissue engineering." *Biotechnol Bioeng* 110 (5):1430-43. doi: 10.1002/bit.24784.

195. Yau, J. W., H. Teoh, and S. Verma. 2015. "Endothelial cell control of thrombosis." *BMC Cardiovasc Disord* 15 (1):130. doi: 10.1186/s12872-015-0124-z.

196. Yoder, M. C. 2012. "Human endothelial progenitor cells." *Cold Spring Harb Perspect Med* 2 (7):a006692. doi: 10.1101/cshperspect.a006692.

197. Youngstrom, D. W., J. G. Barrett, R. R. Jose, and D. L. Kaplan. 2013. "Functional characterization of detergent-decellularized equine tendon extracellular matrix for tissue engineering applications." *PLoS One* 8 (5):e64151. doi: 10.1371/journal.pone.0064151.

198. Yu, L., M. C. Chen, and K. C. Cheung. 2010. "Droplet-based microfluidic system for multicellular tumor spheroid formation and anticancer drug testing." *Lab Chip* 10 (18):2424-32. doi: 10.1039/c004590j.

199. Zhang, R., B. A. Le, W. Xu, K. Guo, X. M. Sun, H. Y. Su, L. Huang, J. Y. Huang, T. Shen, T. Liao, Y. Y. Liang, J. X. J. Zhang, H. J. Dai, and K. Qian. 2019. "Magnetic "Squashing" of Circulating Tumor Cells on Plasmonic Substrates for Ultrasensitive NIR Fluorescence Detection." *Small Methods* 3 (2). doi: 10.1002/smtd.201800474.

200. Zhang, R., C. Rejeeth, W. Xu, C. Zhu, X. Liu, J. Wan, M. Jiang, and K. Qian. 2019. "Label-Free Electrochemical Sensor for CD44 by Ligand-Protein Interaction." *Anal Chem* 91 (11):7078-7085. doi: 10.1021/acs.analchem.8b05966.

201. Zhao, X., S. Liu, L. Yildirimer, H. Zhao, R. H. Ding, H. N. Wang, W. G. Cui, and D. Weitz. 2016. "Injectable Stem Cell-Laden Photocrosslinkable Microspheres Fabricated Using Microfluidics for Rapid Generation of Osteogenic Tissue Constructs." *Advanced Functional Materials* 26 (17):2809-2819. doi: 10.1002/adfm.201504943.